University of São Paulo
"Luiz de Queiroz" College of Agriculture

Quantitative parameterization of soil surface structure with increasing rainfall volumes

Edison Aparecido Mome Filho

Thesis presented to obtain the degree of Doctor in Science. Area: Soil and Plant Nutrition

Piracicaba
2016

Edison Aparecido Mome Filho
Agronomist

Quantitative parameterization of soil surface structure with increasing rainfall volumes

versão revisada de acordo com a resolução CoPGr 6018 de 2011

Advisor:
Prof. Dr. **MIGUEL COOPER**

Thesis presented to obtain the degree of Doctor in Science. Area: Soil and Plant Nutrition

Piracicaba
2016

Dados Internacionais de Catalogação na Publicação
DIVISÃO DE BIBLIOTECA - DIBD/ESALQ/USP

Mome Filho, Edison Aparecido
Quantitative parameterization of soil surface structure with increasing rainfall volumes / Edison Aparecido Mome Filho. - - versão revisada de acordo com a resolução CoPGr 6018 de 2011. - - Piracicaba, 2016.
94 p. : il.

Tese (Doutorado) - - Escola Superior de Agricultura “Luiz de Queiroz”.

1. Erosão pela água 2. Microrelevo 3. Escala 4. Sistema poroso I. Título

CDD 631.45
M732q

DEDICATE

To my parents,

Edison and Izabel,

for all their believe and support, since my early years.

“Barulho de trovoada, coriscos em profusão
A chuva caindo em cascata, na terra fofa do chão
Virando em lama a poeira, poeira vermelha
Poeira, poeira do meu sertão
Poeira entra meus olhos, não fico zangado não
Pois sei que quando eu morrer, meu corpo irá para o chão
Se transformar em poeira, poeira vermelha...”

music by

Luiz Bonan and Serafim C. Gomes

AKNOWLEDGEMENTS

After 4 years, I believe that the most difficult part was not to discuss my dataset, but trying to remember all the people that helped me along the way. Therefore, I ask in advance, please forgive me if your name is not cited in these next lines. Nevertheless, if you did anything, does not matter how small it was, to help me achieve the results exposed in this text, know that I own you a life debt, even if I do not remember it.

First of all, I want to thank FAPESP for the scholarships, under processes 2013/08736-6 and 2014/05738-0, that allowed this project to become true.

Secondly, but not less, I would like to thank my family, my parents, Edison and Izabel, my brother and sister, Ricardo and Erica, my sister in law, Maria, as well as my nephew and niece, Giacomo and Isabel, for soften my life during such hard years.

To "older" friends of the Soil Science department, Osvaldo, Sueli, Sâmala, Getúlio, Lorena, Raul, Renata Beltz, Selene, Mariana and Laura, I thank the hours of discussion, where you were patient enough to hear much more than speak.

To "newer" friends, Hélio, Renato, Sara and Raquel, thanks for all the coffee hours.

To the whole class of 2005 from the best Unesp *campus* in the world, thank you for being part of my early career years, that prepared me for this moment. Special thanks to Rufião and Salsicha, whom made my time in Piracicaba to look like it was just a continuation of my undergrad period.

Thanks to Erreinaldo and everybody at the LPV for allowing me to use their area for my experimentation, and for giving me support every time that I needed.

Thanks to all the interns that helped me in all steps of my field and lab work: Julia, Katharina, Patrick, Marte, Felipe and Vitor.

Thanks to Dr. Alvaro Pires da Silva for letting me use his lab facilities, and to his crew, Jair and Rossi, that helped me during part of my analysis.

Thanks to Sonia and Chiquinho for all the good work in the manufacturing of excellent impregnated soil blocks, and for helping me at the lab whenever you could.

Thanks to Dr. Daniel Gimenez and Dr. Richard Heck, for all the learning and support during my time in foreign lands.

Thanks to Eliana for correcting this text, and everybody that work at the library from the College of Agriculture, for all the help during my master's and doctorate.

We are coming to an end. Again, hope your name was cited here, if not, know that only four names are in my mind now. I know what you are thinking - “you ungrateful b…!”. Well, get over it and let us continue.

First, I would like to thank Virginia and Gonzalo for all the good moments. But especial thanks must be given to Virginia. If you can see 12 beautiful and long tables along this text, filled with the most interesting data about surface sealing and all that science stuff, is because she organized those tables. I have to say, is not every day that you have an intern with a Master degree working for you.

Secondly, I would like to thank Rodrigo Zenero. Without your work, there would be no thesis. Normally, we do not read about problems in the final work. However, I must declare that, if in this world, demons and evil creatures are real, part of them must live inside electrical devices. And a half of the population live inside our “dear” MicroRelief Meter. You should be canonized for being able to make it finish my readings when I most needed it.

Thirdly, thanks to my advisor, Dr. Miguel Cooper. After four years, you have learned how stubborn I can be. And, even so, during all this time you gave me your support and advise. I cannot say that I changed, but I sure have matured during the time working with you. Hope to continue our partnership in the years to come.

And last, but not least. During the last years I am getting more and more certain that there is no supreme being in the middle of the universe controlling our lives. No master in the universe. No after, just now. However, I cannot deny the faith of my parents, that, by holding them up, it kept me strait on my path. At the same time, a dear friend of mine, already thanked previously, gave me good moments of discussion about God, life and its mysteries, during this last semester. The overall lesson that I take from it all, is that we born, live, and die, without knowing nothing for sure. Doubt, as logic, is the very essence of the human race. So, if I do not even know it for sure if multifractal parameters do really mean something, whom am I to deny the existence of something? Thus, in the name of my parents, I thank their God, who, by making them happier in some way, made me a blessed man.

SUMMARY

RESUMO

Parametrização quantitativa da estrutura da superfície do solo em volumes crescentes de chuva

O estudo da estrutura do solo permite inferências sobre seu comportamento. Parâmetros quantitativos são comumente utilizados na avaliação da estrutura e os multifractais ainda são subutilizados na ciência do solo. Alguns estudos mostraram relação entre parâmetros multifractais com a diminuição da rugosidade superficial do solo devido à chuva e a heterogeneidade do sistema poroso. No entanto, uma assinatura multifractal relacionada a um comportamento específico do solo ainda não está estabelecida. Portanto, os objetivos desta pesquisa foram: (i) relacionar parâmetros multifractais com mudanças na estrutura do solo por meio da análise de mapas de rugosidade superficial e de imagens 2D provenientes de blocos impregnados de solo; e (ii) utilizar estes parâmetros para identificar as etapas de degradação do solo devido ao selamento e encrostamento superficial. Um experimento com chuva simulada com intensidade de 120 mm h^{-1} foi montado em uma Nitossolo Vermelho eutroférrico argiloso em parcelas quadruplas onde aplicou-se volumes de 40, 80 e 120 mm, mais um controle sem-chuva. A evolução da rugosidade superficial foi avaliada em três escalas: um rugosímetro de campo (MRM) reuniu leituras numa grade fixa (10 x 10 mm, 640000 mm²); um escâner com triangulação de lasers em multilinhas (MLT) foi usado em laboratório, sobre blocos de solo, criando uma grade aleatório (0,5 mm de resolução, 5625 mm²); um tomógrafo de raios-X (XRT) reuniu leituras de um bloco de solo em uma grade fixa (0,074 x 0,074 mm, de 900 mm²). Para a análise micromorfométrica, amostras de solo indeformado (0,12 x 0,07 x 0,05 m) foram impregnadas, cortadas em blocos, polidas e subdivididas em três camadas (0 a 10 mm, 20 a 30 mm e de 40 a 50 mm), paralelas à superfície, tendo cinco imagens (ampliação de 10x, 156,25 μm^2 $pixel^{-1}$) geradas por camada. Após a segmentação, três imagens foram selecionadas por camada e o sistema poroso foi avaliado. Análises de rugosidade não mostraram diferenças ($p > 0.10$) entre parâmetros multifractais nas medições da escala MRM, enquanto MLT e XRT puderam ser utilizadas para modelar a degradação da rugosidade com o aumento do volume de chuva. Como essas duas ultimas escalas apresentaram resultados similares, MLT poderia substituir o uso de XRT em tais análises, devido ao seu menor custo e possibilidade de cobrir área mais vasta durante as análises. O comportamento multifractal dos poros mudou de acordo com o desenvolvimento do selamento superficial e da camada avaliada, sendo sensitivo a mudanças no grau de fragmentação (número de poros) dentro de cada classe de tamanho de poros. As dimensões de Hausdorff a esquerda do espectro (*Lf(α)min*, *LΔf(α)* and *D2*) tiveram relação linear com o aumento de volume de chuva para ambas medições de rugosidade superficial do solo e de área de poros. Entretanto, *D2* não foi significativo ($p > 0.10$) entre volumes de chuva para diferenciar a porosidade próxima a superfície, embora os parâmetros *D0-D1*, *D0-D2* e *D1-D2* pudessem ser utilizados para descrever mudanças nessa camada. Conclui-se que o espectro multifractal é sensível à mudanças estruturais no solo causadas pela chuva e que pode ser utilizado na parametrização da degradação da rugosidade superficial do solo e da porosidade.

Palavras-chave: Erosão pela água; Microrelevo; Escala; Sistema poroso

ABSTRACT

Quantitative parameterization of soil surface structure with increasing rainfall volumes

The study of soil structure allows inferences on soil behavior. Quantitative parameters are oftentimes required to describe soil structure and the multifractal ones are still underused in soil science. Some studies have shown relations between the multifractal spectrum and both soil surface roughness decay by rainfall and porous system heterogeneity, however, a particular multifractal response to a specific soil behavior is not established yet. Therefore, the objectives of this research were: (i) to establish relations between multifractal parameters and soil structure changes by analyzing both soil surface roughness maps and 2D images from impregnated soil blocks; and (ii) to utilize these parameters to evaluate soil surface degradation by the processes of crusting and sealing. An experiment with simulated rainfall was assembled on a Fine Rhodic Kandiudalf with an intensity of 120 mm h^{-1} in quadruplicate plots at amounts of 40, 80, and 120 mm, plus a no-rainfall control. The evolution of the surface roughness was evaluated in three scales of measurement: a field microrelief meter (MRM) gathered readings on a fixed grid (10 x 10 mm, 640,000 mm²); a multistripe laser triangulation (MLT) scanner was used in the laboratory in soil blocks, creating a random mesh (0.5 mm of resolution, 5625 mm²); an X-ray tomography (XRT) scanner gathered readings of a soil block on a fixed grid (0.074 x 0.074 mm, 900 mm²). For micromorphometrical analysis, undisturbed soil samples (0.12 x 0.07 x 0.05 m) were impregnated, sliced in blocks and polished. Each block was divided into three layers (0 to 10 mm, 20 to 30 mm and 40 to 50 mm), parallel to surface, and five images (10X magnification, 156.25 μm^2 $pixel^{-1}$) were taken by layer. After segmentation, three representative images were chosen by layer and the pore system was evaluated. Roughness analyzes showed no differences ($p > 0.10$) between multifractal parameters across rainfall amounts for MRM measurements, while both MLT and XRT could be used to model roughness degradation by rainfall increase. Since the last two scales presented similar results, MLT could replace XRT in such analysis, due to its lower cost and possibility of a larger area coverage. The multifractal behavior of pores changed according to sealing development and depth of measurement, being sensitive to the changes on size distribution and fragmentation degree (number of pores) within each size class. The Hausdorff dimensions at the left side of the spectrum (*Lf(α)min*, *LΔf(α)* and *D2*) showed a linear behavior with increasing rainfall amount, considering both soil surface roughness and area of pores measurements. However, *D2* was not different ($p > 0.10$) along rainfalls for the porosity closer to surface, although parameters *D0-D1*, *D0-D2* and *D1-D2* could be used to described the changes in this layer. Was concluded that the multifractal spectrum is sensitive to structure changes caused by rainfall and that it can be used to parameterize both soil surface and pores degradation.

Keywords: Water erosiom; Microtopography; Scale; Porous system

1 INTRODUCTION

The description of the soil structure assists the understanding of its behavior in the environment, which is important to explain complex processes that occur in the soil, such as water and air movement, nutrient cycling and erosion. However, characterization of the structure must not depend only on its visual description if we want to logically describe the system. Particularly, to understand a physical process, a mathematical approach is very often the most appropriate, because it uses a logical organization of thoughts to explain the system. As a result, soil physicists rely on both mathematical and statistical modeling to describe processes in soil, and a range of indexes are used to characterize physical quality of a soil.

In the last century, several methods were used to estimate numerical data, which were used to express soil structure regarding its stability and functioning. These methods are mainly based on direct measurements of one or more soil physical attributes that, after some mathematical reasoning are linked to a determined behavior. For instance, aggregates size distribution can be used to calculate the weighted mean diameter, which is commonly used to describe the stability of the soil structure. On the other side both pores size and shape distribution are associated to several flux equations and used to model both inputs and outputs in soil, which basically governs soil functioning. The association between stability and functioning dictates the physical quality of a soil, that may be addressed in different ways. For example, to achieve high crop productivity, the ideal relation between stability and functioning may not be the same as to the one to reduce erosion rates to a minimum. Therefore, the term soil physical quality can be ambiguous. This subject will be developed during the section 2.1.2 to clarify the objectives and the methodology used during this research.

Nonetheless, since soil presents several functions on the ecosystem, which may lead to a range of indexes used to characterize it, it may be considered as a complex system. This brings up the importance of finding a parameter that relates to several soil attributes, allowing its interpretation in several areas of research. The fractal theory was broadly employed in the study of chaotic systems, such as turbulence, and in soil science it was used as a parameter to describe patterns of spatial distribution of different materials, from fungi and bacterial communities until scaling properties of soil aggregation, that interferes in both pores size and shape distribution. However, the range of interpretations that can be uniquely drawn from fractal results is very narrow. The main issue with interpretations only based in a fractal approach is to rely on a unique number so that it will describe several processes occurring at the same time. Thus, the fractal dimension of a dataset is often correlated to other variables

before conclusions can be made. In that sense, the multifractal approach allows more flexibility, as it will be scrutinized throughout this text, and a range of interpretations can be made without the need of other variables input. However, its use is still incipient in soil science. This fact may be associated to the multiplicity of parameters displayed by such analysis, many of whom still lack physical interpretation.

Therefore, the objectives of this research were: (i) to establish relations between multifractal parameters and soil structure changes by analyzing both soil surface roughness maps and 2D images from impregnated soil blocks; and (ii) to utilize these parameters to evaluate soil surface degradation by the processes of crusting and sealing.

The hypothesis tested were: i) The multifractal spectra is sensitive to structure changes caused by a range of rainfall amounts; ii) some multifractal parameters can be used to model the steps of soil surface degradation by rainfall.

2 DEVELOPMENT

2.1 Literature review

2.1.1 Analyses of complex systems: soil as a multifractal

A complex system is one that presents a challenge against universal modeling. In other words, when it is difficult to find a suitable model to describe phenomena, because these occur in a system that has too many variables, we call this system complex (CHU, 2011). The fractal theory has aided the understanding of several complex systems where other mathematical approaches have shown to be laborious, or even erroneous. Because of that, a quick review of this theory is provided.

2.1.1.1 Fractal theory

In Mathematics, the dimension of a space can be described as the minimum set of coordinates to specify any points within it. The theory of measure, by Henri Labesgue, gives the notion of linear measure on a straight line, of plane measure on a bi-dimensional plane, of volume measure in three dimensional space (BESICOVITCH, 1928). Knowing that length exists not only in straight lines, but also in a space, Constantin Carathéodory defined the s-dimension of a set in a q-dimensional space as any integer number considering $q \geq s$. This states the dimensions in a Euclidean space, which are always integer numbers (BESICOVITCH, 1928).

With the development of the set theory and Georg Cantor's idea of the existence of uncountable sets (an infinite of infinities), the Euclidean point of view, traced by general topology, changed and mathematicians proved the possibility of non-integer dimensions. Hausdorff (1919) using the axiomatic of set theory wrote a paper on his definitions of dimensions, and Besicovitch (1928, 1937) applied Hausdorff theorems on the description of sets of fractional dimensions. The definition is as follows, and can be similarly applied to higher dimensional spaces: considering a finite sequence of sets U_i (U_1,U_2,…,U_n) that cover a set A ($U_i \subset A$) in a q-dimensional space (q equals a positive integer), and knowing d_i is the sequence (d_1, d_2,…, d_n) of the diameters of U_i, which $d_i \leq \delta$, and δ is a positive number, the s-dimension of the measure A (s-dimA) can be defined as:

$$\mathrm{s-dimA} = \lim_{\delta \to 0} \sum_{U_i} d^s \qquad (1)$$

In a linear set Besicovitch assumed three possibilities: (i) there exists $0 \leq s \leq 1$, if $s' > s$ for $s' - dimA = 0$ and $s' < s$ for $s' - dimA = \infty$, then A is a s-dimensional set; (ii) if $s - dimA = \infty$ for any $s < 1$, then A is one-dimensional; (ii) if $s - dimA = 0$ for any

$s > 0$, then A is 0-dimensional. This was called the Hausdorff dimension of a set and, due to the possibility of fractional dimensions, was useful to describe the geometry of some strange sets.

To compute the dimension of an object is easier to calculate the Minkowski-Bouligand dimension, which is, in most occasions, similar to the Hausdorff dimension. A way to calculate this is to cover the object with boxes with different side lengths L. The relation between L and the number of boxes N(L) that cover the object follows a power law

$$N(L) \sim \left(\frac{1}{L}\right)^{D} \tag{2}$$

and, when $L \rightarrow 0$, the boxes approximate the real shape and size of the object, expressing Equation 3.

$$N(L) = \lim_{L \to 0} k \left(\frac{1}{L}\right)^{D} \tag{3}$$

D is Minkowski-Bouligand dimension, also called the box-counting dimension, and k is a proportionality constant that represents the number of initiators of the object. This equation can also calculate the topological dimension of lines, squares and cubes, but nothing prevents D of being a non-integer number.

If the boxes are square, there is a scale relation when L decreases and a more insightful way of writing Equation 3 is:

$$N\left(\frac{1}{b^i}\right) = \lim_{i \to \infty} k \left[\frac{1}{b^i}\right]^{-D} \tag{4}$$

Where $N\left(\frac{1}{b^i}\right)$ is the number of boxes with size $\frac{1}{b^i}$, and b^i is the scale factor. When k is 1, D can be expressed by using logarithm in Equation 5, where we can calculate D by two forms, approximately, by the slope of the log log plot of $N\left(\frac{1}{b^i}\right)$ *vs* $\left(\frac{1}{b^i}\right)$, or exactly, by finding the limit of this function.

$$D = \lim_{i \to \infty} \frac{log\, N\left(\frac{1}{b^i}\right)}{log\left(\frac{1}{b^i}\right)} \tag{5}$$

2.1.1.2 Fractals in Nature

As stated before, the fractional dimension is not new in mathematics. However, its use to explain physical phenomena started only in 1967. By measuring the coast of several countries and continents in different scales, Richardson (1961) showed that conventional measurement techniques could give enormously distinct results, with lengths increasing rapidly according to the magnification of the scale. Based on plots of scale *vs* length,

Richardson saw a power law relation. Therefore, he used a log plotting to calculate the slopes of such relations and propose to use this parameter to distinguish the coastlines.

Mandelbrot (1967) made a mathematical interpretation of Richardson's measurements using Equation 3 as basis, considering that the number N(d) of segments of length d needed to walk across the coastline was proportional to $(1/d)^D$, for some exponent D and a proportionality constant k (Equation 6).

$$N(d) = \lim_{d \to 0} k \left(\frac{1}{d}\right)^D \tag{6}$$

The length $L(d)$ of the coastline would be equal to the sum of all d:

$$L(d) = N(d)\, d \tag{7}$$

Therefore, by joining Equations 6 and 7:

$$L(d) = \lim_{d \to 0} k (d)^{1-D} \tag{8}$$

Applying logarithms:

$$log\, L(d) = \lim_{d \to 0} [(1 - D)\, log\, d + log\, k] \tag{9}$$

If the initiator is a unique line, $k = 1$, and because its length would depend on the scale of measurement, d may be substituted by $\frac{1}{b^i}$, where b^i is a scale factor, generating Equation 10:

$$D = 1 + \lim_{i \to \infty} \frac{log\, L\left(\frac{1}{b^i}\right)}{log\left(\frac{1}{b^i}\right)} \tag{10}$$

If the data points of Richardson's log log plots lied along a straight line, the assumption on Equation 6 was justified, and Mandelbrot called the exponent D as the "fractal dimension" of the coastline, permitting Richardson's data to be interpreted by this value. This was the first proof that, at some scales, natural systems could be represented by a simple power law that relates the characteristics of an object to an exponent, which was considered as a dimension of the system.

Mandelbrot used the term "fractal" to designate the objects that exhibit repeating patterns at different scales and did extensive work on reviewing, theorizing and describing such objects and their relations with physical systems. Such interpretations were impacting in the study of chaotic systems, since the fractal dimension helps to explain the scale relation of complex shapes, where details appear to contain more information than the general analysis of the object. Therefore, the fractal theory defines spatial and temporal models of systems that

exhibit a range of symmetry, characterized by a power law dependent on the number of repetitions of a given characteristic.

2.1.1.3 Multifractal theory

Although the fractal theory presents an easy way of characterize a system, complex structures of nature present variations that cannot be analyzed by a simple fractal model. In nature most of the processes are stochastic, and the mass distribution along the systems is not homogeneous. The multifractal analysis includes this density variation, which are expressed in a multifractal spectrum (CHHABRA et al., 1989; CHHABRA; JENSEN, 1989) that gives a quantitative description of a heterogeneous phenomenon (STANLEY; MEAKIN, 1988). Perfect and Kay (1995) describes the fractal dimension as "a non-integer dimension that determines the capacity of a generator in occupying a space" and Stanley and Meakin (1988) said a "…multifractal phenomena describes the concept that different regions of an object have different fractal properties". Therefore, the multifractal approach brings much more information of a process that happens at different scales, since it considers the heterogeneity of the system.

If a system presents areas of different densities, it means that at each step of its formation, different probabilities occurred at different regions. For example, in a volume of soil, the formation of soil aggregates occurs at different amounts in each region, and areas with higher concentration of solids are going to present morphology different to areas with higher porosity. This shows that the distribution of probabilities of the mass along the object can be used to describe the system and to interpret the system's organization.

Once again recurring to the counting-box technique, the mass probability of the *ith* box $P_i(L)$ can be considered as the ratio between the number of points with mass of the *ith* box $N_i(L)$ and the total mass of the system N.

$$P_i(L) = \frac{N_i(L)}{N} \tag{11}$$

Smaller the box size, smaller is the mass contained in that box compared to the rest of the image. Therefore, there is a dependence between $P_i(L)$ and L, decreasing the probability of each box with the decreasing of L, which may be expressed by a power law.

$$P_i(L) \sim L^{\alpha_i} \tag{12}$$

α_i is called the Lipschitz-Holder exponent, or the strength of singularity (CHHABRA; JENSEN, 1989). This exponent characterizes the scale in the *ith* region or spatial location and can be interpreted as the local behavior of $P_i(L)$ in the center of a box with diameter L

(POSADAS et al., 2003). We can calculate α_i by Equation 10 and, because the probability measures the fraction of the points that occupy a region, we think of this ratio as a dimension.

$$\alpha_i = \lim_{L \to 0} \frac{log\, P_i(L)}{log(L)} \tag{13}$$

Because of a logarithm property, smaller probabilities gives higher values of α_i, being the contrary true. Since α_i turns into a local exponent when $L \to 0$, and similar values can be found in different regions (boxes) of the system, the measure is called a "multifractal" (PARISI et al., 1985), exhibiting a range of power laws (Equation 11).

$$N(\alpha) \sim \left(\frac{1}{L}\right)^{f(\alpha)} \tag{14}$$

The number of boxes $N(\alpha)$ where $P_i(L)$ has exponents $\alpha + d\alpha$ is proportional to the inverse of the box size L and to an exponent f(α), which is the Hausdorff dimension of a set of boxes having the same strength singularity and can be loosely defined as a set of "fractal dimensions". Plotting f(α) *vs* α we obtain a parabolic curve, with concavity up, known as the singularity spectrum, or the multifractal spectrum of the object. As cited by Chhabra and Jensen (1989) this curve "…provides us with a precise mathematical description of the multifractal behavior of a data set of an object".

Due to difficulties in direct computation of f(α), various methods where proposed to obtain it. Two main methods will be described here: the Legendre transformation of the τ(q) curve and the use of partition function $\mu_i(q, L)$.

2.1.1.3.1 Legendre transformation of τ(q)

From Equation 11 is possible to note a conservation of probability:

$$\sum_{i=1}^{N} P_i(L) = 1 \tag{15}$$

Rearranging Equations 11 and 15, and adding a distortion exponent q to evaluate the behavior of the distribution of mass in the measure, we get to the Equation 16 (BENZI et al., 1984):

$$\sum_{i=1}^{N} P_i(L)^q = \frac{\sum_{i=1}^{N} N_i(L)^q}{N} \tag{16}$$

We note that the distortion depends on the L size of the box, and it follows a power law (MANDELBROT, 1974; HENTSCHEL; PROCACCIA, 1983; BENZI et al., 1984):

$$\sum_{i=1}^{n} P_i(L)^q \sim L^{\tau(q)} \quad (18)$$

Where $\tau(q)$ is a non-linear function of q if the fractal is not uniform, i.e. in the case of a multifractal measure, and it relates to an infinite number of generalized dimensions Dq as showed by Hentschel and Procaccia (1983):

$$\tau(q) = (q-1)Dq \quad (19)$$

Joining Equations 19 and 18, applying logarithms and limit, so $L \to 0$, we get the definition of the generalized dimensions used by Hentschel and Procaccia (1983):

$$Dq = \frac{1}{q-1} \lim_{L \to 0} \frac{\sum_{i=1}^{N(L)} \log P_i(L)^q}{\log L} \quad (20)$$

The slope of the curve $\tau(q)\ vs\ q$ is α:

$$\alpha = \frac{d\tau}{dq} \quad (21)$$

And due to the non-linearity of $\tau(q)$ there exists a range of α_i from which there are equivalent intercepts $f_i(\alpha)$ (i =1,2,…,N):

$$f_i(\alpha) = q\alpha_i - \tau \quad (22)$$

Thus, using the Legendre transformations of the $\tau(q)\ vs\ q$ curve is possible to get an $f(\alpha)\ vs\ \alpha$ spectrum.

2.1.1.3.2 Partition function ($\mu_i(q, L)$)

Chhabra and Jensen (1989) proposed a direct method to determine the $f(\alpha)$ spectrum, without recurring to the Legendre transformations. For this, they used the comparison of the distortion of the mass probabilities over the sum of all boxes at this size (Equation 23).

$$\mu_i(q, L) = \frac{P_i^q}{\sum_{i=1}^{N(L)} P_i^q} \quad (23)$$

Using a relationship between the Hausdorff dimension and Shannon's entropy, Equation 22 can generate Equations 24 and 25.

$$f(q) = \lim_{L \to 0} \frac{\sum_{i=1}^{N(L)} \mu_i(q, L)\ \log[\mu_i(q, L)]}{\log L} \quad (24)$$

$$\alpha(q) = \lim_{L \to 0} \frac{\sum_{i=1}^{N(L)} \mu_i(q, L)\ \log[P_i(L)]}{\log L} \quad (25)$$

Considering the intervals where the linear correlation between the numerators of equations 23 and 24 *vs* log *L* is high, we can estimate the f(α) spectrum.

2.1.1.3.3 Multifractal spectrum parameters

The *f(α)* spectra presents a convex parabolic shape, from where several parameters are known (Figure 1). The maximum Hausdorff dimension ($f(\alpha)_{max}$) occurs at q = 0 and it is known as the capacity or the box counting fractal dimension (*D0*), representing the global information or system average (VOSS, 1988). When the Hausdorff dimension equalizes the Lipschitz-Holder exponent (*f(α) = α*), *q* is 1 and this is called the entropy dimension (*D1*), since is related to the Shannon entropy (SHANNON; WEAVER, 1949). When *q* is 2, f(α) is mathematically associated with the correlation function (HENTSCHEL; PROCACCIA, 1983) and represents the correlation of the measures contained in a *L* size box, being called correlation dimension (*D2*). If a process is indeed multifractal, these sorts as $D2 \leq D1 \leq D0$ (HENTSCHEL; PROCACCIA, 1983).

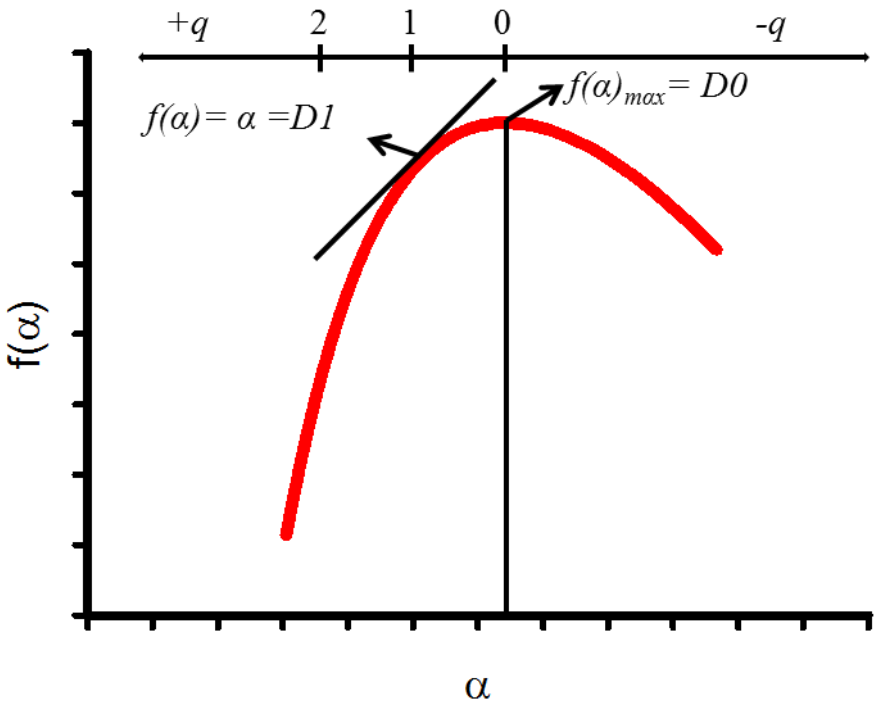

Figure 1 – Schematic of a multifractal spectrum and graphical interpretations of the capacity dimension ($f(\alpha)_{max}$ =*D0*) and the entropy dimension (*f(α)≡α =D1*).

Other parameters can be assessed from the spectrum and their physical interpretation may help describe soil structure changes (Figure 2).

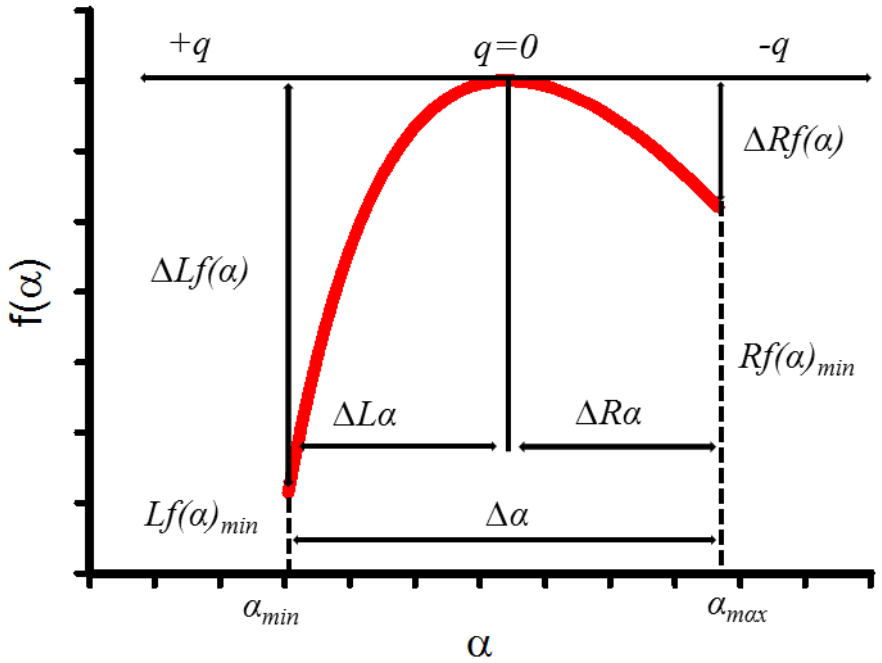

Figure 2 – Schematic of a multifractal spectrum and parameters that can be estimated: $Rf(\alpha)_{min}$: minimum Hausdorff dimension at right of *D0*; $Lf(\alpha)_{min}$: minimum Hausdorff dimension at left of *D0*; $\Delta Rf(\alpha)$: range of Hausdorff dimensions at right of *D0*; $\Delta Lf(\alpha)$: range of Hausdorff dimensions at left of *D0*; $f(\alpha)_{ratio}$: ratio between $\Delta Rf(\alpha)$ and $\Delta Lf(\alpha)$; α_{min}: minimum Lipschitz-Holder exponent; α_{max}: maximum Lipschitz-Holder exponent; $\Delta\alpha$: the complete range of Lipschitz-Holder exponents; $\Delta R\alpha$: range of Lipschitz-Holder exponents at right of *D0*; $\Delta L\alpha$: range of Lipschitz-Holder exponents at left of *D0*; α_{ratio}: ratio between $\Delta R\alpha$ and $\Delta L\alpha$

The minimum Hausdorff dimension at left of *D0* ($Lf(\alpha)_{min}$) is related to positive range of *q*'s, so it can be interpreted as the fractal dimension of areas presenting higher probabilities. The range between *D0* and the $Lf(\alpha)_{min}$ ($\Delta Lf(\alpha)$) represents how uniform the fragmentation process occurs at areas with higher probabilities, and values closer to 0 may show a homogeneous process, or one dominated by smaller probabilities. Similarly, the minimum Hausdorff dimension at right of *D0* ($Rf(\alpha)_{min}$) represents the fractal dimensions of areas with smaller probabilities, and the range between this and *D0* ($\Delta Rf(\alpha)$) shows the diversity of dimensions of these areas. While the ordinate axe relates to the fragmentation process at different ranges of probabilities, the Lipschitz-Holder exponent (α) shows how probabilities change along scales. Thus, its minimum (α_{min}) shows how the distribution changes over scale in areas of higher density, and its maximum (α_{max}) how it happens for the areas with lower density. The range at left and at right of $\alpha(D0)$ ($\Delta L\alpha$ and $\Delta R\alpha$) indicate which class changes more over scale when compared to the systems' mean. The whole range ($\Delta\alpha$) represents how diverse the system is along scales. Both ratios ($f(\alpha)_{\text{ratio}}$ and α_{ratio}) relates the behavior of areas with small probabilities to those with high probabilities, and show which class is more

fragmented and changes more across scale, respectively. They are calculated according to Equations 26 and 27.

$$f(\alpha)_{\text{ratio}} = \frac{\Delta R f(\alpha)}{\Delta L f(\alpha)} \quad (26)$$

$$\alpha_{\text{ratio}} = \frac{\Delta R \alpha}{\Delta L \alpha} \quad (27)$$

2.1.1.4 Fractal and multifractal applications in soil science

Fractal techniques have been used in soil science as an alternative to conventional geometry (PACHEPSKY et al., 1996; GIMENEZ et al., 1997). The fractal dimension assumes that a soil property is scale dependent and can be represented by a power law. In soil biology it was used in evaluation of mycelial morphology of different fungi species (BODDY et al, 1999). In the soil chemistry area, Rice and Lin (1993) were the first to evaluate the fractal nature of humic materials, followed by Senesi (1999), Rizzi et al. (2004) and Fedotov and Shoba (2013). Also Rice et al. (1999) and Sokolowska et al. (2009) considered patterns of the distribution of soil organic matter. Fractal dimensions were also used in many other areas of soil chemistry, e.g., as a parameter to estimate cation exchange capacity (ERSAHIN et al., 2006; BAYAT et al., 2014), to evaluate mineral dissolution (GUARRACINO et al., 2013), nitrogen adsorption isotherms (PAZ FERREIRO; WILSON; VIDAL VÁZQUEZ, 2009), soil metal contamination (GERANIAN; MOKHTARI; COHEN, 2013), amongst others.

The field of soil physics is where the use of fractal analysis started, and, because of that, is the area with most vast use for such theory. It started in the analysis of soil particles distribution (ORFORD; WHALLEY, 1983), and have been widely used until today for the same purpose (TYLER; WHEATCRAFT, 1992; STANCHI et al, 2006, BIEGANOWSKI et al., 2013; PENG et al., 2014). In the analysis of the structure Turcotte's (1986) paper on soil fragmentation was a pioneer, while publications by Young and Crawford (1991), and Crawford, Sleeman and Young (1993), are the classical base for fractal modeling of aggregates size distribution. In the field of pore analysis its use was really expanded, especially considering the image analysis of soil pore systems. The first work considering the pore system was the one from Rieu; Sposito (1991), and was followed for more than 30 publications on the same subject, considering methodological problems and specific applications. There are several review papers about fractal under the structure scope. Ghanbarian-Alavijeh et al. (2011) reviewed the pore-solid-fractal approach; Perfect and Kay

(1995) the applications in soil and tillage researchs. All things considered, the fractal theory was, and still have been, well explored in soil science.

However, the fractal approach characterizes the mean properties of a dataset and cannot provide information on average behavior deviations of a power law (POSADAS et al., 2003). The multifractal analysis includes density variations and can be expressed in a multifractal spectrum (CHHABRA et al., 1989; CHHABRA; JENSEN, 1989), which integrates and quantifies the spatial properties of the studied object (POSADAS et al., 2003). The multifractal tool is much newer if compared to the fractal approach, especially applied to the soil science field. For example, during the literature review for this research, it was found 10 papers which used multifractal analysis for particle size distribution, 4 in the analysis of soil structure and 21 considering the pore system, being 5 about water retention modeling. The respective number of papers considering the fractal applications were 19, 46, 27 and 45.

Some parameters of the multifractal spectrum are well known and related to the heterogeneity of the porous system (POSADAS et al., 2003). However, due to its still incipient use in soil science, soil properties leading to a multifractal behavior are not established yet, which makes the interpretation of soil multifractal parameters an important subject of investigation.

2.1.2 Definition of soil physical quality – stability and functioning

The description of any system demands the creation of an ordered list of parameters with specific definitions that allows us to explain each step of the phenomena occurring in such system. Let us take as example the term “soil science”. Before knowing its significance, it is necessary to define separately what is “soil” and what is “science”. Soil (from Latin *solum*, Anglo-French *soy* and Middle-English *soile*, meaning “ground”) can be defined as a triphasic (consisting of air, liquids and solids) and tridimensional body that occupies the Earth’s surface. It is bordered by the atmosphere above, the lithosphere below and by water bodies laterally (i.e. lakes, rivers, seas and oceans) and beholds life. Its genesis arises from the interaction between a parental material with climate and organisms over time, being affected by the relief. Science (from Latin *scientia*, meaning "knowledge") is a systematic enterprise that builds and organizes knowledge in the form of testable explanations and predictions about the universe. Science is also associated with the scientific method itself, which the Oxford English Dictionary (2015) defines as "a method or procedure … consisting in systematic observation, measurement, and experiment, and the formulation, testing, and modification of hypotheses". Thus, “soil science” can now be defined as a systematic

organization of the knowledge achieved of the subject “soil” by experimentation. It is developed by the study of soil as a natural resource of the surface of the Earth, based on the description of its genesis, classification and mapping, using physical, chemical and biological attributes, and aiming to enhance its use, management and conservation.

Although very broad, we can follow the same premise to define “soil physical quality”. Is important to state that the aim of this work is not to create a global definition for this term, but the reader needs to understand our scope when referring to it during this text. A brief comment on the definition of soil structure is needed. As stated before, soil is triphasic. How the three phases interact forming different arrangements between solids and pores (i.e. the spaces not occupied by solids that can be filled up by liquid or air) is defined as “soil structure”.

“Soil quality” can be defined as “the ability of a soil to perform functions that are essential to people and the environment” (DORAN et al., 1994). Since soil structure affects water and air movement, influencing its ability to execute vital functions, and all of the above are physical processes occurring in soil, the term “soil physical quality” will be considered in this text as a measure of the ability that soil structure has to perform functions that are essential to mankind and the environment. Thus, a soil with good physical quality presents a soil matrix resistant to disaggregation, at the same time allowing life to exist. In other words, a soil with high physical quality must be resistant to erosion and exhibit a degree of organization that allows the development of flora and fauna.

All classical soil physical properties (texture, bulk density, aggregates shape and size) allow inferences about soil physical quality, because they all relate to the matrix arrangement. However, it is common to find that most publications on soil physical quality are associated to some physical index, in an attempt to resume several soil attributes into fewer variables. Such index may be linked to properties that command crop development, like compaction and resistance to penetration. Some examples are the aggregates tensile resistance (DEXTER; KROESBERGEN, 1985; MULLINS et al., 1992), relative bulk density (HÅKANSSON, 1990) and the least limiting water range (SEVERIANO et al., 2011). On the other hand, soil structural stability, which is a measure of how soil structure maintains its coherence over time, is also an important physical qualifier. In this case, clay dispersion (LEVY et al., 1993) and distinct measures of aggregates stability (Le BISSONNAIS, 1996) are widely used to produce indexes, since they show how soil behaves against erosion.

We can consider the soil functioning as the third pillar of soil physical quality. The term “function” relates to how the soil plays its role in the ecosystem. Then, its “functioning” is

any process that leads to this end. The main physical processes in soil are modeled via flux equations. These are used to model water (RAATS, 2001) and air (MOLDRUP et al., 2001) movement in soil. In that way, properties that represent these processes are also indicative of the degree of physical quality of a soil. Examples are the use of the classical water retention curve (DEXTER, 2004a, 2004b), the surface water infiltration rate (ZHOU; LIN; WHITE, 2008), the air permeability (BALL et al., 1997), hydraulic conductivity (PAGLIAI; VIGNOZZI; PELLEGRINI, 2004), amongst others. Some of these will be explored in this text.

2.1.3 Soil erosion: its mechanic and the "sealing" process

Soil erosion is a set of natural processes that changes a soil, diminishing its capability on exercising its function in the ecosystem. These processes cause physical, chemical and biological changes. They are marked by: the selective removal of particles, which changes the structure, interfering in the dynamics of fluids and heat; the decline in the content of organic matter and nutrients, causing decay in soil fertility; and, as a result, a reduction in the biota.

Human accelerated erosion is a major cause of cultivable soils depletion, making them unsuitable for exploitation. To change this feature, several soil conservation techniques are used to reduce erosion to a minimum rate. These techniques are the result of extensive research on the causes of erosion, which are explained by the mechanics of the erosion process, that relates the soil and the erosive agents.

2.1.3.1 Physical Erosion

It is common to divide erosion into physical, chemical and biological, according to its cause (LAL, 2001). The physical erosion is the process in which a natural agent causes the breakdown, transport and deposition of soil particles and aggregates (MORGAN, 2005). During this text we will only discuss this type of erosion and address it simply by "soil erosion".

The natural agents cited above are any force of nature capable of implementing sufficient energy to detach soil particles and aggregates, and move them, until they deposit at a location different from its origin. Wind and water are those agents, but they may be assisted by fire (SHAKESBY, 2011; GABET, 2014), since fire weakness the structure, and gravity as supporter agents (LAL, 2001). However, wind or water are still needed to detach and carry the soil to a lower gravitational reference (e.g. point closer to earth's center).

In the case of water, erosion may occur due to its performance in liquid form, through the action of rainfall, rivers and sea waves (LAL, 2001), or in solid form, due to expansive action of water during the condensation process, or to the melting that destabilizes the structure (ANDERSLAND; WIGGERT; DAVIES, 1996). In tropical regions, which represents a major area of Brazil, the main erosion agent is rainwater, since summer rainstorms are very common in such climate. The rainfall is primarily responsible for the erosion in places where the soil bares unprotected, due to tillage operations, and prone to crumbling.

2.1.3.1.1 Mechanics of erosion caused by rainfall

2.1.3.1.1.1 Rainfall erosivity and soil erodibility

Considering rainfall itself, several attributes interfere in its "erosivity", i.e. its capacity in causing erosion (WISCHMEIER; SMITH, 1960; SALLES; POESEN; GOVERS, 2000). We can summarize the main attributes as: the raindrop size (UIJLENHOET; STRICKER, 1999), pressure exerted over the soil (NEARING; PARKER, 1994) and velocity when reaching the target (GUO et al., 2013); the rainfall intensity (ASSOULINE; BEN-HUR, 2006) and amount (DALLA ROSA et al., 2012); and the composition of the rainwater (BORSELLI et al., 2001). Most studies on soil erosion process keep one or two of these attributes as variables, while maintaining all others constant. In studies with simulated rainfall, the raindrop size, velocity, pressure and angle of contact can be controlled by the devices sets. Then, is left to the researcher to decide on the intensity and amount to be used during experimentation.

Once rainfall impacts on soil surface, the erosion starts to be controlled by its intrinsic properties, such as: soil type and steepness, that are dependent on the parental material, regional climate and landform (WISCHMEIER; MANNERING, 1969); tillage and cover, factors that are controlled by man (i.e. land use) (DALLA ROSA et al., 2012). Once again, these are attributes that can be controlled or evaluated separately, to comprehend their relationship with erosion rates (VAN OOST; GOVERS; DESMET, 2000; LAL, 2001).

Rainfall erosion begins with the impact of raindrops over the soil surface (NEARING; BRADFORD; HOLTZ, 1987), continues through disintegration of clods and aggregates (Les BISSONNAIS, 1996), extends up to the runoff (NEARING; PARKER, 1994) and it ends with the sedimentation. Part of the sediments formed during the rainfall event are carried along with the water to the watercourses and are deposited in the lower parts of the relief (e.g. riparian zones). However, part of these particles and aggregates can also settle very close to

its origin, causing local changes in soil surface structure by forming a “seal”. Since the whole erosion process consists of these three main steps (particles and aggregates detachment, runoff and sedimentation) this will be further discussed.

2.1.3.1.1.2 Particles and aggregates detachment and transport

The detachment of the particles is the first stage of the erosion process and occurs mainly by three causes: the raindrop impact, which releases its kinetic energy on the soil surface, breaking aggregates and clods where the structure has weak points, and spreading particles around; slaking, due to rapid moistening, that increases aggregates internal pressure, causing micro-implosions that create ruptures that induce crumbing; and by water induced structure weakness, since water acts as a lubricant that allow structural sliding when soil is saturated (Les BISSONNAIS, 1996).

The second stage of erosion is the transport of aggregates and particles. It starts with the spreading caused by the impact of the raindrop, and continues when water starts to flow in surface, carrying sediments downhill (MORGAN, 2005). Water surface flow only happens if rainfall intensity exceeds soil hydraulic conductivity capacity (DARBOUX et al., 2001). To be transported, the sediment must be detached from the soil matrix (SHARMA, 1996), and the rate and distance is dependent on the energy of the water flux at surface (DARBOUX at al., 2001), which is dependent on the steepness (NEARING; PARKER, 1994) and roughness of the surface (DARBOUX; HUANG, 2005). During the superficial flux of particles, i.e. the runoff, more particles can be detached and transported, depending on the shear capacity of the flux and the shear resistance of the soil (HUANG; BRADFORD; LAFLEN, 1996).

If the water flow at surface is laminar, particles removal is of uniform thickness over the area, causing what is called as sheet or interrow erosion (DESCROIX et al., 2008). When the flux concentrates and the flow becomes turbulent, soil removal occurs by forming intermittent rills (MORGAN, 2005). If these evolve to become persistent and deeper, the so called gullies are formed. In the current specialized literature, these have been divided into ephemeral gullies and gullies according to their depth and width (CHESWORTH, 2008).

2.1.3.1.1.3 Particles and aggregates deposition – sealing and crust formation

The last step of the erosive process is the deposition of particles and aggregates that were detached from the soil matrix. The deposition happens according to the size and weight of sediments. The first particles and aggregates to deposit are those with low transportability, i.e. the heavier and wider ones (BERTONI; LOMBARDI NETO, 2005). The lightest

materials are the last ones to deposit, reaching larger distances from its origin. The runoff flow energy also influences the morphology and distribution of particles. Irregular depositions suggest erosive events with turbulent flow, while uniform deposits, with well-selected grain sizes, are an indicative of laminar flow (MOMOLI et al., 2007).

Sediments properties differ according to their origin and, many times, can be distinguished from local horizons by color, particles size distribution, organic carbon content, pH and exchange complex constitution (FULLEN et al., 1996). Local sediments are, in essence, of coarser fractions, since clay and silt can be transported through larger distances. The amount of clay and silt also increases in proportion to the slope, since the steeper slopes contribute to the acceleration of runoff, increasing the soil erodibility. Hence, parental material, relief and precipitation are the determinant factor influencing the size distribution of the sediments.

The deposition of particles and aggregates over the original soil surface forms a layer with different structure from the one underlying. The increase in thickness of this layer may change the surface bulk density, due to an decrease in the porosity, followed by an decrease in its hydraulic properties, fact why this layer is called a “soil seal”. When this layer of soil dries out, is common to occur an increase in the resistance to penetration, while its aspect becomes brittle and laminar, forming a so called “soil crust”. Although sometimes the terms soil crusting and soil sealing are considered as synonymous, soil sealing describes the wet process in which porosity decreases due to a rearrangement of structure, while soil crusting marks the increase in soil strength due to the drying of this rearranged structure (BERGSMA et al., 2000).

Considering the above, crusts can be separated into two types: structural and depositional. These two types give birth to different microstructure morphologies, and may occur successively, initiating with the sealing of the surface by an structural brokenness, followed by an depositional process of particles on its top. Structural crusts are formed by the reorganization of the soil surface due to a local displacement of fragments, i.e., clods and aggregates, without the sedimentation of particles. They are the result of gradual packaging and coalescence of small clods and aggregates, which are mainly produced by the breakdown of bigger aggregates due to an increased internal stress during wetting, i.e., slaking (NORTON; SCHROEDER; MOLDENHAUER, 1986). Depositional crusts are the result from the displacement of fragments and particles due selective decantation in puddles, formed during the runoff process, where the water slowly infiltrate into the soil (KOOISTRA; SIDERIUS, 1986).

2.1.4 Soil surface roughness *vs* soil physical quality

The behavior of the soil surface structure has an important role on air, water and nutrients dynamics. In tropical and subtropical regions it is common to have high intensity rainfall events during summer seasons, and rainfall erosivity can lead to greater problems on bare and/or tilled soil. The raindrop impact changes soil microtopography, which controls surface depressional water storage (BURWELL et al., 1963; HANSEN et al., 1999; BORSELLI; TORRI, 2010), drainage and runoff (SEGINER, 1969; ROMKENS et al., 2001), and even interferes on infiltration rates (BURWELL; LARSON, 1969; MAGUNDA et al., 1997; GUZHA, 2004). Therefore, the state of the soil microtopography is dependent on, and controls, soil erosion (MAGUNDA et al., 1997; DARBOUX et al., 2005; RODRÍGUEZ-CABALLERO et al., 2012).

Very often, the roughness of a surface is a measure of its state. Smith (2014) ratify that "surface roughness" generically defines any "…resulting parameter…that determines the minimum amount of information necessary to parameterize topographic complexity at a degraded scale in the most physically meaningful way". He also states that this is subjective and dependent on the objectives of a study. Therefore, in soil science, the surface roughness is considered as a parameter that represents the variability of a set of (z) heights inside an (x, y) area and can be used to interpret the morphology of the microtopography. Commonly, this parameterization separates roughness into two classes: the Oriented Roughness, governed by the slope and tillage marks, and the Random Roughness (RR), representing the distribution of soil clods and particles (ALLMARAS et al., 1966; CURRENCE; LOVELY, 1970; KAMPHORST et al., 2000). The latter one, a major percentage of total roughness, is the most relevant considering fluxes at surface, since it controls the dynamics of runoff and it is governed by soil intrinsic attributes (i.e. particles and clods size distribution, water dispersed clay and aggregates stability).

Consequently, several devices that collect data are used to estimate roughness parameters. The pin meter (BURWELL et al., 1963), the laser profilometer (CURRENCE; LOVELY, 1970) and the infrared microrelief meter (MRM) (CASTRO et al., 2006; CASTILHO et al., 2011) are examples of equipments used in field, that perform readings of (z) heights in square grids with a (x,y) resolution $\geq$ 1 mm. Other devices, generally used in the laboratory, case of Huang's laser scanner (HUANG et al., 1988) and the Multistripe Laser Triangulation (MLT) scanner (HIRMAS et al., 2016), reach finer horizontal resolutions, up to 0.5 mm. In addition, computed tomography allows the generation of even higher resolution images, as far as 0.02 mm (20 μm) by using standard X-ray computed tomography (XRT)

(ELLIOT; REYNOLDS; HECK, 2010) or even 0.001 mm (1 μm) using X-ray microtomography (μXRT) (ZHOU et al., 2013). Information on increasing scales stimulates the study of fragmentation processes caused by rainfall, because it allows mapping clods disruption by reaching scales close to the actual size of the soil's primary particles, which was only possible previously via mathematical and/or statistical modeling. Furthermore, the gathering of real physical data on different scales can help enhance models used to estimate more complex variables (i.e. drainage, runoff, soil loss).

Apart from the above, the roughness parameterization depends on distinct mathematical approaches as well. Allmaras et al. (1966) first used the standard error of log of heights, and Currence and Lovely (1970) showed the standard deviation of heights was enough if Oriented Roughness was corrected. Since these indexes only represent the vertical range of roughness, without considering the spatial component (KAMPHORST et al., 2000), several authors tried a geostatistical approach (VIDAL VÁSQUEZ et al., 2009; DALLA ROSA et al., 2012). However, the scale factor is also important and fractal models were also used in conjunction to spatial modeling (HUANG; BRADFORD, 1992; VIDAL VÁSQUEZ et al., 2005, 2010). Two facts restrain the use of fractal theory on roughness analysis: (1) it relies on a single number to describe the whole system; (2) although fractal indices may represent morphological responses to rainfall, they cannot be used to actually quantify fluids dynamics at the surface (KAMPHORST et al., 2000). In this sense, multifractal models excel. The multifractal approach consider several dimensions related to local occurrence of probabilities of a process, which merges the information of scale and spatial distribution, making it possible to generate indexes that may be used to model complex variables. This rising technique in soil science is still little explored in the evaluation of surface roughness (GARCÍA MORENO et al., 2008; SAN JOSÉ MARTÍNEZ et al., 2009; VIDAL VÁSQUEZ et al., 2010), but it is very promising in the generation of parameters that may express structural changes of the soil surface.

2.1.5 Soil structure image analysis

Micromorphometrical analysis consists on the evaluation of thin sections taken from soil blocks impregnated with polyester resin. This technique allows the study of the soil microstructure and to quantify the shape, size and soil pore connectivity using quantitative indexes related to pores and aggregate morphology (RINGROSE-VOASE, 1987; HORGAN, 1998; HOLDEN, 2001). Since the pore system morphology is related to water movement and the matrix arrangement is associated to pedogenic processes and biological activity (BOUMA

et al., 1977; RINGROSE-VOASE, 1987; PAGLIAI; DENOBILI, 1993) this technique has aided in the study of the soil structure (RINGROSE-VOASE; BULLOCK, 1984).

The selection and interpretation of soil pore morphological parameters still requires research (DROOGERS et al., 1998; HOLDEN, 2001) and, although this approach allows to systematically analyze a soil sample, it provides a partial result, since the analysis are made in two-dimensional soil sections.

The computed tomography scan is an alternative to the bidimensional problem. This is a relatively new technique in soil analysis, since X-rays were discovered only in the late nineteenth century by WC Roentgen (HECK, 2009). The X-rays attenuation index calculus obtained mathematical foundations only in 1963 by Cormack (CARVALHO, 2007) and initial works using this technique to study the soil emerged only in the 1980s. It was widely used in the study of soil porosity and hydraulic properties, initiating with innovative studies in the 1980s, related to soil bulk density (HAINSWORTH; AYLMORE, 1983), water movement in soil-plant system (PETROVIC et al., 1982) and soil moisture (CRESTANA, 1985). In the early 1990s, it was used aiming to understand the structure morphology and behavior, by macroporosity measurements (PHOGAT; AYLMORE, 1989; GREVERS et al., 1989; ANDERSON et al., 1990), biopores reconstruction (JOSCHKO et al., 1992, 1993) and effect of aggregate size on solute transportation (ANDERSON et al., 1992). In the late 1990s and early 2000s, the main use of this technique switched to understanding structure modifications in soils, such as due to cropping system (OLSEN; BØRRESEN, 1997), decomposition of organic waste (De GRYZE et al., 2006) and to wetting and drying cycles (PIRES et al., 2007).

Nevertheless, although the studies using CT brought a new approach to image analysis, there was not a distinguished language used to describe soil structural quality that implicated in a leap between these and classical techniques. And the calculation of indexes that are actually based on a tridimensional approach is still scarce, since much work has been done analyzing the bidimensional slices that form the reconstructed 3d image.

2.2 Material and methods

An experiment with simulated rainfall was assembled on a Fine Rhodic Kandiudalf (SOIL SURVEY STAFF, 2014), i.e., a Nitossolo Vermelho eutroférrico argiloso (EMBRAPA, 2013), located at 22º41’51.5” S and 47º37’53.2” W, at the “Luiz de Queiroz” College of Agriculture – University of Sao Paulo, in the city of Piracicaba, Sao Paulo, Brazil (Figure 3). Piracicaba is in an altitude of 554 meters, in a subtropical region of the state of Sao Paulo. Its climate is Cwa, according to the classification of Köppen-Geiger. Temperatures

through the year vary from a maximum of 310.65 K to a 289.15 K minimum. The annual average rainfall is 1230 millimeters, with typically three dry months during the year (June, July and August).

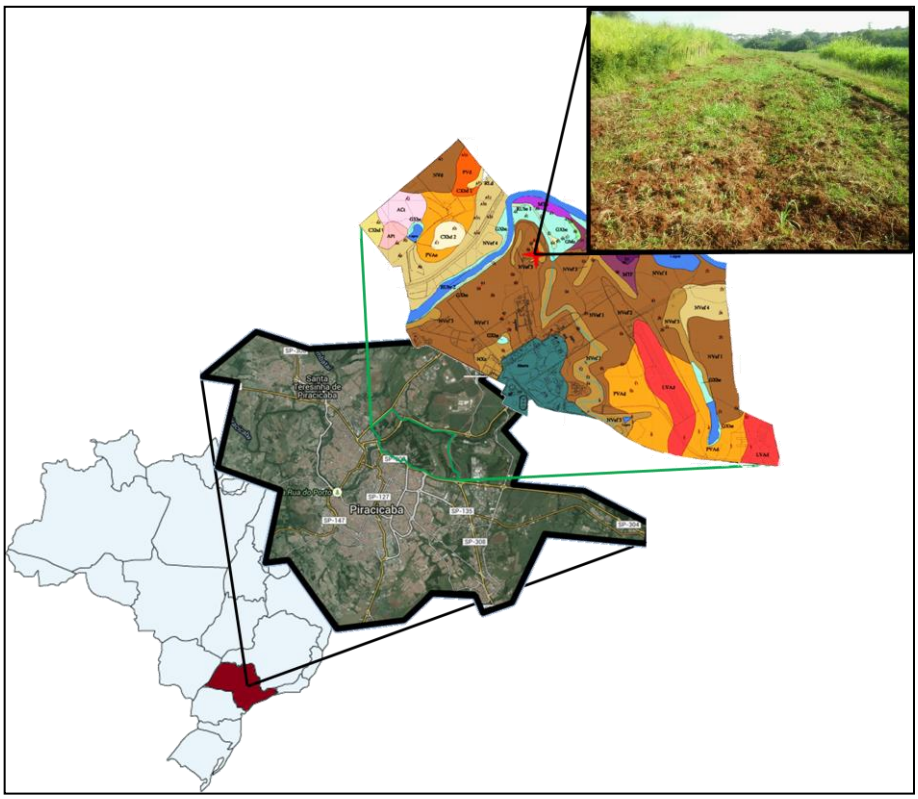

Figure 3 – Schematic showing the localization of a Fine Rhodic Kandiudalf (22º41'51.5" S; 47º37'53.2" W), at "Luiz de Queiroz" College of Agriculture, Piracicaba, Sao Paulo, Brazil, where an experiment with simulated rainfall was assembled with quadruplicate plots divided in four blocks, each one containing the treatments No-rainfall, 40, 80 and 120 mm of rainfall

The preparation of the soil, the sampling design and all measurements are described next.

2.2.2 Soil preparation and experimental design

Soil preparation was carried at the end of March 2014, by two disk harrowing (24 discs x 50.80 cm) operations: the first was for soil breakdown and disturbance of grass clumps, and the second, two weeks later, to simulate the conventional preparation of the seedbed. After the tillage operations, the soil was fully bare, presenting broken and partially decomposed straws of the previous crop (*Gossypium hirsutum* L.) and a distribution of different size clods. We removed tillage marks using a rake, in order to diminish its interference in the Oriented Roughness. Then, the area was fenced, to impede animal passage, and 16 plots (1 m^2) were established in a contour line following the elevation of the terrain. A gap of 0.5 m was left

between plots to avoid drifts from neighboring treatments. A random blocks design divided the contour line in 4 blocks wherein rainfall applications were randomized (Figure 4).

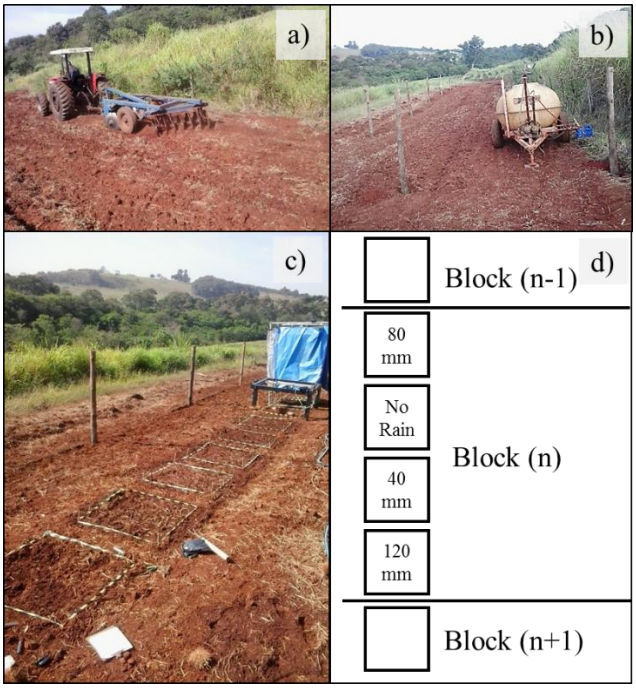

Figure 4 – (a) Picture of a Rhodic Kandiudalf after the second passage of a leveling harrow, (b) image showing how was the slope of the area and the localization of the water tank, and (c) leveled photo from the 1 m^2 plots, demarcated by a black/yellow tape and arranged in a line perpendicular to the slope. (d) The scheme of the experimental design in randomized blocks (d), showing how the blocks were divided along the line and an example of how the rainfall was randomized within each one of the four blocks.

After rainfall application (item 2.2.3), following a 24 h drying period, elevation data was collected from each plot with a laser microrelief meter (item 2.2.4). Six undisturbed samples were collected by plot: two soil blocks (12 x 12 x 5 cm) were scanned by a multistripe laser triangulation (MLT) scanner and a X-ray tomography (XRT) scanner, respectively, to obtain information about surface roughness (item 2.2.4); two cylinders (2.5 x 5 cm) were collected to measure the bulk density (item 2.2.5.2), and to model the water retention curve (item 2.2.5.3); two soil blocks (12 x 7 x 5 cm) were used in aggregate stability tests (item 2.2.5.2) and micromorphometrical analyses (item 2.2.6.1). One disturbed sample was collected by experimental block at the surface (0-5 cm), to characterize the soil particles distribution (item 2.2.5.2), pH and exchange complex composition (item 2.2.5.1) (Figure 5).

The particles size distribution and chemical composition of the exchange complex are summarized on Table 1 and Table 2. The blocks were homogeneous. However, during statistical procedures the block design was maintained due to other possible causes of variance (e.g. terrain slope, machinery passage, etc.).

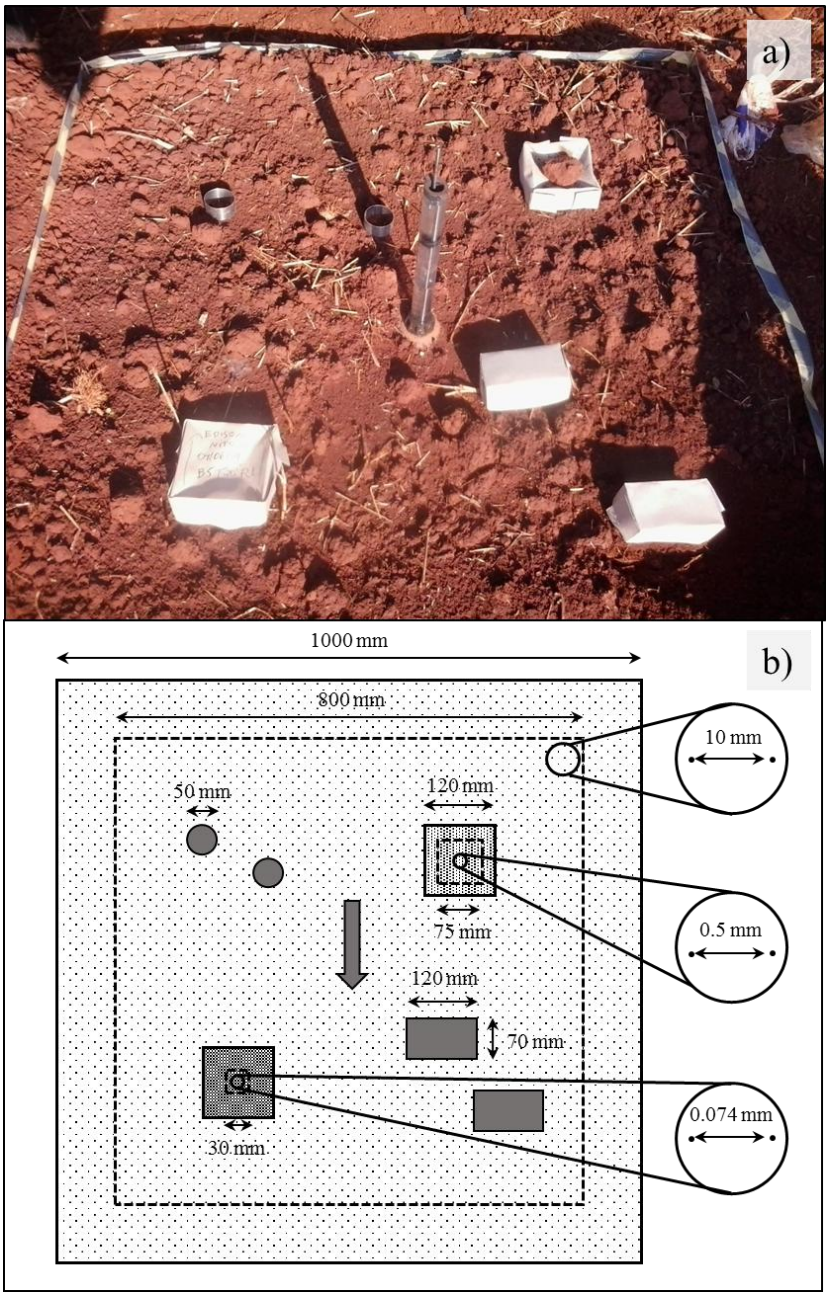

Figure 5 – (a) Disposition of the sampling inside each plot and (b) scheme with the measures of each sample: two cylinders with 50 mm in diameter, that were used for bulk density and water retention curve evaluations; two rectangular blocks (120 x 70 mm), that were used in micromorphometrical and aggregates stability analyses; and two square soil blocks (120 mm x 120 mm) that were used in roughness analyses. The dots represent the resolution of roughness measurements. A field microrelief meter was used to gather information of the whole 1 m^2 plot (10 mm resolution). For each square soil block there were different scales of measurement, using a multistripe laser scanner (right, 0.5 mm resolution) and a X-ray tomography scanner (left, 0.074 mm resolution). Solid lines represent the area of collected data, while dashed lines represent the cropped area used during analyses. The arrow in the middle indicate the position of the infiltrometer, used to measure unsaturated soil hydraulic conductivity

Table 1 – Values of pH, organic carbon content (OC) and particles size distribution of a Fine Rhodic Kandiudalf (22º41'51.5" S, 47º37'53.2" W) at surface (0-5 cm) after two disk harrowing operations

Block	pH			Clay	Silt	Sand	OC
	H_2O	$CaCl_2$	KCl	g kg^{-1}			
1	6.1	5.4	5.0	521	222	257	15.99
2	6.2	5.5	5.1	547	205	248	15.23
3	6.2	5.5	5.1	547	211	241	15.23
4	6.1	5.5	5.1	547	210	243	14.85

Table 2 – Chemical composition of the exchange complex of a Fine Rhodic Kandiudalf (22º41'51.5" S, 47º37'53.2" W) at surface (0-5 cm) after two disk harrowing operations

Block	P	K	Ca	Mg	Al	H+Al	SB	CEC	V	M
	mg Kg^{-1}	$mmol_c$ kg^{-1}							%	
1	0.198	10.61	52.91	23.00	0.00	0.60	86.52	87.12	99.31	0.00
2	0.148	10.87	54.56	22.54	0.00	11.60	87.97	99.57	88.35	0.00
3	0.119	9.08	55.11	23.36	0.00	9.00	87.55	96.55	90.68	0.00
4	0.122	12.02	52.58	23.81	0.20	18.00	88.42	106.42	83.09	0.23

P:phosphorus; K: potassium; Ca: calcium; Mg: magnesium; Al: exchangeable aluminum; H+Al: hydrogen and aluminum (soil potential acidity); SB: sum of bases; V: base saturation; m: aluminum saturation

2.2.3 Rainfall simulation

Rainfall was applied at an intensity of 120 mm h^{-1} in the quadruplicate plots at amounts of 40, 80, and 120 mm, plus a control treatment with no-rainfall. The simulator operates at a height of 2.4 m above the soil and consists of a oscillating spray nozzle (VeeJet Nozzle, H/U-80100, Spraying Systems, Co.) connected to a system that maintain a pendulum movement to simulate rainfall in a total area of $1m^2$. The entire system is supported by metal pipes that brings lightness and firmness at the same time. To avoid the effects of drift a plastic cover was placed around the equipment (Figure 6a).

The rainfall intensity was chosen based on regional climate characteristics and soil structural features. For example, Hudson (1965) stated that rainfall intensities over 25 mm h^{-1} are erosive for most tropical and subtropical soils. However, soil erosion is a combination between rainfall erosivity and soil erodibility, which depends on intrinsic properties of soil, such as structural stability. Castilho et al. (2011), studying the same soil of this research (Rhodic Kandiudalf), found undisrupted clods even after 10 natural rainfalls with intensities higher than 25 mm h^{-1}. Magunda et al. (1997), in a similar soil (Mollic Kandiudalf), found minimal changes on soil surface roughness after 126 mm of simulated rainfall with an intensity of 63 mm h^{-1}. These are evidences that such soils possess a highly stable structure.

Considering that, to fully understand this soil disruption behavior due to cumulative rainfall, higher intensities must be used during simulation tests, so that a wider range of structural changes may be captured.

2.2.4 Soil surface roughness measurements

The evolution of the surface roughness was evaluated in three scales of measurement. In the field, a portable field microrelief meter (MRM) was used, coupled with an infrared sensor (GP2Y0A21YK0F, SHARP Corporation) with ±0.05 mm resolution, and making readings on a fixed grid (10 x 10 mm), totaling 10,201 points per plot (Figure 6a). In the laboratory two finer scales were obtained from soil blocks. One block from each plot was scanned by a multistripe laser triangulation (MLT) scanner (NextEngine, Inc.), creating a random mesh averaging 60,000 points (resolution of 0.5 mm) (Figure 6c). A second block from each plot was scanned using an X-ray tomography (XRT) scanner model XT H 225st, third generation, with a total of 1918x1534 detectors (Figure 6b). To reduce artifacts and image noise a high passage filter was used. The acquisition voxel size was of 74.5 x 74.5 x 74.5 µm. This process results in average of 3018 two-dimensional projection images that are reconstructed to portray a three-dimensional soil structure. The final image was reconstructed using maximum resolution, and the process was filtered by back projection, using CT PR O 3D and VGSTUDIO.

To minimize influences of artifacts and disturbances on samples edge, only a central area from each resulting mesh was analyzed, cropping areas of 800 x 800 mm, 75 x 75 mm and 30 x 30 mm for MRM, MLT and XRT, respectively.

2.2.5 Soil attributes

2.2.5.1 Chemical analyses

The determinations of pH in water, $CaCl_2$ 0.01 mol L^{-1}, KCl 1 mol L^{-1}, and of the content of exchangeable aluminum (Al), potassium (K), phosphorus (P), calcium (Ca) and magnesium (Mg) were performed according to Raij et al. (2001). The Walkey-Black method was used for the determination of the organic carbon content (OC), as described in Anderson and Ingram (1992). All soil samples were air dried and sieved (< 2 mm) prior to each analysis.

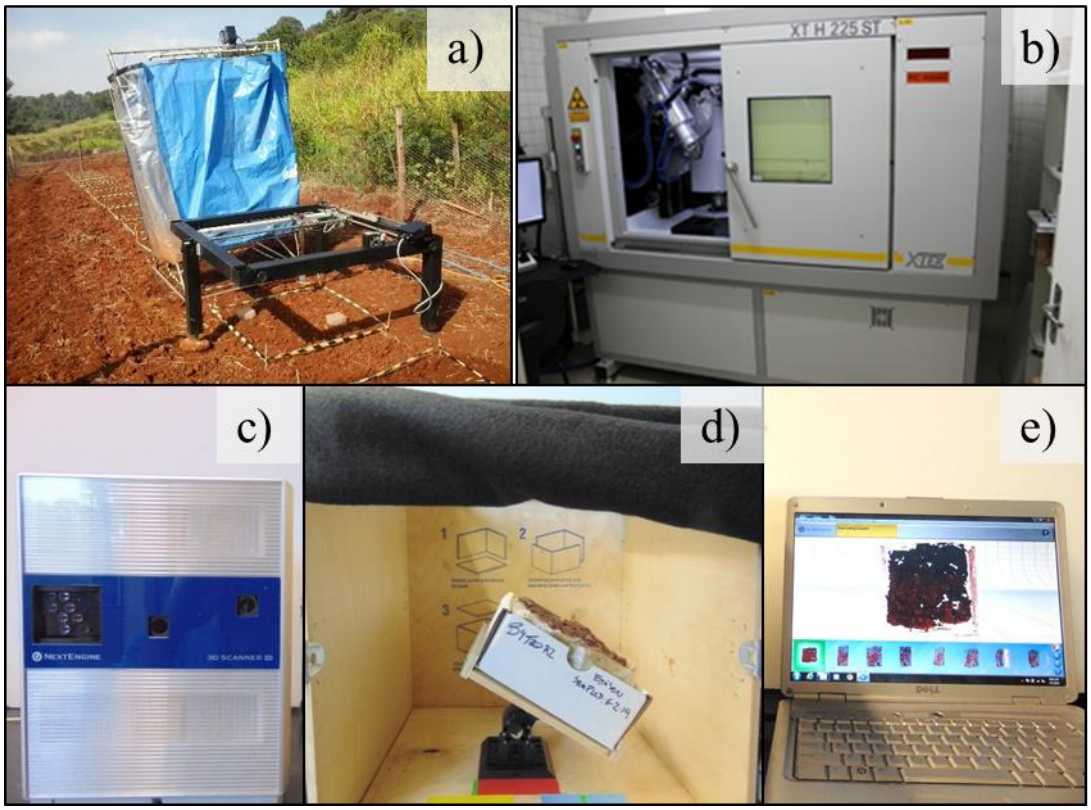

Figure 6 – (a) Rainfall simulator (with a blue cape) and field microrelief meter (MRM) sensor (black device); (b) X-ray tomography (XRT) third generation scanner, with a total of 1918x1534 detectors (c) multistripe laser triangulation (MLT) scanner; (d) soil block (120 x 120 mm) aligned at 150º and ready to be scanned by the MLT scanner; (e) example of a reconstructed image using the MLT accompanying software

2.2.5.2 Physical analyses

The bulk density (*BD*) (Mg m^{-3}) was determined using the cylinder method according to Grossman and Reinsch (2002). Cylinders (2.5 x 2.5 cm) were collected in quadruplicates by rainfall amount. The particle size distribution was determined by the hydrometer method (GEE; OR, 2002), using 40 g of sieved disturbed samples (< 2 mm) after air dried. The number of replicates was the same as for the cylinder method used for BD. The particles density (*PD*) (Mg m^{-3}) was determined from the same disturbed samples (< 2 mm) using a Helium pycnometer (AccuPyc 1330, Micromeritics Instrument Corporation ®). The ratio of volume of pores (P_r) (m^3 m^{-3}) was calculated from *BD* and *PD* (Equation 28), indicating the relative amount of voids of the soil (VOMOCIL, 1965).

$$P_r\ (m^3 m^{-3}) = 1 - \left(\frac{BD}{PD}\right) \quad (28)$$

An aggregates stability test was conducted according to Le Bissonnais (1996) using blocks of soil (12 x 7 x 5 cm) collected in quadruplicates according to rainfall amount. The surface of each block (0-10 mm) was ripped off, from which, aggregates were manually

broken and normalized to a diameter between 4 and 2 mm. The 10 mm layer was chosen in an attempt to boost the chances of detecting the changes caused by sealing. After, pre-treatments were applied in triplicates of 5 g of normalized aggregates, dried at 313,15 K for 24 h. The pre-treatments were: slow wetting, where dry aggregates were placed in a filter paper over a saturated sponge and slowly moistened by capillary forces; fast wetting, where dry aggregates were submerged directly into water; and mechanical breakdown, when dry aggregates were previously moistened with alcohol and shaken, while submerged in water, with controlled energy. After each pre-treatment, the aggregates were immersed in alcohol and sieved (0.053 mm), with the retained soil once again dried (313,15 K for 24 h). These dry aggregates were then passed through a set of six sieves (2, 1, 0.5, 0.106 and 0.053 mm), generating an aggregates size distribution, which was consequently used to calculate the weighted mean diameter (WMD) (Equation 29).

$$\text{WMD}\ (mm) = \sum_{i=1}^{n} d_i \frac{m_i}{m_t} \tag{29}$$

WMD considers the equivalent diameter of aggregates (d_i), which is the average diameter between a subsequent set of sieves (e.g. between sieves 2 mm and 1 mm d_i = 1.5 mm), having the relative mass of aggregates ($\frac{m_i}{m_t}$) as weights. m_t is the total mass of aggregates (5 g) and m_i is the mass of aggregates retained at each sieve *i*.

2.2.5.3 Hydrological analyses

Soil water retention curve (SWRC): The SWRC is the correlation between the gravimetric water content (θ) and the matric potential in the soil (Φ_m). Undisturbed soil samples were collected in cylinders (2.5 x 2.5 cm). Using a nylon string, each cylinder was subdivided into three parts (top, middle and bottom) while maintaining the original structure. The subsamples were relocated to smaller cylinders (2.5 x 0.8 cm). Since there were quadruplicate samples for each rainfall amount, it totaled 48 subsamples. Curves were generated using these subsamples in pressure plates for potentials of -0.001; -0.003; -0.006; -0.008; -0.010; -0.033 -0.070 MPa and -0.100, and disturbed samples (< 2 mm) in high pressure plates for potentials of -0.300, -0.500 and 1.5 MPa. The curves were fitted using the empirical model proposed by van Genuchten (1980), which parameters are the soil water contents at saturation θ_s and residual θ_r, plus the empirical parameters *n* and α (Equation 30). Changes in the inclination of the curves were evaluated using parameters *n* and α.

$$\theta = \theta_r + \frac{(\theta_s - \theta_r)}{[1 + (\alpha h)^n]^{(1-1/n)}} \quad (30)$$

Soil hydraulic conductivity [K(θ)]: The hydraulic conductivity of the unsaturated soil was calculated by measurements with a mini disk infiltrometer (Mini Disk Infiltrometer, Decagon Devices) at four potentials (-1.5, -3.0, -4.5 and -6 cm) (Figure 5). To calculate the unsaturated hydraulic conductivity, the method by Zhang (1997) was used.

2.2.6 Image analyses

2.2.6.1 Micromorphometrical analyses

Undisturbed soil samples, oriented to the surface and collected in cardboard boxes (0.12 x 0.07 x 0.05 m), were impregnated using a polyester resin (MURPHY, 1986), styrene monomer (CASTRO et al., 2003), a catalyzer (RINGROSE-VOASE, 1991) and a fluorescent pigment (MURPHY et al., 1977). The impregnation procedure and image acquisition was done as described by Castro et al. (2003).

In the laboratory, the samples were air dried for 10 days and at 313.15 K with forced air circulation for 48 hours. These samples were put in containers and placed in a desiccator connected to a vacuum pump, which helps the solution to penetrate the pores. The impregnation was held by a solution of polyester resin and styrene monomer (1/1), using a hardening solute (Butanox M50, 10 drops L^{-1} of solution) and a fluorescent colorant (Tinopal OB, Ciba-Geigy®, 5 g L^{-1} of solution). After drying, the samples were sliced in blocks and polished. Image (1024x768 pixels) acquisition using a digital color camera (Sony DFW-X700) in 10X magnification (156.25 μm^2 pixel^{-1}) was made using a charged couple device (CCD) system, connected to a magnifying glass with a polarizer (Zeiss).

Each block was divided into three layers (0 to 10 mm, 20 to 30 mm and 40 to 50 mm), parallel to surface, and five images were taken from each layer. After taking the pictures, images analyses, using software ImageJ, followed the steps showed in Figure 7: each RGB image (24 bits) was converted to 8 bits (256 gray-levels); since most images showed artifacts related to illumination, with central pixels presenting higher values than those from the edge, a filter was applied around the image to smooth the values around the image center; after this correction, plugin “CTofsoil” was used to select areas of low variance in an attempt to smooth the histogram and facilitate the segmentation process; an average histogram was calculated for all blocks and used to choose the threshold between pores and solids; after segmentation, pores with equivalent diameter less than 50 μm (≤13 pixels) were excluded prior to any calculations. Then, three representative images, from each layer, were used in further analysis.

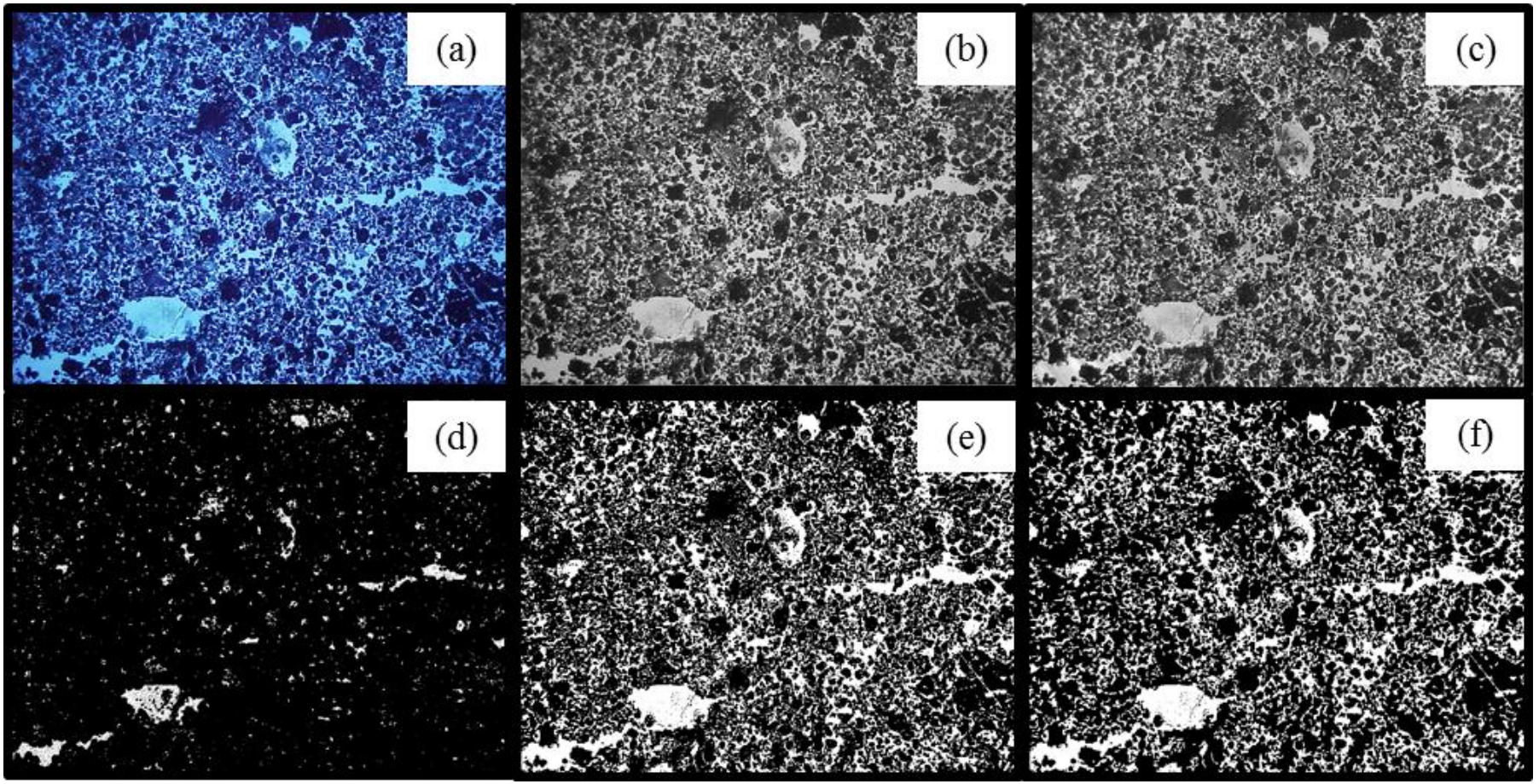

Figure 7 – Example from steps of the binarization of a bidimensional image. (a) RGB image taken using a digital color camera (Sony DFW-X700) in 10X magnification; (b) image transformed to a unique 8 bit channel of 256 grey-level colors; (c) 8 bit image after correcting the illumination distribution; (d) 8 bit image where areas with low variance (grey) were demarked to calculate a histogram; (e) binary image with white pores (255) and black matrix (0); (f) binary image after deleting pores with diameter less than 50 µm (<13 pixels)

The total area of pores (%) was estimated by the ratio between the number of pixels representing the pore system and the total number of pixels of the image (MORAN et al. 1988). The classification of pores by shape and size was executed using software Soil Pore Image Analysis - SPIA (COOPER et al., 2016).

2.2.6.2 Soil surface roughness analyses

Both MRM and MLT generate (*x*, *y*, *z*) data frames to create Digital Elevation Models (DEM). These were rasterized into matrices, whose rows and columns dimensions represents (*x*, *y*) coordinates and cell values are (*z*) heights, which were interpreted as grey-level images, having the cells as pixels and the heights as bit depth. For XRT three-dimensional binary images, the surface was estimated by adding the number of (*z*) axe voxels, at each (*x*, *y*) position, from the first bidimensional slice of the surface (pure air) until the first one representing the solid phase. Then, by subtracting the total number of slices and multiplying the resulting two-dimensional image by the scan's resolution (0.0745 mm) we obtained a representation of the surface of the soil.

Once we gathered the images from all scales, general trends of terrain slope (Oriented Roughness) were removed by linear regressions, and all calculations were made using the absolute value of the models deviations. Data were rearranged to present a minimum height of 1 mm. Since MLT scanner measures the distortion patterns of lasers over an object (HIRMAS et al., 2016), places where light is lost (cracks) creates gaps in the DEM. These gaps were not considered in descriptive statistics and interpreted as zero (0) during multifractal calculations, which interferes in some spectra features that will be explained next.

There are several roughness indexes that have been used in rainfall simulation studies (BERTUZZI et al., 1990). However, the facility of calculation and the good correlation with rainfall (ELTZ; NORTON, 1997), as to other important variables (KAMPHORST et al., 2000; GARCÍA MORENO et al., 2008), makes the random roughness index RR_i a suitable index to be used on describing soil roughness behavior across rainfall increase, reason to why it was used as an standard measure in this study (Equation 31). It is the standard deviation of k heights h_i within a plot with average height $\bar{h}$ (KAMPHORST et al., 2000).

$$RR_i = \left[\frac{1}{k}\sum_{i=1}^{k}(h_i - \bar{h})^2\right]^{1/2} \quad (31)$$

2.2.6.3 Multifractal analysis

For all images the multifractal spectrum f(α) was calculated using the partition function $\mu_i(q, L)$ (Equation 22) and a box-counting technique. By covering an image with boxes of different sizes L and applying Equation 23 for a range of q values ($q \in R$) is possible to calculate $\alpha(q)$ and $f(q)$ (Equations 24 and 25). In this method, a grid of boxes of size L covers the image and the number of boxes that contain at least one pixel representing the object of study is counted (POSADAS et al., 2003).

Multifractal spectra from the 2d images and the maps were calculated according to Posadas et al. (2003) with the software Multifractal Analysis System 3.0 (http://inrm.cip.cgiar.org/home/downmod.htm; accessed on 27 June 2015). For the calculations using the 3d images an ImageJ plugin was used. For each image, maximum and minimum q values were selected when f(q) and α(q) were linear functions ($R^2 \geq 0.98$). Values of q were estimated using a Δq of 0.1 to create a more detailed spectrum.

As shown in Figures 1 and 2 the $f(\alpha)$ spectra presents a convex parabolic shape, from where several parameters are known or can be estimated. The parameters evaluated during this research were: *D0*, *D1*, *D2*, *D0-D1*, *D0-D2*, *D1-D2*, $Lf(\alpha)_{min}$, $\Delta Lf(\alpha)$, $Rf(\alpha)_{min}$,, $\Delta Rf(\alpha)$, α_{min},, α_{max}, $\Delta L\alpha$, $\Delta R\alpha$, $\Delta\alpha$, $f(\alpha)_{\text{ratio}}$ and α_{ratio}.

It was discussed that *D0* is a fractional dimension of the mass contained in a fragmented system, i.e. one that possesses parts with and without mass. For example, if someone wants to analyze the pore system of a soil, the pore phase is considered as the one containing the mass of the system, while the solids are considered weightless during the analyses. When all points have mass, *D0* is equal to the object's topological dimension. Since roughness analyses consider a surface, *D0* should be equal to 2 for all plots. However, the MLT data, as explained in item XXX, present gaps, and *D0* was not exactly 2 for this dataset. Nevertheless, how *D0* relates to other dimensions is less affected by the gaps if the covered area (i.e. the area containing mass) is prevalent, since points with mass have major influence over spectrum format, especially considering its left side. All MLT images presented 90% or more of covered area, thus this feature was not considered as a problem.

Although previous information from each parameter was presented on section 2.1.1.3.3, specific interpretations are presented here. $Lf(\alpha)_{min}$ can be interpreted as the fractal dimension of micro-watersheds in roughness analyses, or large macropores in pore system analyses. $\Delta Lf(\alpha)$ represents the homogeneity of the fragmentation at these areas, and values closer to 0 may show a unifractal process, or one dominated by micro-valleys and smaller macropores. Similar interpretations can be made at the right side for $Rf(\alpha)_{min}$ and $\Delta Rf(\alpha)$. α shows how the

same range of heights, or pores sizes, change across scales. Thus, α_{min} shows how the distribution of the highest micro-watersheds, or larger macropores, changes over scale, and α_{max} how it happens for the lowest micro-valleys and smaller macropores. $\Delta L\alpha$ and $\Delta R\alpha$ indicate which class of heights and macropores changes more over scale when compared to the systems' mean. $\Delta\alpha$ represents diversity across scales, i.e. how differentiated it is its roughness or porosity. $f(\alpha)_{\text{ratio}}$ and α_{ratio} shows the ratio between micro-valleys and micro-watersheds, or between large and small macropores, and it is an indicative of which class is more fragmented or changes more across scales.

2.2.7 Statistical analyses

In the case of soil roughness, since the datasets were large (e.g. the smallest grid had more than 6,000 points), initial evaluation was made by descriptive statistics (maximum, minimum, mean, median, mode, variance, skewness and kurtosis) of each heights and exploratory analysis using histograms. Although all calculations were carried out with original height values, histograms present a logarithmic abscissa, for better visual interpretations. In the case of the aggregates stability an exploratory analysis was made using the plot of the distribution of masses of aggregates according the equivalent diameters. These variables were important to characterize the behavior of soil surface according to rainfall amount before interpreting the multifractal parameters. For bulk density, ratio volume of pores, aggregates size distribution, random roughness index, unsaturated soil hydraulic conductivity, image pores distribution and all multifractal parameters, direct measures of differences between means were used in interpretations.

An Anova with randomized blocks was applied to all variables and each multifractal parameter, and significant differences ($p < 0.10$) were considered in further analyses. In the analysis of the soil surface roughness, the scale of measurement was used as an additional factor to rainfall amount as a cause of variance. For images pore analysis and water retention curves depth was the additional factor, since the impregnated blocks and the cylinders were divided in three layers before each analysis.

Before comparing means, we checked the homogeneity of variances amongst treatments using Levene's test. In case of homoscedasticity, Tukey-Kramer Honest Significance Distance (Tukey HSD) was used, as for heteroscedasticity, Dunnett's modified Tukey-Kramer (DTK) pairwise multiple comparison was used instead. When differences in means across rainfall amounts were significant ($p < 0.10$) and a linear pattern was observed, linear regressions were used to explain behavior across rainfall. The coefficient of determination

(R^2) was used to check the models explained variance, and the significance of the angular coefficient (slope) was used for comparisons and interpretations.

All tests and regressions were made using R-project software (R CORE TEAM, 2015). Homogeneity test used functions of package "car" (FOX; WEISBERG, 2011), and mean tests from packages "agricolae" and "DTK" (LAU, 2013; MENDIBURU, 2015).

2.3 Results and discussion

2.3.1 Soil surface roughness

In an initial glance over samples' DEMs on each scale, we notice that physical changes happens on all scales with rainfall application, considering the opposite treatments of no-rainfall and 120 mm (

Figure *8*). Even in a coarser scale (MRM), there is a smoothing after rainfall, with a diminishing appearance of peaks and a spreading of the valley over the area. The persistent peaks represent very stable clods that do not disrupt even after 120 mm of rainfall. In higher scales there is a more pronounced flattening. This happens mainly because sample size is smaller and covers an area smaller than the average size clod. Thus, on such scales, disruption of very small clods (MLT) and particles spreading (XRT) are expected to be the dominant processes. This may be seen in the flatter and smother image from MLT after rainfall, indicating general dismantlement of clods, and flatter, but more rugged, image from XRT, indicating the presence of small particles covering the surface.

Looking on descriptive statistical parameters of heights response to rainfall increase, we note, a general negative linear behavior for the variance of MRM, while its maximum, mean, median and mode, and all variables (less skewness and kurtosis) of MLT and XRT, present a negative quadratic behavior, with maxima around 80 mm (MRM) and 40 mm (MLT and XRT) of rainfall (Table 3). The negative linear behavior of variance was expected, since it is reasonable to think that when rainfall increases, more clods disrupt, and heights tend to diminish, as well as its variability. The initial increase of these parameters on MLT and XRT show that, at the beginning of the disruption process, the surface becomes more complex, i.e. rougher. It is easy to imagine that, at the beginning of the rainfall event, some clods disrupt more easily than others, and that not all pulverize entirely, instead they break into increasingly smaller clods. This increases heterogeneity of heights, especially in areas closer to more stable clods. As stated before, MRM gathers information of larger features, showing how average size clods behave with rainfall increase. In this case, a linear decrease of heights is expected,

because it represents the average behavior of the system, which is a general flattening. However, at a larger scale, where the small clods are responsible for the aspect of the roughness, anything that increases the quantity of this type of clods will favor the increase of height differences.

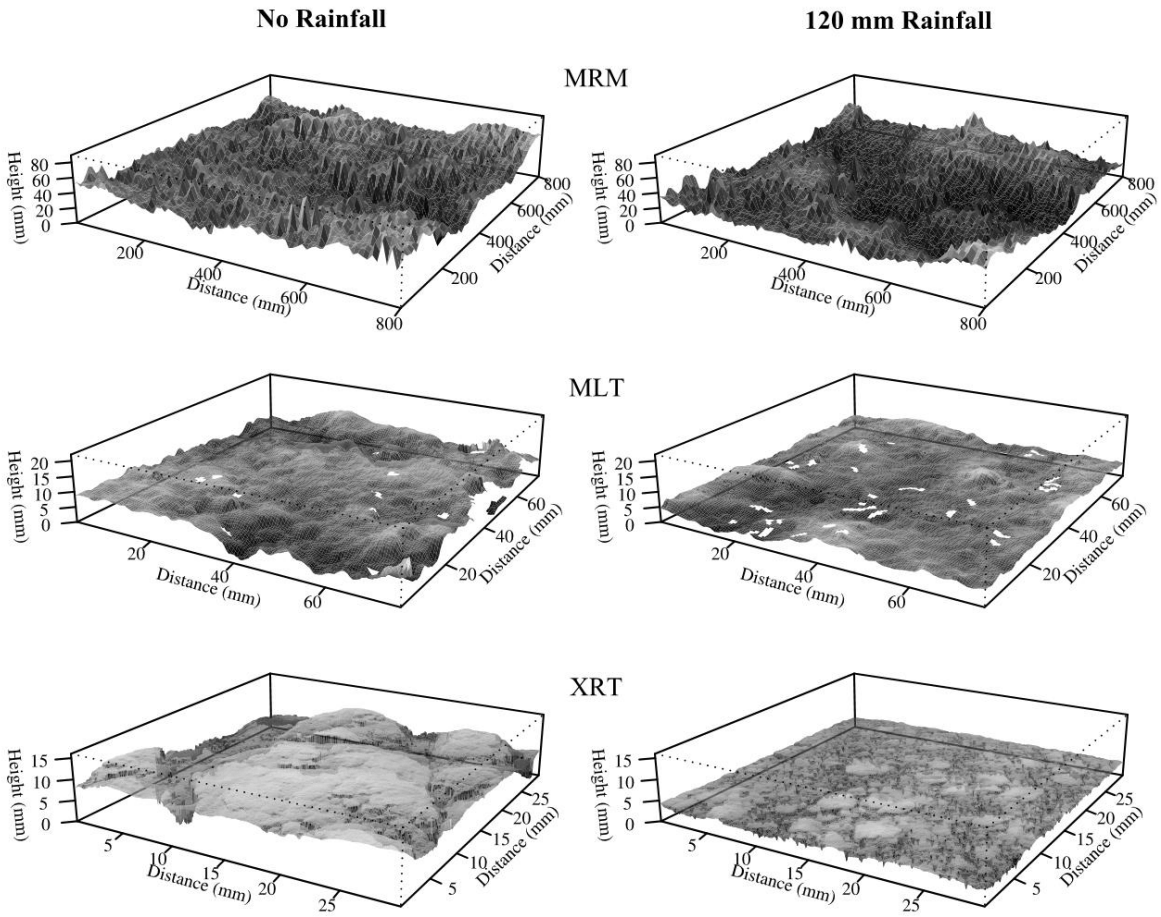

Figure 8 – Digital elevation models from the surface of a fine Rhodic Kandiudalf, before (No rainfall) and after rainfall simulation (120 mm), obtained in three scales, by: a field microrelief meter sensor (MRM, 10 – 800 mm); a multistripe laser triangulation scanner (MLT, 0.5 – 50 mm); and an X-ray tomographer (XRT, 0.0745 - 30 mm)

The mean, the median and the mode represent the central tendency, which means that an increase in these variables is not always accompanied by an increase in variance, but can show that the distribution has shifted right. MRM skewness at 80 mm shows a light skewness left (-0.04), which may represent such displacement. However, since the variance reduces, the increase of these variables just means that during clod breakdown micro-valleys are filled faster than peaks are destroyed. In summary, proximity between means, medians and modes

within rainfall amount, plus skewness and kurtosis data, show that heights behave very close to normal [$P \sim N(\mu, \sigma^2)$] in all scales. Along scales, proportion seems to be the basic difference,

Table 3 – Descriptive statistics from surface elevation measurements on a fine Rhodic Kandiudalf, before (No rainfall) and after rainfall simulations (40, 80 and 120 mm), obtained in three scales, by: a field microrelief meter sensor (MRM, 10 – 800 mm); a multistripe laser triangulation scanner (MLT, 0.5 – 50 mm); and an X-ray tomographer (XRT, 0.0745 - 30 mm)

	MRM				**MLT**				**XRT**			
Rainfall (mm)	**No Rainfall**	**40 mm**	**80 mm**	**120 mm**	**No Rainfall**	**40 mm**	**80 mm**	**120 mm**	**No Rainfall**	**40 mm**	**80 mm**	**120 mm**
						(mm)						
Maximum	64.38	67.67	67.34	59.68	14.26	18.12	11.48	10.27	12.74	14.53	7.90	6.62
Mean	29.73	27.04	33.44	23.60	8.08	9.93	6.00	5.78	8.45	9.06	4.79	4.47
Median	29.51	26.35	33.45	23.22	8.14	9.76	5.93	5.80	8.55	8.90	4.70	4.40
Mode	29.10	25.44	33.15	24.70	8.27	9.65	5.92	5.70	8.55	8.33	4.68	4.33
						(mm²)						
Variance	73.52	72.38	67.49	64.72	4.95	5.47	2.32	2.13	3.91	5.57	1.23	0.69
						(dimensionless)						
Skewness	0.25	0.42	-0.04	0.44	-0.10	0.55	0.44	-0.04	-0.15	0.19	0.20	0.09
Kurtosis	0.47	0.33	0.61	0.40	-0.38	2.45	0.64	0.37	-0.25	0.32	-0.16	-0.26

Obs: the minimum height for all rainfall amounts and scales was rearranged to 1 mm.

since MRM, MLT and XRT ranged to a Maximum of 64.38, 14.26 and 12.74 mm before rainfall simulation, and 59.68, 10.27 and 6.62 mm after the last application, respectively.

We matched these observations with histograms (Figure 9). When rainfall has not occurred yet, both MLT and XRT show very similar distributions. MRM has a larger distribution of heights. More or less, all distributions could be extrapolated to a normal after 80 mm of rainfall. However, at 40 mm, MLT and XRT present a bimodal distribution. This agrees with the initial increment in variance after the first rainfall, since, as explained before, soon after rainfall, the heterogeneity is enhanced, and different classes of clods size are created in a short space of time during disruption process. This contributes to the appearance of peaks that represent each new clod size class that dominate the surface. Nevertheless, considering all other rainfall amounts and scales, there is nothing that extrapolates to much normality. Allmaras et al. (1966) recommended the logarithm transformation of heights, but Currance and Lovely (1970), and Kamphorst et al. (2000), also stated that most heights distributions behave as normal. Considering all histograms, and skewness and kurtosis values, no transformations were used to normalize the dataset.

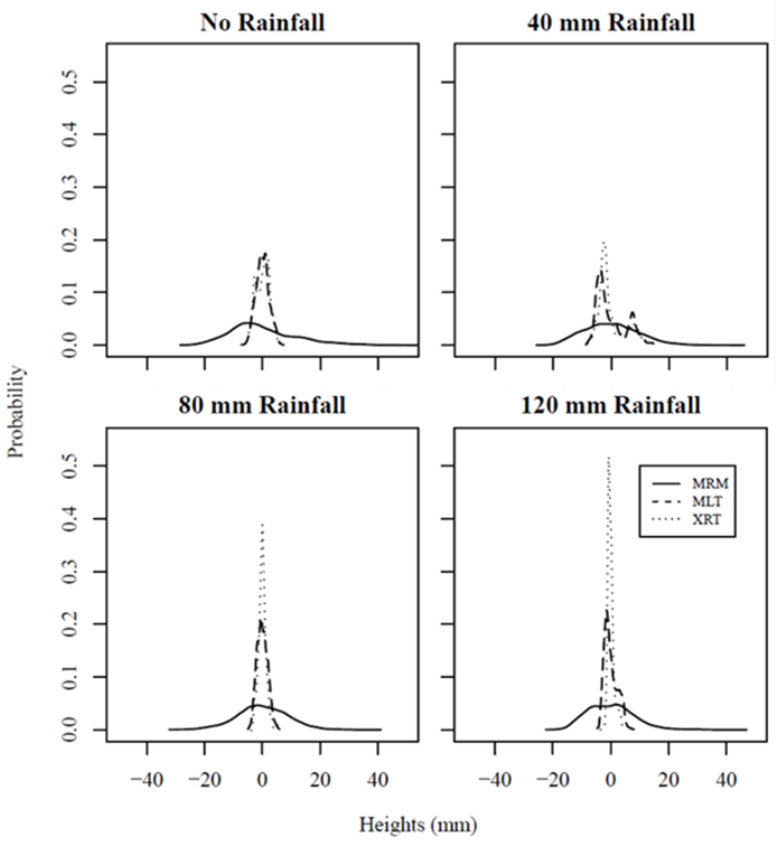

Figure 9 – Histograms from surface elevation measurements on a fine Rhodic Kandiudalf, before (No rainfall) and after rainfall simulations (40, 80 and 120 mm), obtained in three scales, by: a field microrelief meter sensor (MRM, 10 – 800 mm); a multistripe laser triangulation scanner (MLT, 0.5 – 50 mm); and an X-ray tomography scanner (XRT, 0.0745 - 30 mm)

Rainfall increase appears to concentrate distributions over all scales, with more markedly features on MLT and XRT, where we see more narrow and peaked distributions after 120 mm of rainfall. XRT becomes very narrow at 120 mm, when its central value represents more than 50% of the distribution. At the same rainfall amount, MRM have bigger tails on both sides and presents more subtle changes, concentrating on a uniform distribution between 15 and 25 mm. Increasing rainfall augment the possibility of clods disruption, which is expected to homogenize heights, which would cause the narrowing of the histograms. Differences in scales are basically related to range. While MLT and XRT present very similar histograms: on first two rainfall amounts both are centered around 8 mm, and after 120 mm present distinct narrowing degrees; MRM is always centered above 20 mm. Thus, different parametrization is expected for each scale.

2.3.1.1 Random Roughness - RR_i

In

Table 4 we find the average from all variables (RR_i and multifractal parameters) of each factor (rainfall and scale). The Anova showed that *RRi* had differences ($p < 0.10$) among scales within all rainfall amounts, and among rainfalls only for MLT and XRT. After testing pairwise means, differences among rainfalls presented no significance ($p > 0.10$), while MRM was considered significantly different from MLT and XRT. The difference in range was enough to differentiate scales; however, the subtle narrowing of distributions was not expressed by RR_i. Magunda et al. (1997) also found, in a Mollic Kandiudalf with similar particles size distribution and carbon content as the soil of this study, only 5% reduction in RR_i after 126 mm of simulated rainfall in a scale from 25 to 200 mm. Hence, in stable soils it seems to be difficult to find more accentuated differences along rainfall application. This corroborates results showed on section 2.3.2.2, where aggregates size distributions did not present significant differences ($p > 0.10$) along rainfall application.

Several studies use RR_i as an independent variable to model more difficult to obtain soil attributes. Considering that, we did a linear regression between average RR_i and rainfall amount for each scale (Figure 10). For rainfall amount, only MRM had a very significant ($p < 0.05$) slope ($\beta_1 = -0.0048$), but still not very far from 0. The heteroscedasticity of MLT and XRT, confirmed by Levene's test, must be the contributing factor to diminish the significance ($p < 0.2$) on these scales, since they present increasingly smaller coefficients ($\beta_1 = -0.0078$; $\beta_1 = -0.0112$), which would indicate a more accentuated response to rainfall by magnifying the

scale of measurement. Even if there is a general decreasing behavior of RR_i according to rainfall amount, the lack of significance makes it difficult to consider this variable as a good indicator of surface behavior. Significance appears to be linked specifically to the range of variances within each factor. This can lead to two hypothesis: (i) RR_i is not effective in evaluating rainfall effects in this type of soil; or (ii) the lack of significance is related to the actual inexistence of physical differences on soil surface after rainfall. Since the second hypothesis is easily refuted by visual examinations of surface before and after rainfall, other parameters may explain better changes of soil surface with rainfall across scales.

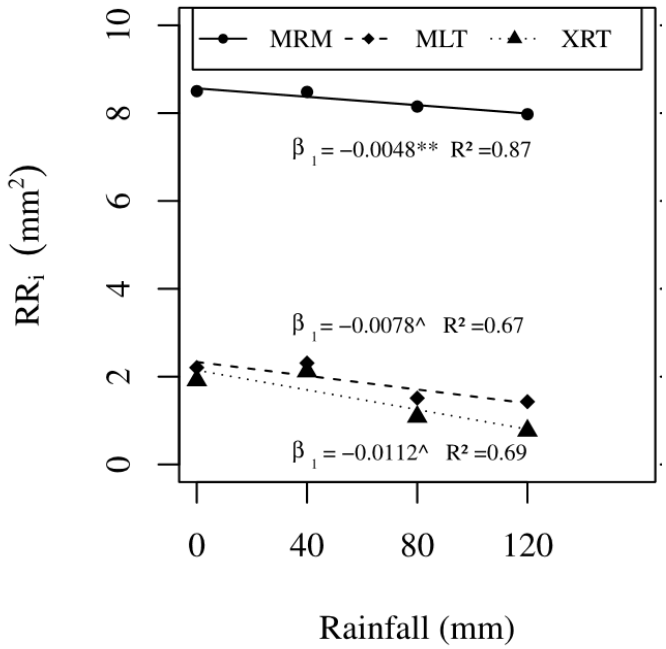

Slope (β_1) *p*-values: "^^"< 0.35, "^" < 0.2, "*" < 0.1 and "**" < 0.05

Figure 10 – Linear regressions from Random Roughness indexes (RR_i) of a fine Rhodic Kandiudalf with rainfall amount as independent variable. Data obtained in three scales, by: a field microrelief meter sensor (MRM, 10 – 800 mm); a multistripe laser triangulation scanner (MLT, 0.5 – 50 mm); and an X-ray tomography scanner (XRT, 0.0745 - 30 mm)

2.3.1.2 Multifractal analyses of the soil surface roughness

At a first sight over the average multifractal spectra (Figure 11), we do not see much differences between rainfall amounts on α range for MRM, although it appears to show some differences on $Lf(\alpha)_{min}$, for 120 mm, and $Rf(\alpha)_{min}$ for 80 mm of rainfall. For MLT and XRT there are clearer differences on both α and f(α) ranges, with a narrowing of α and decreasing of $Lf(\alpha)_{min}$ and $Rf(\alpha)_{min}$ with rainfall increase. Differences between scale have MRM with

wider and longer spectra, while MLT and XRT are more similar, with differences related to range of dimensions.

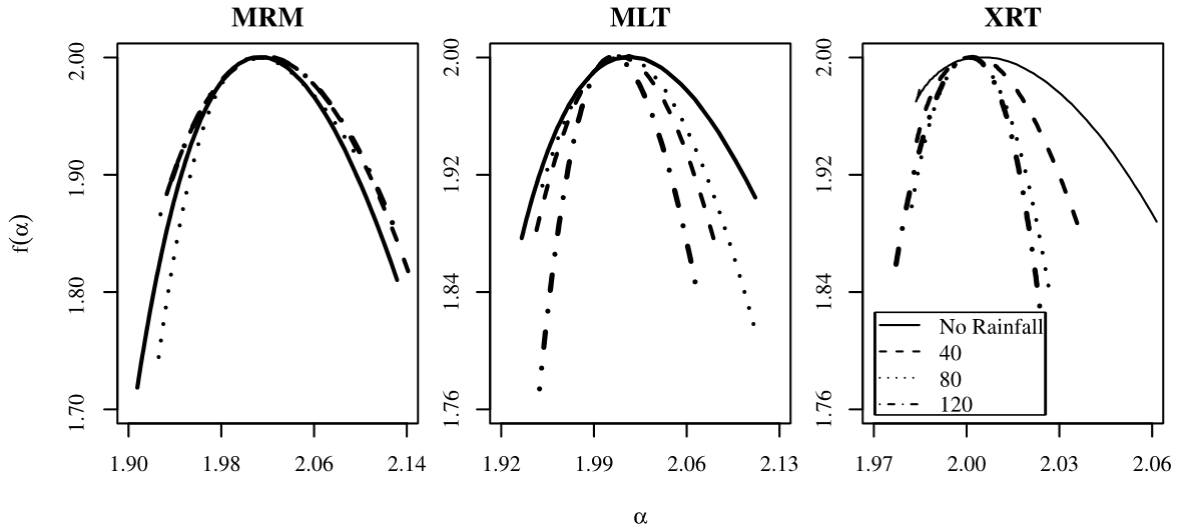

Figure 11 - Multifractal spectra of elevations from a fine Rhodic Kandiudalf before (No rainfall) and after rainfall simulations (40, 80 and 120 mm), obtained in three scales, by: a field microrelief meter sensor (MRM, 10 – 800 mm); a multistripe laser triangulation scanner (MLT, 0.5 – 50 mm); and an X-ray tomography scanner (XRT, 0.0745 - 30 mm)

To simplify interpretations, the parameters on Table 4 were used to unravel the multifractal behavior of soil surface. For MRM, no parameters were significantly different across rainfall, even the ones related to the left spectrum side [$Lf(\alpha)_{min}$, $\Delta Lf(\alpha)$]. Again, for this scale, the variability within rainfall amount was too high to consider average spectra differences as a response to physical differences. This may confirm that on this soil and at this scale (from 10 to 800 mm), rainfall input is not enough to cause a modification on the general multifractal pattern of surface roughness. This type of soil is known to present high stability. Studying roughness changes by natural rainfall at the same soil, Castilho et al. (2011) noticed a reduction in total roughness after rainfall. However, they state that random clods would persist (i.e. undisrupted) even after 10 rainfall events. This stability favors a heterogeneous behavior of surface roughness even with rainfall.

Table 4 – Parameters calculated from roughness maps, from a fine Rhodic Kandiudalf before (No rainfall) and after rainfall simulations (40, 80 and 120 mm), obtained in three scales, by: a field microrelief meter sensor (MRM, 10 – 800 mm); a multistripe laser triangulation scanner (MLT, 0.5 – 50 mm); and an X-ray tomographer (XRT, 0.0745 - 30 mm)

	MRM				MLT				XRT			
	No Rainfall	40 mm	80 mm	120 mm	No Rainfall	40 mm	80 mm	120 mm	No Rainfall	40 mm	80 mm	120 mm
RR_i	8.50 A	8.48 A	8.15 A	7.97 A	2.21 aB	2.31 aB	1.51 aB	1.43 aB	1.92 aB	2.12 aB	1.09 aB	0.77 aB
D1	1.988	1.984 B	1.991 B	1.984 C	1.986 a	1.992 aA	1.990 aB	1.996 aB	1.996	1.999 A	2.000 A	2.000 A
D2	1.958 B	1.944 B	1.970 B	1.945 B	1.952 bAB	1.969 abAB	1.961 abB	1.986 aA	1.987 A	1.994 A	1.997 A	1.996 A
D0-D1	0.0117	0.0158 A	0.0087 A	0.0158 A	0.0155 a	0.0090 aAB	0.0107 aA	0.0045 aB	0.0037	0.0015 B	0.0005 B	0.0005 B
D0-D2	0.0418 A	0.0558 A	0.0298 A	0.0553 A	0.0487 aAB	0.0322 aAB	0.0397 aA	0.0152 aB	0.0127 B	0.0065 B	0.0032 B	0.0037 B
D1-D2	0.0300 A	0.0400 A	0.0210 A	0.0395 A	0.0333 aAB	0.0233 aAB	0.0290 aA	0.0108 aB	0.0090 B	0.0050 B	0.0028 B	0.0033 B
$Rf(\alpha)_{min}$	1.726	1.662	1.716	1.769	1.819 a	1.783 a	1.711 a	1.717 a	1.703	1.707	1.787	1.712
$Lf(\alpha)_{min}$	1.694 B	1.681 B	1.658 B	1.669	1.827 aA	1.743 abAB	1.739 abAB	1.614 b	1.930 aA	1.875 abA	1.803 bcA	1.693 c
$R\Delta f(\alpha)$	0.275	0.339	0.284	0.231	0.183 a	0.218 a	0.290 a	0.284 a	0.315	0.293	0.214	0.288
$L\Delta f(\alpha)$	0.306 A	0.319 A	0.342 A	0.331	0.174 bB	0.258 abAB	0.262 abAB	0.387 a	0.088 bB	0.125 bB	0.197 abB	0.308 a
$f(\alpha)_{ratio}$	0.915 A	1.230 B	0.841	0.908	1.045 A	0.950 B	1.109	0.785	5.710 aA	2.416 aA	1.071 a	0.979 a
α_{min}	1.904 B	1.895 B	1.916 B	1.898 B	1.925 AB	1.923 B	1.916 B	1.936 AB	1.979 aA	1.979 aA	1.977 aA	1.971 aA
α_{max}	2.157 A	2.185 A	2.165 A	2.156 A	2.141 A	2.102 B	2.136 A	2.087 B	2.090 aA	2.048 abB	2.030 bB	2.028 bC
$\Delta\alpha$	0.253 A	0.290 A	0.249 A	0.258 A	0.216 AB	0.179 B	0.219 A	0.151 B	0.111 B	0.069 C	0.053 B	0.057 C
$\Delta R\alpha$	0.144 A	0.168 A	0.154 A	0.139 A	0.125 A	0.093 B	0.125 A	0.083 B	0.085 aA	0.046 abB	0.029 bB	0.027 bC
$\Delta L\alpha$	0.109 A	0.122 A	0.095 A	0.119 A	0.091 AB	0.086 B	0.094 A	0.069 B	0.026 B	0.023 C	0.024 B	0.030 B
α_{ratio}	1.344 B	1.373	1.650 A	1.240 A	1.435 B	1.048	1.356 A	1.180 A	3.218 aA	2.056 ab	1.087 bA	0.829 bA
q_{min}	-3.43 A	-3.95 A	-3.28 A	-3.10 A	-2.85 A	-4.80 A	-4.08 A	-6.80 A	-8.10 aB	-18.68 aA	-17.50 aB	-36.48 aA
q_{max}	6.93 A	6.28 B	8.88 B	7.30 A	8.68 A	6.15 B	6.50 B	12.98 A	18.40 A	17.90 A	21.23 A	34.90 A

Lower case letters represent significant differences ($p < 0.10$) between rainfall amounts within scales and uppercase letters represent significant differences ($p < 0.10$) between scales within rainfall. Differences were checked by Tukey HSD test in case of homoscedasticity, otherwise, DTK test was applied. RR_i: random roughness index; *D0*: capacity dimension; *D1*: entropy dimension; *D2*: correlation dimension; $Rf(\alpha)_{min}$: minimum Hausdorff dimension at right of *D0*; $Lf(\alpha)_{min}$: minimum Hausdorff dimension at left of *D0*; $\Delta Rf(\alpha)$: range of Hausdorff dimensions at right of *D0*; $\Delta Lf(\alpha)$: range of Hausdorff dimensions at left of *D0*; $f(\alpha)_{ratio}$: ratio between $\Delta Rf(\alpha)$ and $\Delta Lf(\alpha)$; α_{min}: minimum Lipschitz-Holder exponent; α_{max}: maximum Lipschitz-Holder exponent; $\Delta\alpha$: the complete range of Lipschitz-Holder exponents; $\Delta R\alpha$: range of Lipschitz-Holder exponents at right of *D0*; $\Delta L\alpha$: range of Lipschitz-Holder exponents at left of *D0*; α_{ratio}: ratio between $\Delta R\alpha$ and $\Delta L\alpha$; q_{min}: minimum generalized dimension; q_{max}: maximum generalized dimension

Areas with a larger amount of stable clods will suffer less flatting by raindrop impact and/or moistening dismantlement, responding unpredictably to rainfall increase, which may create even rougher patterns. This behavior contributes to maintain a high variability of surface roughness even after rainfall application, which would reflect on the spectra.

For MLT, that represents a larger scale, from 0.5 and 75 mm, the case was different. There were significant differences ($p < 0.10$) for $f(\alpha)$ parameters $D2$, $Lf(\alpha)_{min}$ and $L\Delta f(\alpha)$. As explained before, $f(\alpha)$ can be interpreted as the fractal dimension of areas with same probability, and which scale organization relates to the magnitude of an specific α range ($\alpha + \partial\alpha$). In other words, $f(\alpha)$ is a fragmentation index of an specific class of probabilities, represented by a fractional number between 1 and 2 (i.e. topological dimension of a surface). Smaller the value of $f(\alpha)$, more fragmented is the region represented by this range of probabilities and smaller is the area covered by such features. On MLT, $Lf(\alpha)_{min}$ significantly ($p < 0.10$) decreases from 1.827, before rainfall, to 1.614, after 120 mm of rainfall. The $Lf(\alpha)_{min}$ represents the dimension of areas with high probabilities (peaks). Therefore, the decrease in $Lf(\alpha)_{min}$ means that peak areas are becoming more sparse, which would happen if the surface is getting flatter. Not only $Lf(\alpha)_{min}$ is related to the flattening process, but it also shows at what degree the process diminishes at each rainfall amount, since it represents the area filling capacity of one class of probabilities. This may be better observed by $L\Delta f(\alpha)$. It shows that the interval between $D0$, the average filling capacity of the system, and $Lf(\alpha)_{min}$, significantly ($p < 0.10$) increase from 0.174 to 0.387. This means that after 120 mm of rainfall the peaks has twice less filling capacity than before rainfall, which implicates in twice less chance of finding high points over the surface.

For reasons explained in section 2.2.6.3, MLT does not have $D0 = 2$ for all images, which may dislocate $D2$. However, without considering the gross value of $D0$, the behavior across rainfalls must be explored. D2 is an specific value of $f(\alpha)$ that represents the correlation of the measures contained in a L size box. Thus, the increase from 1.952, before rainfall, to 1.986, after 120 mm of rainfall, shows that the correlation is increasing with rainfall increase. That is, the local dimensions of different areas within an L size box, are becoming similar. This shows once again how the surface becomes homogeneous with rainfall increase, and that there is a positive spatial pattern, where higher heights will have more probability of being surround by other high points.

For XRT the behavior was similar on $f(\alpha)$, with significant ($p < 0.10$) differences on $Lf(\alpha)_{min}$, decreasing from 1.930 to 1.693, and $L\Delta f(\alpha)$, increasing from 0.088 to 0.308. Nevertheless, XRT also had significant ($p < 0.10$) differences for α parameters α_{max}, $\Delta R\alpha$ and

α_{ratio}. We have to remember that α values show how height distribution changes proportionally to scale. It represents the slope of the linear relation of [$logP_i(L)/logL$], and, because of the logarithm, smaller probabilities relate to higher α values. That is why the right side of the spectrum is related to the micro-valleys (i.e. areas with small probabilities). Since it is a slope, α represent the rate in which probabilities change along scales. α_{max} then represents how fast areas with smaller probabilities change across scale. For XRT, rainfall increase changes α_{max} from 2.090 to 2.028. Thus, rainfall enables a reduction in rate on which the micro-valleys distribution will change along scale. $\Delta R\alpha$, which show how α_{max} distances from the systems average, decreases from 0.085 to 0.027, showing that, after rainfall, scale has four times less influence over low probabilities areas when compared with the average height of the surface. α_{ratio} is the relation between right and left side of the spectrum. That is, it shows which range of probabilities change more along the scales. Before rainfall, α_{ratio} is 3.218, which means that valleys change more than peaks along the scales. At 80 mm of rainfall, the ratio almost becomes one (1.087), which indicate that extremes (i.e. peaks and micro-valleys) behave similarly among the scales. After 120 mm of rainfall α_{ratio} is 0.829, indicating that the low probabilities area changes less across scales than the peaks. Considering there were no significant differences ($p > 0.10$) on $Rf(\alpha)_{min}$, the fragmentation of the micro-valleys is the same across rainfall, but with smaller differences among scales, which means the heights are closer to the average, i.e. more homogeneous.

Differences across scales of measurement happened for almost all variables. Once again *D2*, $Lf(\alpha)_{min}$, $L\Delta f(\alpha)$, α_{max}, $\Delta R\alpha$ and α_{ratio} had significant differences ($p < 0.10$), but also there were differences ($p < 0.10$) on *D1*, *D0-D1*, *D0-D2*, *D1-D2*, $f(\alpha)_{ratio}$, $\Delta L\alpha$, $\Delta R\alpha$, α_{min} and α_{ratio}. Only $Rf(\alpha)_{min}$ and $R\Delta f(\alpha)$, were not different across scales ($p > 0.10$). This means the variance on the right side of spectra is too high to permit average differences between scales. The right side relates to the negative range of *q*'s, which mathematically contributes to enhance the variance of the estimates on this part of the spectrum. To circumvent such problem, some authors have used a method called "gliding box" to increase the number of L size boxes during calculations and diminish the variance on the right side of the spectra (GARCÍA MORENO et al., 2008). However, since 18 parameters were sensitive in differentiating scales in this research, the box-counting method seems to be suffice in analysis of this kind. In almost all comparison between $f(\alpha)$ parameters (*D2*, *D0-D2*, *D1-D2*, $Lf(\alpha)_{min}$, $L\Delta f(\alpha)$) MLT is not different ($p > 0.10$) from XRT. For α parameters ($\Delta L\alpha$, $\Delta R\alpha$ and α_{ratio}) this was not always true, with XRT presenting significantly smaller $\Delta L\alpha$ and $\Delta R\alpha$ and larger α_{ratio} values at different rainfall amounts. This diversity is related to the narrowing of the α range with grid

increment. The finer grid, associated to a smaller area of measurement, influence the scale arrangement of probabilities, since differences in height start to diminish. However, it is interesting to note that the fragmentation is similar on these two scales of measurement.

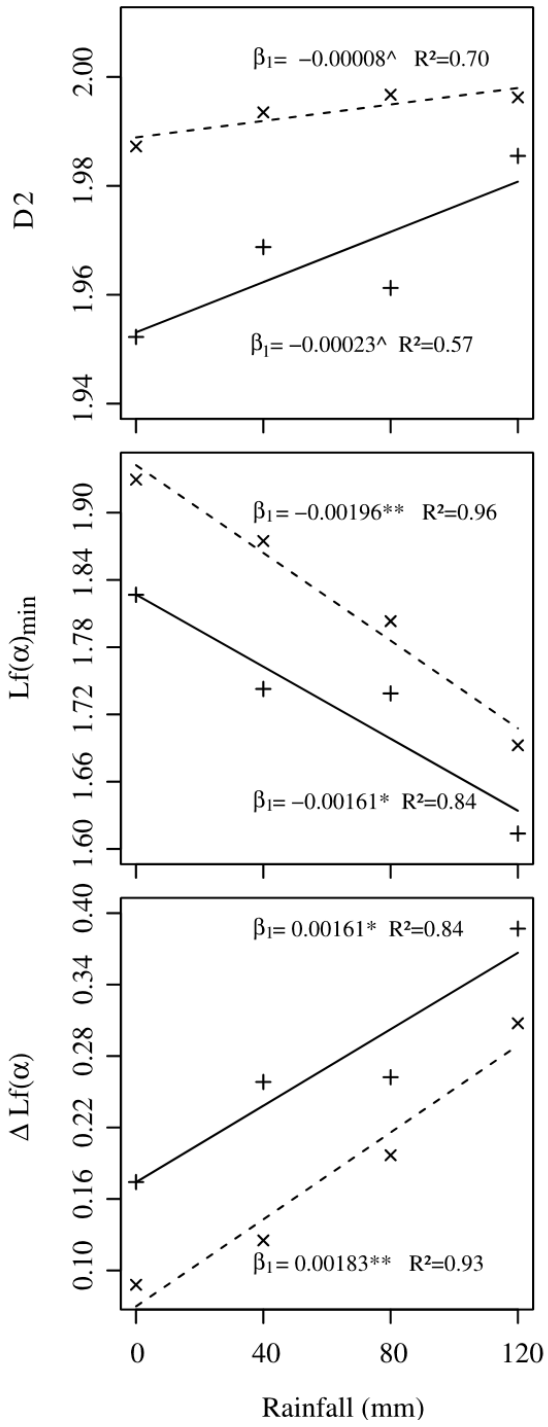

Slope (β_1) *p*-values: "^^"< 0.35, "^" < 0.2, "*" < 0.1 and "**" < 0.05

Figure 12 - Linear regressions from parameters D2: correlation dimension, $Lf(\alpha)_{min}$: minimum Hausdorff dimension at left of D0, $\Delta Lf(\alpha)$: range of Hausdorff dimensions at left of D0, estimated from multifractal spectra of a fine Rhodic Kandiudalf before (No rainfall = 0 mm) and after rainfall simulations (40, 80 and 120 mm), obtained in two scales of measurement, by: a multistripe laser triangulation scanner (MLT, 0.5 – 50 mm; solid line and + symbols); and an X-ray tomography scanner (XRT, 0.0745 - 30 mm; dashed line and x symbols)

Since no parameters were significant for MRM, we can only use the mutltifractal parameterization on MLT and XRT data. Considering the previous discussion, the regressions, according to rainfall, of the average parameters *D2*, $Lf(\alpha)_{min}$ and $L\Delta f(\alpha)$ from these two scales are displayed on Figure 12. Parameter *D2* has the lowest R^2 (0.57, 0.70), and slopes (-0.00023, -0.00008) are very close to 0, with relatively high *p*-values (0.16, 0.11). $Lf(\alpha)_{min}$ and $L\Delta f(\alpha)$ had more significant (p > 0.05, 0.01; 0.05, 0.02) slopes (-0.00161, -0.00196; 0.00161, 0.00183), and models that better explain the variability along rainfall (R^2= 0.84, 0.96; 0.84, 0.93). Hence, these two variables are the most import for describing the soil surface roughness variability across rainfalls. Most importantly, since there are no significant differences (p > 0.44, 0.65) between slopes of different measurement methods, one may be chosen over the other in the evaluation of the surface roughness.

2.3.2 Physical attributes

2.3.2.1 Bulk Density and Ratio of Volume of Pores

In an initial evaluation we can use simple parameters that relate to soil structural changes. The average bulk density (*BD*) and ratio of volume of pores (P_r) are showed in Table 5. Although we note an increase in *BD* after rainfall simulation, which causes a diminishing in P_r, differences were not significant (p > 0.10).

Table 5 - Averages of Bulk Density and Ratio of Volume of Pores from quadruplicates of a Fine Rhodic Kandiudalf (22º41'51.5" S, 47º37'53.2" W) at surface (0 - 2.5 cm) before (No-rainfall) and after rainfall simulations (40, 80, 120 mm)

	No-rainfall	40 mm	80 mm	120 mm
Bulk Density	($Mg\ m^{-3}$)			
	1.20	1.25	1.24	1.24
Ratio of Volume of Pores	($m^3\ m^{-3}$)			
	0.55	0.53	0.54	0.53

There were no differences (p >0.10) between rainfall amounts.

One of the difficulties on trying to evaluate soil surface processes is to consider the scale in which they happen. The depth in which the sealing occurs for this soil is very narrow, as discussed in section 2.3.4. When observed in the microscope, most of the crusts, even after 120 mm of rainfall, were smaller than 10 mm (i.e. 0.10 cm). Therefore, the height of the cylinder used for BD measurements had 2.5 times the width of the crust. Bergsma et al. (2000) cites that a crust can vary from a few millimeters to a maximum of 2 or 3 cm wide. This wide variance given by the authors is because their text try to create an international literature for soil erosion and conservation studies, which make it reasonable, in a world

scenario, to consider several classes of soils. As reported before, the soil of this study presents a very stable structure, theme that is going to be explored in section 2.3.2.2. Thus, is convenient to infer that the cylinder size was not enough to find differences between rainfall amounts, reason to why it was decided to divide the samples in narrower depths when computing the water retention curves that are showed in section 2.3.3.2.

2.3.2.2 Aggregates stability

The aggregates size distribution (*ASD*) and the weighted mean diameters (*WMD*) are shown in Table 6. Differences were not significant ($p > 0.10$) between rainfall amounts for all pre-treatments, which reflects the high stability of such soil. However, a pattern is observed. Slow wetting (*SW*) had a higher concentration of aggregates bigger than 2 mm (903.15, 916.23, 898.98 and 894.31 g kg^{-1}), followed by the values from mechanical breakdown (*MB*) (585.29, 594.13, 551.66 and 534.27 g kg^{-1}) and fast wetting (*FW*) (215.24, 193.83, 223.92 and 184.92 g kg^{-1}). Le Bissonnais (1996) states that it is common to find much smaller values for FW, since it relates to the slaking of dry soils when they are rapidly moistened (e.g. during tropical storms common during summer). Since this process is related to the raising pressure inside aggregates and clods, that may cause several internal ruptures in different parts of the structure, it is expected to have a higher degree of dismantlement, after all, it occurs simultaneously in several parts of the aggregate.

Two facts are promptly noted by checking all pre-treatments. First, with regard to the differences between treatments, all distributions present relatively high *WMD*. Second, different distribution patterns occur after each pre-treatment, as can be seen in Figure 13, that shows the distributions according to equivalent diameters. *FW* curves covers a wider range of diameters, concentrating between 0.75 and 3.5 mm. *MB* is more concentrated around 1.5 and 3.5 mm, and SW is dominated by aggregates with 3.5 mm of diameter. Although there were no differences ($p > 0.10$) amongst rainfall amount, in *FW* we can better differentiate the curves according to rainfall, where 120 mm of rainfall decreases the amount of big aggregates, while increasing the concentration of very small aggregates (< 0.053 mm). The curves for *MB* and *SW* behave similarly according to rainfall amount, being difficult to distinguish differences between simulations.

With this information we can theorize which process is going to be dominant during clods disruption in this soil according to rainfall. At first, if the soil is dry when rainfall starts, big clods will suffer slaking, which will create wider distributions, with sizes reaching from centimeters to a few millimeters. When water starts to accumulate and the moisture

standardizes at the surface, the breakdown due to raindrop impact will be the dominant process, but not as effective, since most clods remain bigger than 1 mm. The results for *SW* show that almost no clod crumbles when the soil is already humid and water flux is slow. When studying surface roughness in the same area, Castilho et al. (2011) noticed the persistence of undisrupted random clods even after 10 natural rainfall events (with intensity > 25 mm h^{-1}). This resistance is a natural feature of this class of soil. Brazilian Rhodic Kandiudalfs (SOIL SURVEY STAFF, 2014), i.e., Nitossolos Vermelhos eutroférrico (EMBRAPA, 2013), are known to present high contents of iron oxides, even in silt and sand fractions (FERREIRA et al., 2003), because of their parental material (basalt). That generates cohesive bonds that are difficult to break. The cohesive forces of such elements prevents dispersion by water alone, maintaining the structure stable for longer periods of time. Such soils even present a challenge during particles size analysis, since its total dispersion is very difficult due to these strong cohesive forces (CORÁ et al., 2009).

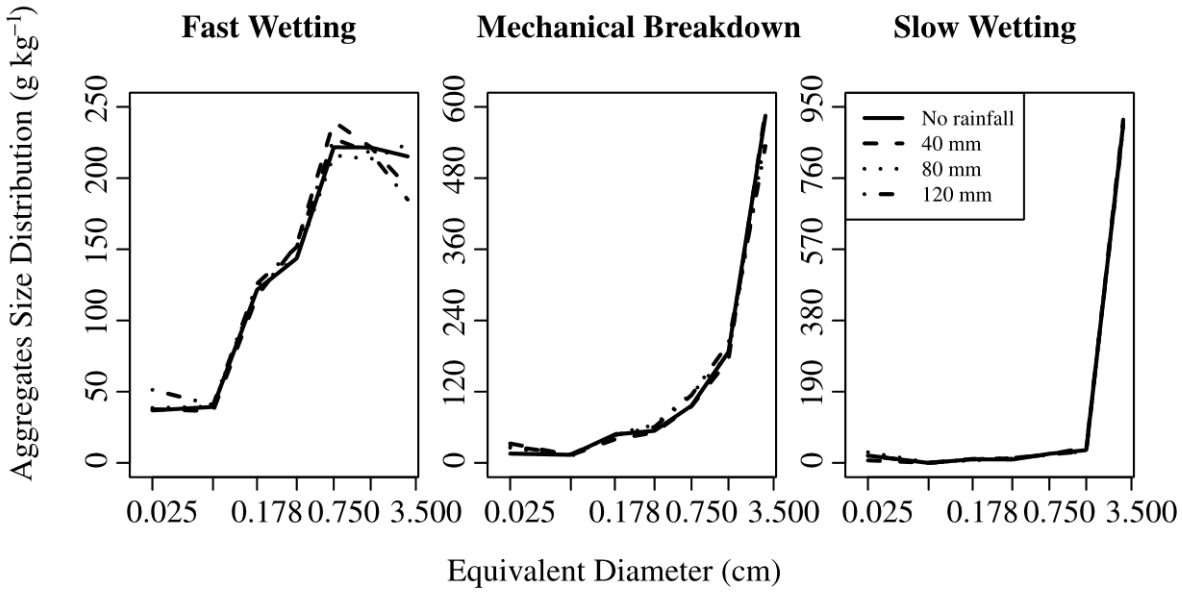

Figure 13 – Aggregates size distribution at surface (0-10 mm) of a Fine Rhodic Kandiudalf before (No-rainfall) and after rainfall simulations (40, 80 and 120 mm). Values represent the mass of aggregates, in g kg^{-1} of soil, distributed according to diameter. Each plot represent a distinct pre-treatment: dry aggregates slowly moistened by capillary forces (slow wetting); dry aggregates directly submerged in water (fast wetting); dry aggregates, previously moistened with alcohol, and shaken in water with controlled energy (mechanical breakdown)

Table 6 – Results of a stability test (Le Bissonnais, 1996) from aggregates of the surface (0-10 mm) of a Fine Rhodic Kandiudalf before (No-rainfall) and after rainfall simulations (40, 80 and 120 mm). Values on the upper part of the table represent the mass of aggregates, in g kg^{-1} of soil, retained by a respective sieve after pre-treatments: dry aggregates slowly moistened by capillary forces (slow wetting); dry aggregates thrown in water (fast wetting); dry aggregates are previously moistened with alcohol and then shaken, with controlled energy, inside water (mechanical break)

Aggregates diameter (Φ)	Slow Wetting				Fast Wetting				Mechanical Break			
	No-rainfall	40 mm	80 mm	120 mm	No-rainfall	40 mm	80 mm	120 mm	No-rainfall	40 mm	80 mm	120 mm
(mm)	g kg^{-1}											
Φ > 2	903.15 A	916.23 a	898.98 a	894.31 a	215.24 c	193.83 c	223.92 c	184.92 c	585.29 b	594.13 b	551.66 b	534.27 b
2 < Φ < 1	34.02 C	31.48 c	31.01 c	41.12 b	221.52 a	221.76 a	213.35 a	217.76 a	186.89 b	173.54 b	182.14 b	201.54 a
1 < Φ < 0.5	24.47 C	22.79 c	21.82 c	22.94 c	221.67 a	239.71 a	216.00 a	227.69 a	96.38 b	95.38 b	116.71 b	114.24 b
0.5 < Φ < 0.25	9.11 C	12.13 c	11.65 c	12.96 c	143.74 a	153.32 a	144.37 a	151.67 a	54.18 b	51.26 b	64.05 b	60.66 b
0.25 < Φ < 0.106	9.64 C	10.63 c	6.85 c	9.58 c	121.58 a	117.46 a	124.24 a	126.12 a	47.94 b	39.95 b	48.77 b	47.04 b
0.106 < Φ < 0.05	0.00 C	0.00 c	1.00 c	0.00 c	39.35 a	35.97 a	39.29 a	40.24 a	13.63 b	12.88 b	10.89 b	14.04 b
Φ < 0.05	19.63 A	6.75 b	28.70 a	19.10 b	36.91 a	37.94 a	38.83 a	51.60 a	15.70 a	32.87 a	25.79 a	28.21 b
	mm											
Weighted Mean Diameter	3.24 a	3.28 a	3.22 a	3.22 a	1.33 c	1.27 C	1.34 c	1.22 c	2.43 b	2.44 b	2.32 b	2.29 b

Lower case letters represent significant differences ($p < 0.10$) between pre-treatments at same rainfall amount. There were no significant differences between rainfall amounts within pre-treatments. Differences were checked by Tukey HSD test in case of homoscedasticity, otherwise, DTK test was applied

2.3.3 Hydrological attributes

2.3.3.1 Unsaturated soil hydraulic conductivity - K(θ)

In Table 7 are the values of K(θ) in four tensions (1.5, 3, 4.5 and 6 cm). There were significant differences ($p < 0.10$) between rainfall amounts and between tensions. *K(θ)* was almost always significantly bigger at 1.5 cm, that represent pores with equivalent diameter of 1.98 mm. At 40 mm of rainfall, for all tensions, *K(θ)* drops almost to one third of its initial value in all tensions, which does not significantly change with increasing rainfall. In 40 mm differences between tensions starts to fade, with no significant differences between tensions of 1.5 and 3 cm. At 120 mm of rainfall there were no significant differences ($p > 0.10$) between all tensions. That means that with increasing rainfall the reorganization of the pores close to the surface causes a drastic change in the structure, probably standardizing pore sizes to a smaller equivalent diameter.

Table 7 – Values of unsaturated soil hydraulic conductivity at surface from a Rhodic Kandiudalf before (No rainfall) and after rainfall simulations (40, 80 and 120 mm). Measurements were made with a MiniDisk Infiltrometer at four tensions (τ = 1.5, 3, 4.5 and 6 cm)

τ (cm)	Equivalent Diameter (mm)	No-rainfall	40 mm	80 mm	120 mm
		cm s^{-1}			
1.5	1.98	0.00157 aA	0.00048 aB	0.00060 aB	0.00060 aB
3	0.99	0.00087 bA	0.00028 abB	0.00034 bB	0.00031 aB
4.5	0.66	0.00069 bA	0.00020 bB	0.00023 bB	0.00020 aB
6	0.50	0.00050 bA	0.00016 bA	0.00015 bA	0.00013 aA

At a tension of 6 cm there were no differences ($p > 0.10$) between rainfall amounts. Thus, the porosity with equivalent diameter smaller than 0.50 mm was not affected by rainfall. Instead, rainfall caused pronounced changes in macropores bigger than 0.66 mm. Hence, changes in soil hydraulic conductivity from pores with equivalent diameter between 0.66 and 1.98 mm may be related to changes in their size distribution, which would be reflected in the beginning of the water retention curve (*WRC*), and/or to changes in pores shape and connectivity, that can be evaluated by micromorphometrical analysis.

2.3.3.2 Water Retention Curve – *WRC*

In Figure 14 is possible to observe differences in average *WRC*s by rainfall amount and depth of measurement. There is a general decreasing in the dispersion of points with increasing rainfall, which is related to the homogenization of the structure within each

treatment. The curves show that rainfall causes differences in all three layers with increasing amount. However, main distinction occur at the superficial layer. In all rainfall amounts, the curves at surface stay beneath others (middle and subsurface) for most potentials (showed in pF, i.e., $\log_{10}|-h|$ cm).

Before rainfall, all curves presented similar shape and were closer to one another. This indicates that before rainfall the structure does not change from surface till the depth of 2.4 mm. We can verify that by checking the *WRC* fitted parameters in Table 8. There are no differences between layers before rainfall for θs (1.00, 1.00 and 1.00 kg kg^{-1}) and θr values are very close (0.14, 0.08 and 0.12 kg kg^{-1}). Equality between θs values shows that there is homogeneity in the part of the curve that represent structural pores. The θr is more affected by the inclination of the curve, since it depends on the location of the inflection point at a lower potential (van GENUCHTEN, 1980), which shows when the porosity changes from structural to textural (DEXTER, 2004a). This can be observed by the α and *n* parameters. Parameter α presented a little increase on the middle curve (1.98, 2.48 and 1.31) while *n* presented a small decrease (1.30, 1.21 and 1.27). The parameter α is related to the position of the inflection points, while *n* to the steepness of the curve (van GENUCHTEN, 1980). Higher α indicates inflections closer to the end of the curve, i.e. higher percentage of structural pores, and lower *n* relates to smaller gradients $\partial\theta/\partial h$, which is typical of curves that are less steep. Since the shape and θs and θr are very similar, there is no reason to consider differences between curves before rainfall.

After 40 mm of rainfall, the curves of deeper layers (middle and subsurface) presented a different curvature when compared to the surface. Just with one rainfall there were changes in θs (1.00, 0.49 and 0.49 kg kg^{-1}) and a positive linear behavior of θr (0.16, 0.18 and 0.19 kg kg^{-1}). It is easy to imagine that rainfall would decrease θs at surface, due structural changes caused by sealing. However, values of α (3.13, 0.06 and 0.03) and *n* (1.34, 1.64 and 1.83) show that deeper layers suffered more changes with the first application of simulated rainfall. The increase in steepness (i.e. increasing *n*) and decrease of structural porosity (i.e. decrease of α), along with a linear increase in θr, may point to an increase in clay content due to illuviation from the upper layer. The clay padding would explain the reduction of θs. Imagining that structural pores are the first to be filled, a decrease of α would also be plausible, and it is noteworthy that an increase in clay content would explain the rising of θr.

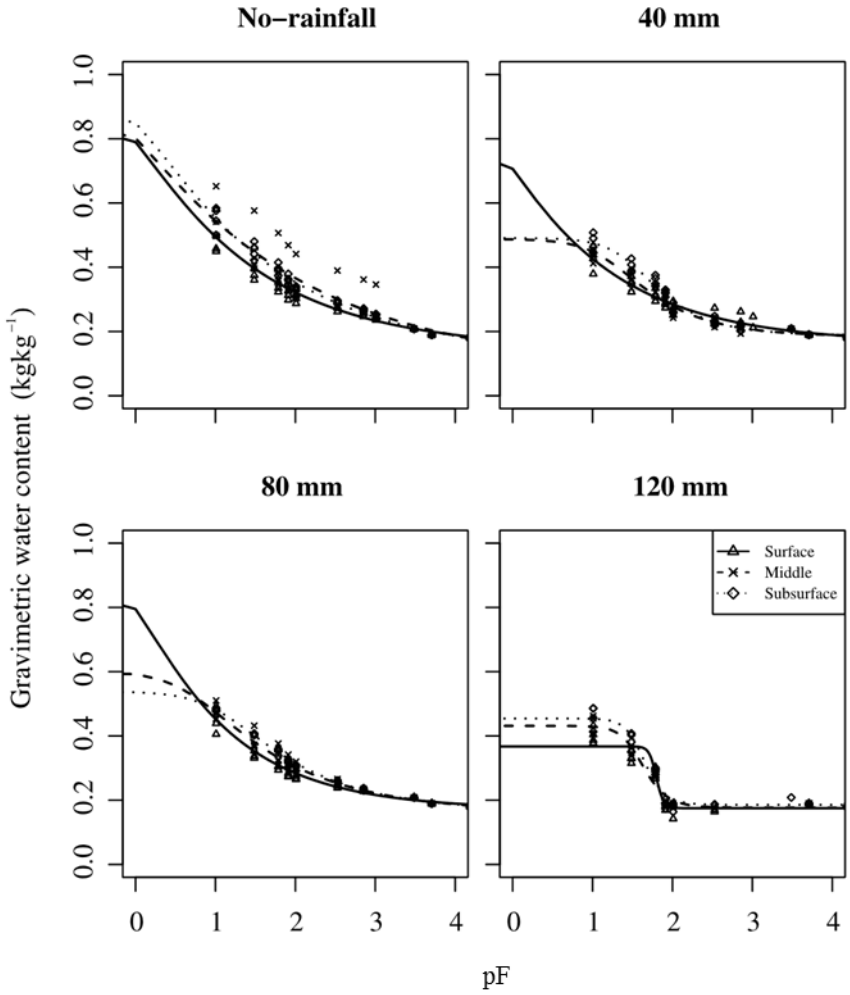

Figure 14 – Average water retention curves from a Rhodic Kandiudalf before (No-rainfall) and after rainfall simulations (40, 80 and 120 mm). Averages calculated from quadruplicate soil cylinders (2.5 x 2.5 cm) collected by rainfall amount. Each cylinder was divided in three parts (0.8 x 2.5 cm) to capture the transitions caused by soil sealing. Depths represent layers very close to soil actual surface (surface, 0 - 0.8 mm), an intermediate layer between parts that can be affected by sealing and the soil original structure (middle, 0.8 – 1.6 mm) and the layer less directly affected by rainfall (subsurface. 1.6 – 2.4 mm)

At 80 mm all curves are once again very similar in shape and more superimposed. Nevertheless, they are less steep and displaced downward when compared to before rainfall, indicating a loss of structural porosity. Although ranges between θs (1.00, 0.60 and 0.54 kg kg^{-1}) and θr (0.17, 0.16 and 0.17 kg kg^{-1}) is larger than it was after 40 mm of rainfall, α values (1.46, 0.20 and 0.08) are smaller at surface and *n* values are very similar (1.40, 1.38 and 1.43), corroborating the less steep shape.

After 120 mm of rainfall there are profound differences between layers, with three very distinct curves. There is a huge difference between the values of θs (0.37, 0.43 and 0.45 kg kg^{-1}), while θr (0.17, 0.18 and 0.19 kg kg^{-1}) remains very close. This represents an immense difference in structure between the three layers, since at surface the soil retains 0.08 kg kg^{-1}

less than at subsurface. Although the surface layer is the most degraded, changes occur at all depths, since low α values (0.02, 0.03 and 0.03) and high *n* values (10, 3.32 and 3.85) shows a complete change in soil behavior, with values very similar to ones found for sandy soils (van GENUCHTEN, 1980), where the lack of aggregation leads to more steep curves, with inflection occurring right at the beginning of the curve, at higher potentials.

Table 8 – Parameters from average water retention curves of a Rhodic Kandiudalf before (No-rainfall) and after rainfall simulations (40, 80 and 120 mm). Averages calculated from quadruplicate soil cylinders (2.5 x 2.5 cm) collected by rainfall amount. Each cylinder was divided in three parts (0.8 x 2.5 cm) to capture the transitions caused by soil sealing

	Surface				Middle				Subsurface			
Curve Parameters	No-rainfall	40 mm	80 mm	120 mm	No-rainfall	40 mm	80 mm	120 mm	No-rainfall	40 mm	80 mm	120 mm
	kg kg^{-1}											
Θs	1.00	1.00	1.00	0.37	1.00	0.49	0.60	0.43	1.00	0.49	0.54	0.45
Θr	0.14	0.16	0.17	0.17	0.08	0.18	0.16	0.18	0.12	0.19	0.17	0.19
	dimensionless											
A	1.98	3.13	1.46	0.02	2.48	0.06	0.20	0.03	1.31	0.03	0.08	0.03
N	1.30	1.34	1.40	10.00	1.21	1.64	1.38	3.32	1.27	1.83	1.43	3.85
	model accuracy											
R²*	0.99	0.99	0.99	0.95	0.99	0.99	1.00	0.97	0.99	0.99	1.00	0.96
RSE**	0.0100	0.0090	0.0077	0.0263	0.0143	0.0114	0.0065	0.0222	0.0124	0.0150	0.0068	0.0264

Depths represent layers very close to soil actual surface (surface, 0 - 0.8 mm), an intermediate layer between parts that can be affected by sealing and the soil original structure (middle, 0.8 – 1.6 mm) and the layer less directly affected by rainfall (subsurface. 1.6 – 2.4 mm). All parameter were significant ($p < 0.05$) for the regression

*R^2 - coefficient of determination between real and predicted data

**RSE – Residual standard error of the non-linear regression model

Differences amongst rainfall amounts within each layer were more or less linear for deeper layers (middle and subsurface), and more abrupt at surface, with drastic changes from 80 to 120 mm. This shows that the sealing process is not completely linear from surface to the underlying layers. Instead, changes occurs at different amounts at each depth, depending on which process is dominant at surface. For example, if clay dispersion is dominant, deeper layers will suffer faster changes than the overlying soil. If slaking and/or mechanical break starts to rearrange clods, the surface presents more changes.

Since *K(θ)* presents great changes right after the first rainfall, and curves at surface change gradually across rainfall amount, other features must be changing to impede water movement. The *WRC* shows structural differences related to retentions characteristics, that may be extrapolated to pores size distribution if bulk density is known. However, soil conductivity does not only depends on pore sizes, but also on its shape, tortuosity and

connectivity. Shape and connectivity can be easily estimated by micromorphometrical analysis.

2.3.4 Image Pore Analysis

2.3.4.1 Micromorphometrical analysis

The distribution of the percentage of area of pores by format and size are presented in Table 9. A graphical representation can be found in Figure 15. Independently of the rainfall amount and depth, the dominant class of pores was the complex with diameters larger than 1000 µm. This type of pore is associated to the degree of connectivity in a pore system. The definition of "complex" is an allusion to the difficulty to define such pores based on a unique diameter value, since they are not circular or elongated. Thus, complex pores are normally more ramified, and bigger this pore is, higher is the chance of connectivity throughout the system. At the same time that complex pores (> 1000 µm) dominated, they changed ($p < 0.10$) with the rainfall volumes applied on the surface layer, with a decrease in area from 35.360 %, before rainfall, to 20.308 % after 120 mm of rainfall. The fact that this happened only at the surface is associated to the sealing process, which modifies the soil structure only at the first few millimeters of the soil surface. On the other hand, the average of this class of pores was larger at the 40 mm rainfall than before rainfall, but the differences were not significant, which is evidently related to the high variability within this treatment. Analogously to the surface roughness discussion, initial rainfall increases variability within the soil, instead of standardizing it due to clod disruption, especially considering the high stability of the aggregates of this soil. The more stable parts will disrupt less, so at the beginning of the rainfall event the variability increases, until soil moisture standardizes, and the structure at the surface starts to breakdown.

The smaller area occupied by complex pores (> 1000 µm) was followed by an increase in the area of smaller size pores, such as smaller complex (500 – 1000 µm and 100 - 200 µm) and elongated (20 - 50 µm) types. Rounded pores did not present differences ($p > 0.10$) for all sizes within the soil surface among rainfalls. This may be associated to the very small area covered by such pores and the high variability of the pore systems. Analyzing the behavior of the means, an increase of almost all rounded pores as rainfall volume increases can be observed. This may show that the pore structure is becoming less and less connected.

When comparing depths at the same rainfall volume it is interesting to note that, before rainfall, there is practically no differences ($p > 0.10$) between layers, meaning that the whole 5 cm layer is homogeneous. The biggest differences between depths are observed at the 80 mm

volume of rainfall, with all complex pores from 100 to 1000 μm decreasing as depth increases. Although changes by rainfall occur mainly at the surface, the accumulative rainfall can cause a collapse of the structure due to increase moistening, which weakens cohesive bonds, thanks to the lubricant action of water. This favors the increase of the bulk density in deeper layers, which might be confused with crust formation. We can infer that this is not the case here, since the distribution of rounded pores decreases, which is the contrary of what happen in a sealed layer, where the area of rounded pores rises due to fragmentation of big complex and elongated pores. Hence, the pore structure is not being morphologically changed from complex and connected pores into rounded and disconnected ones. Instead, there is an underlying process in which the whole area of pores is diminishing.

Table 9 – Distribution of pore area by shape and size in a Rhodic Kandiudalf before (No-rainfall) and after rainfall simulations (40, 80 and 120 mm). Results are means from quadruplicate soil blocks having triplicate images within rainfall amount and depth of measurement. Images were taken, parallel to the real surface of the soil, for three depths,: surface (0-10 mm), middle (20- 30 mm) and subsurface (40 – 50 mm)

Type of pores by diameter (μm)		Top				Middle				Bottom			
		No-rainfall	40 mm	80 mm	120mm	No-rainfall	40 mm	80 mm	120mm	No-rainfall	40 mm	80 mm	120mm
		(%)											
Complex	>1000	35.360 a	35.798 a	22.925 ab	20.308 B	24.453	43.363	35.593	27.203	29.580	30.890	30.320	23.450
	500-1000	1.485 ab	1.040 b	3.015 aA	2.285 Ab	2.133	0.585	0.755 B	1.873	1.035	0.908	1.008 B	1.705
	400-500	0.323	0.240	0.595 A	0.570 A	0.270	0.098	0.103 B	0.303 B	0.085	0.030	0.060 B	0.135 B
	300-400	0.218 A	0.155	0.378 A	0.490	0.158 A	0.043	0.078 B	0.118 B	0.048 B	0.058	0.045 B	0.180 B
	200-300	0.070	0.065	0.110 A	0.200	0.038	0.025	0.020 B	0.018	0.020 A	0.030	0.003 B	0.060
	100-200	0.005 b	0.008 bA	0.020 abA	0.030 aA	0.000	0.008 A	0.000 B	0.000 B	0.000 b	0.000 bA	0.003 abAB	0.008 aB
	50-100	0.000	0.000	0.000	0.000	0.000	0.000	0.000	0.000	0.000	0.000	0.000	0.000
	20-50	0.000	0.000	0.000	0.000	0.000	0.000	0.000	0.000	0.000	0.000	0.000	0.000
Elongated	>1000	0.000	0.000	0.000	0.000	0.000	0.000	0.000	0.000	0.000	0.000	0.000	0.000
	500-1000	0.000	0.000	0.000	0.520	0.000	0.000	0.000	0.000	0.000	0.000	0.000	0.000
	400-500	0.000	0.000	0.000	0.000	0.000	0.000	0.250	0.000	0.000	0.000	0.000	0.000
	300-400	0.000	0.000	0.000	0.000	0.000	0.000	0.000	0.000	0.000	0.165	0.000	0.263
	200-300	0.153	0.000	0.063	0.093	0.103	0.000	0.068	0.123	0.000	0.293	0.225	0.048
	100-200	0.293	0.275	0.128	0.225	0.368	0.150	0.473	0.758	0.345	0.263	0.320	0.438
	50-100	0.623	0.533	1.085 A	1.095	0.683	0.330	0.458 B	0.793	0.588	0.398	0.490 B	0.930
	20-50	0.358 b	0.303 b	0.650 abA	0.940 aA	0.310	0.140	0.230 B	0.300 B	0.343	0.200	0.175 B	0.350 B
Rounded	>1000	0.085 AB	0.130	0.065	0.418	0.000 B	0.105	0.158	0.060	0.363 A	0.295	0.310	0.268
	500-1000	0.253	0.110	0.248	0.270	0.363	0.553	0.183	0.280	0.258	0.158	0.405	0.248
	400-500	0.078	0.098	0.180	0.160	0.253	0.145	0.158	0.218	0.173	0.095	0.240	0.175
	300-400	0.288	0.185	0.275	0.205 B	0.365	0.383	0.303	0.300 AB	0.300	0.200	0.228	0.403 A
	200-300	0.580	0.495	0.720	0.690	0.648	0.000	0.373	0.545	0.458	0.475	0.413	0.660
	100-200	1.338 A	0.975	1.768 A	1.718	1.130 AB	0.000	0.745 B	1.040	0.895 B	0.773	0.880 B	1.120
	50-100	1.105 A	0.858	1.578 A	1.740 A	0.975 AB	0.040	0.688 B	0.840 B	0.828 B	0.705	0.750 B	0.910 B
	20-50	0.000	0.000	0.000	0.000	0.000	0.695	0.000	0.000	0.000	0.000	0.000	0.000

Lower case letters represent significant differences ($p < 0.10$) between rainfall amounts within scales and uppercase letters represent significant differences ($p < 0.10$) between scales within rainfall. Differences were checked by Tukey HSD test in case of homoscedasticity, otherwise, DTK test was applied

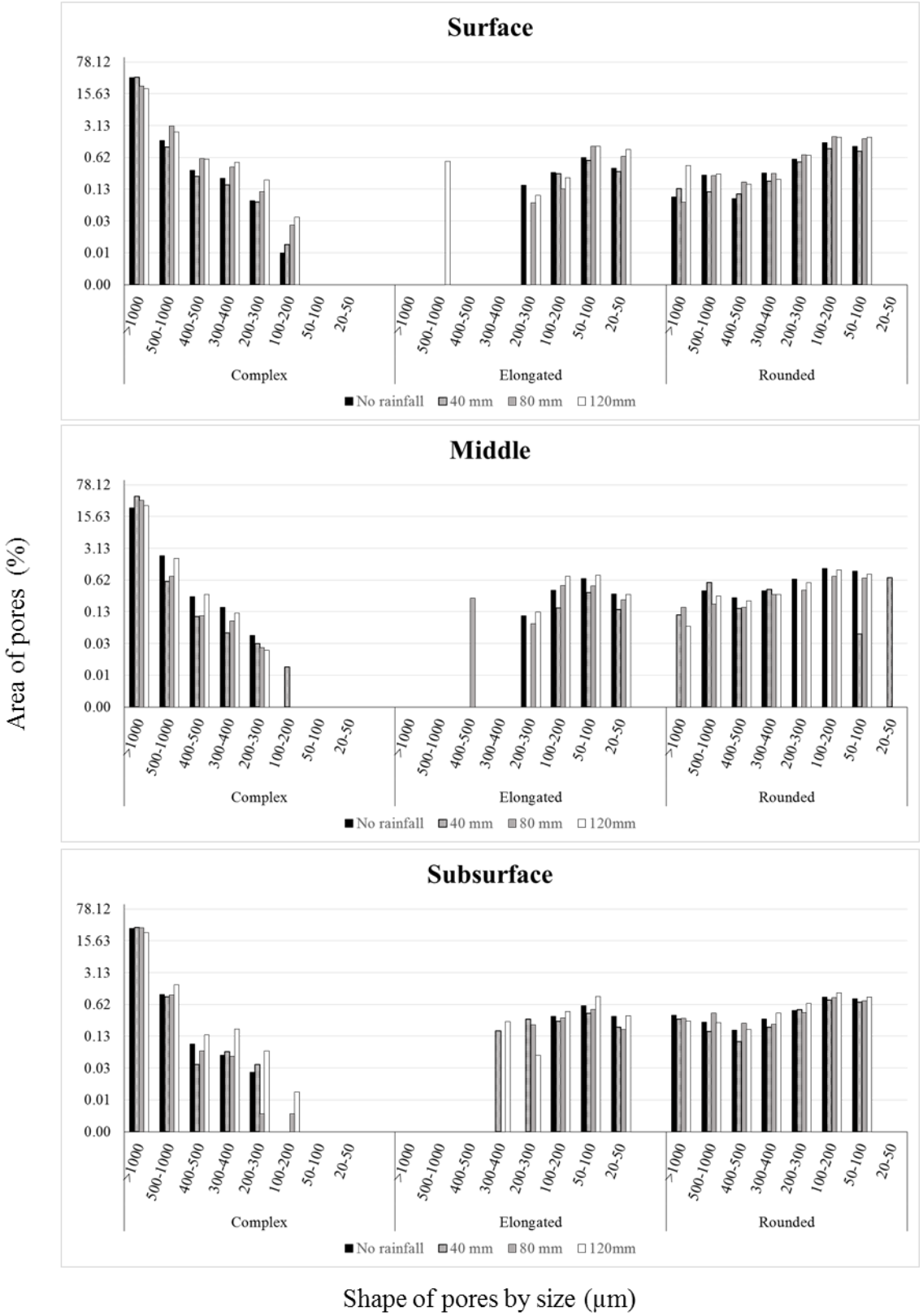

Figure 15 - Distribution of area of pores by shape and size in a Rhodic Kandiudalf before (No-rainfall) and after rainfall simulations (40, 80 and 120 mm). Results are averages from quadruplicate soil blocks having triplicate images within rainfall amount and depth of measurement. Images were taken, parallel to the real surface of the soil, for three depths,: surface (0-10 mm), middle (20- 30 mm) and subsurface (40 – 50 mm)

Another important factor, that must be take into account in the discussion of pore connectivity, is the number of pores. For example, if a soil has a high percentage of area covered by complex pores with diameter larger than 1000 μm, but these are divided into 100 units, it is easy to understand that this pore system would be little connected when compared to one with same area but represented by only 10 units. The idea of connectivity is important in a conservationist point of view, since it allows the soil to infiltrate and percolate water more easily and faster, increasing the initiation time and diminishing the volume of runoff.

The number of pores by type and size are found in Table 10 and the graphical representation is in Figure 16. Again differences ($p < 0.01$) between rainfall amounts occurred only at the surface, with an increase of the number of complex (200 – 400 μm and 500 – 1000 μm), elongated (20 – 50 μm) and rounded (50 – 100 μm) pores. As stated in the area of pores discussion above, the fact that the area of big complex pores was significantly diminished and divided between the types cited above (smaller complex, elongated and rounded pores), one can infer that rainfall is indeed decreasing connectivity at the surface, attributing this to the soil surface sealing process. We note that several size classes are empty, which make it plausible to summarize them into broader size classes to facilitate interpretation. In Table 11, and Figure 17 and Figure 18, we find the same dataset divided into three size classes (large, medium and small). Some differences ($p < 0.10$) are not observed as before, especially because variances within each class are increased. However, the average presented in each condensed class has similar behavior as to the one of the previous classes. At the surface, there is a linear decrease of large complex pores with rainfall increase, followed by a significant ($p < 0.01$) increase in the area of medium complex, medium elongated, small elongated and small rounded pores. Differences ($p < 0.10$) between depths occur primarily after 80 mm of rainfall. Number of pores at the surface increase ($p < 0.10$) substantially with rainfall volume, especially the small rounded ones. Important to note that, after 120 mm of rainfall, the number of pores in several classes is bigger ($p < 0.10$) then the one at the same rainfall in a deeper layer. This shows how significantly the structure has changed at surface due to sealing.

Table 10 - Distribution of number of pores by format and size in a Rhodic Kandiudalf before (No-rainfall) and after rainfall simulations (40, 80 and 120 mm). Results are averages from quadruplicate soil blocks having triplicate images within rainfall amount and depth of measurement. Images were taken, parallel to the real surface of the soil, for three depths,: surface (0-10 mm), middle (20- 30 mm) and subsurface (40 – 50 mm)

Type of pores by diameter (μm)		Top				Middle				Bottom			
		No rainfall	40 mm	80 mm	120mm	No rainfall	40 mm	80 mm	120mm	No rainfall	40 mm	80 mm	120mm
		Number of pores											
Complex	>1000	4	4	5	4	5	4	4	3	4	2	4	4
	500-1000	5 ab	4 B	10 aA	8 ab	6	2	2 B	6	3	2	2 B	5
	400-500	2	2	5 A	4 A	2	1	1 B	2 B	1	0	0 B	1 B
	300-400	2 abA	2 b	4 abA	6 a	2 AB	1	1 AB	1	0 B	1	0 B	2
	200-300	2	2	2 A	4 A	0	0	0 B	0 B	0	0	0 B	1 AB
	100-200	0	0	1 A	1 A	0	0	0 B	0 B	0	0	0 B	0 B
	50-100	0	0	0	0	0	0	0	0	0	0	0	0
	20-50	0	0	0	0	0	0	0	0	0	0	0	0
Elongated	>1000	0	0	0	0	0	0	0	0	0	0	0	0
	500-1000	0	0	0	0	0	0	0	0	0	0	0	0
	400-500	0	0	0	0	0	0	0	0	0	0	0	0
	300-400	0	0	0	0	0	0	0	0	0	0	0	0
	200-300	0	0	0	0	0	0	0	0	0	0	0	0
	100-200	1	1	1	1	2	0	2	2	2	1	1	2
	50-100	8	7	16 A	15	8	4	6 B	10	7	5	6 B	12
	20-50	18 b	15 b	30 abA	47 aA	15	7	10 B	14 B	17	9	10 B	17 B
Rounded	>1000	0	0	0	0	0	0	0	0	0	0	0	0
	500-1000	1	0	1	1	1	0	1	1	1	0	2	1
	400-500	0	1	1	1	2	0	2	2	2	0	2	1
	300-400	4	2	4	3 B	5	2	4	4 AB	4	3	3	5 A
	200-300	16	13	20	19	18	10	10	15	12	13	11	18
	100-200	114 A	82	152 A	150	94 AB	58	64 B	87	76 B	66	74 B	94
	50-100	350 abA	270 b	501 abA	556 aA	311 AB	174	218 B	264 B	264 B	226	240 B	288 B
	20-50	0	0	0	0	0	0	0	0	0	0	0	0

Lower case letters represent significant differences ($p < 0.10$) between rainfall amounts within scales and uppercase letters represent significant differences ($p < 0.10$) between scales within rainfall. Differences were checked by Tukey HSD test in case of homoscedasticity, otherwise, DTK test was applied

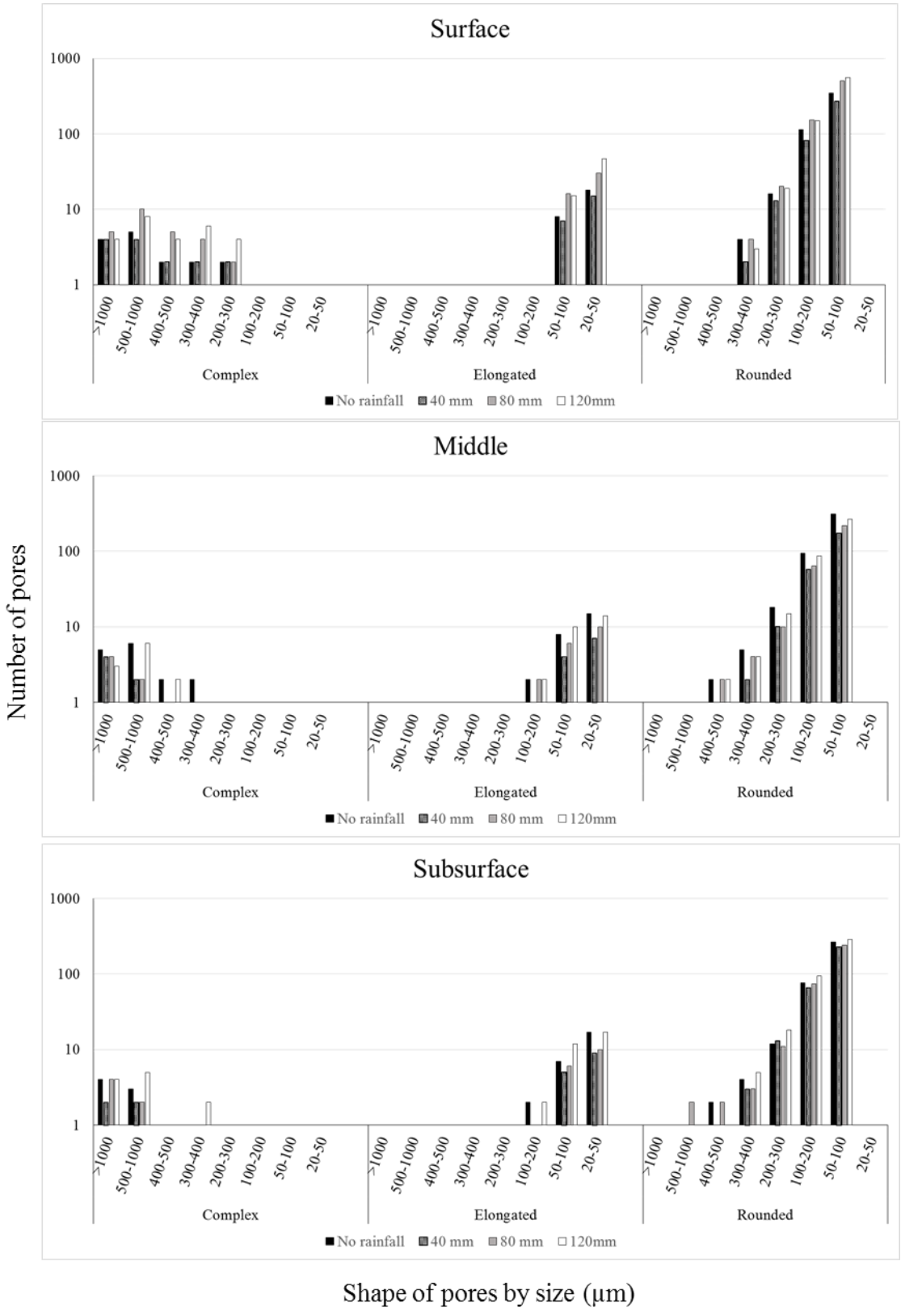

Figure 16 - Distribution of number of pores by shape and size in a Rhodic Kandiudalf before (No-rainfall) and after rainfall simulations (40, 80 and 120 mm). Results are means from quadruplicate soil blocks having triplicate images within rainfall amount and depth of measurement. Images were taken, parallel to the real surface of the soil, for three depths,: surface (0-10 mm), middle (20- 30 mm) and subsurface (40 – 50 mm)

Table 11 - Distribution of area and number of pores by shape and size classes in a Rhodic Kandiudalf before (No-rainfall) and after rainfall simulations (40, 80 and 120 mm). Results are means from quadruplicate soil blocks having triplicate images within rainfall amount and depth of measurement. Images were taken, parallel to the real surface of the soil, for three depths,: surface (0-10 mm), middle (20- 30 mm) and subsurface (40 – 50 mm)

Type and class of pores		Surface				Middle				Subsurface			
		No rainfall	40	80	120	No rainfall	40	80	120	No rainfall	40	80	120
		(%)											
Complex	large	36.99	36.95	24.95	22.58	26.77	43.77	35.84	29.01	30.65	31.73	31.34	28.80
	medium	0.47 A	0.36	0.90 A	1.00 A	0.29 B	0.13	0.13 B	0.27 B	0.12 C	0.11	0.20 B	0.29 B
	small	0.00	0.00	0.00	0.00	0.00	0.00	0.00	0.00	0.00	0.00	0.00	0.00
Elongated	large	0.57	0.35 AB	0.41	0.53 B	0.59	0.18 B	0.87	0.95 AB	0.53	0.84 A	0.62	1.03 A
	medium	0.80	0.72	1.72 A	1.76	0.83	0.41	0.53 B	0.91	0.69	0.48	0.56 B	0.87
	small	0.05	0.04	0.09 A	0.13	0.04	0.02	0.03 B	0.04	0.06	0.02	0.03 B	0.03
Rounded	large	0.39	0.29	0.48	0.46	0.50	0.13	0.37	0.393	0.85	0.52	0.77	0.78
	medium	1.57	1.24	2.02	1.85	1.71	0.87	1.09	1.46	1.29	1.06	1.25	1.66
	small	1.77 abA	1.32 b	2.59 aA	2.77 aA	1.52 AB	0.94	1.09 B	1.37 B	1.28 B	1.07	1.19 B	1.37 B
		number of pores											
Complex	large	10 ab	8 b	16 aA	14 ab	12	6	6 B	10	7	5	6 B	10
	medium	6 A	5	10 A	14 A	4 B	2	2 B	3 B	2 C	2	1 B	4 B
	small	0	0	0	0	0	0	0	0	0	0	0	0
Elongated	large	2	2	2	2	2	1	2	4	2	2	2	3
	medium	20 B	18 ab	39 aA	45 abA	18	8	13 B	18 B	16	11	12 B	20 B
	small	6 ab	4 b	7 Ab	15 aA	4	2	4	4 B	6	2	4	4 B
Rounded	large	1	1	2	2	2	0	2	2	2	1	2	2
	medium	59	45	75 A	68	56	32	36 B	51	42	39	40 B	54
	small	424 abA	323 b	603 aA	662 aA	372 AB	212	260 B	319 B	316 B	269	289 B	327 B

Lower case letters represent significant differences ($p < 0.10$) between rainfall amounts within scales and uppercase letters represent significant differences ($p < 0.10$) between scales within rainfall. Differences were checked by Tukey HSD test in case of homoscedasticity, otherwise, DTK test was applied

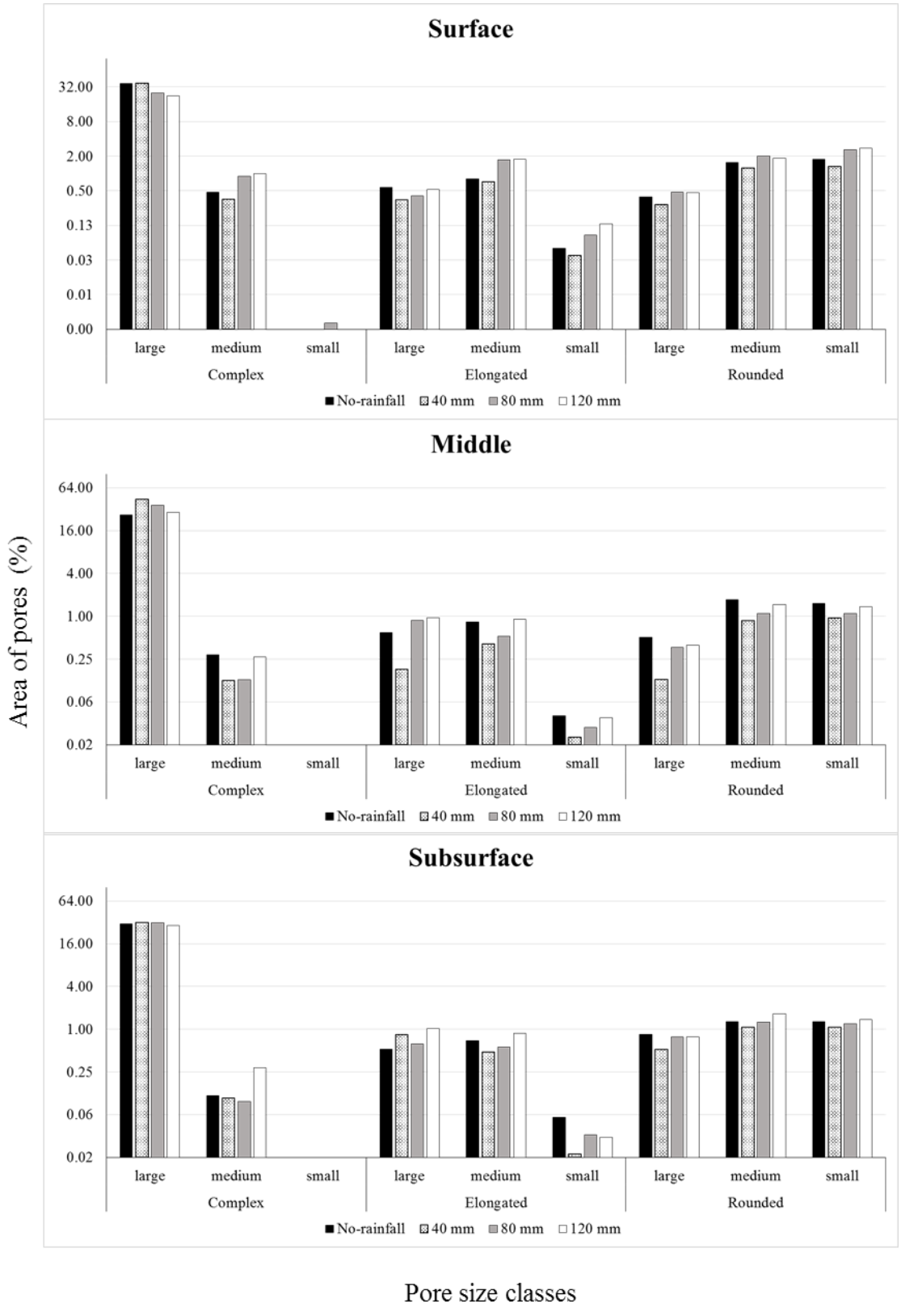

Figure 17 - Distribution of area of pores by shape and size classes in a Rhodic Kandiudalf before (No-rainfall) and after rainfall simulations (40, 80 and 120 mm). Results are means from quadruplicate soil blocks having triplicate images within rainfall amount and depth of measurement. Images were taken, parallel to the real surface of the soil, for three depths,: surface (0-10 mm), middle (20- 30 mm) and subsurface (40 – 50 mm)

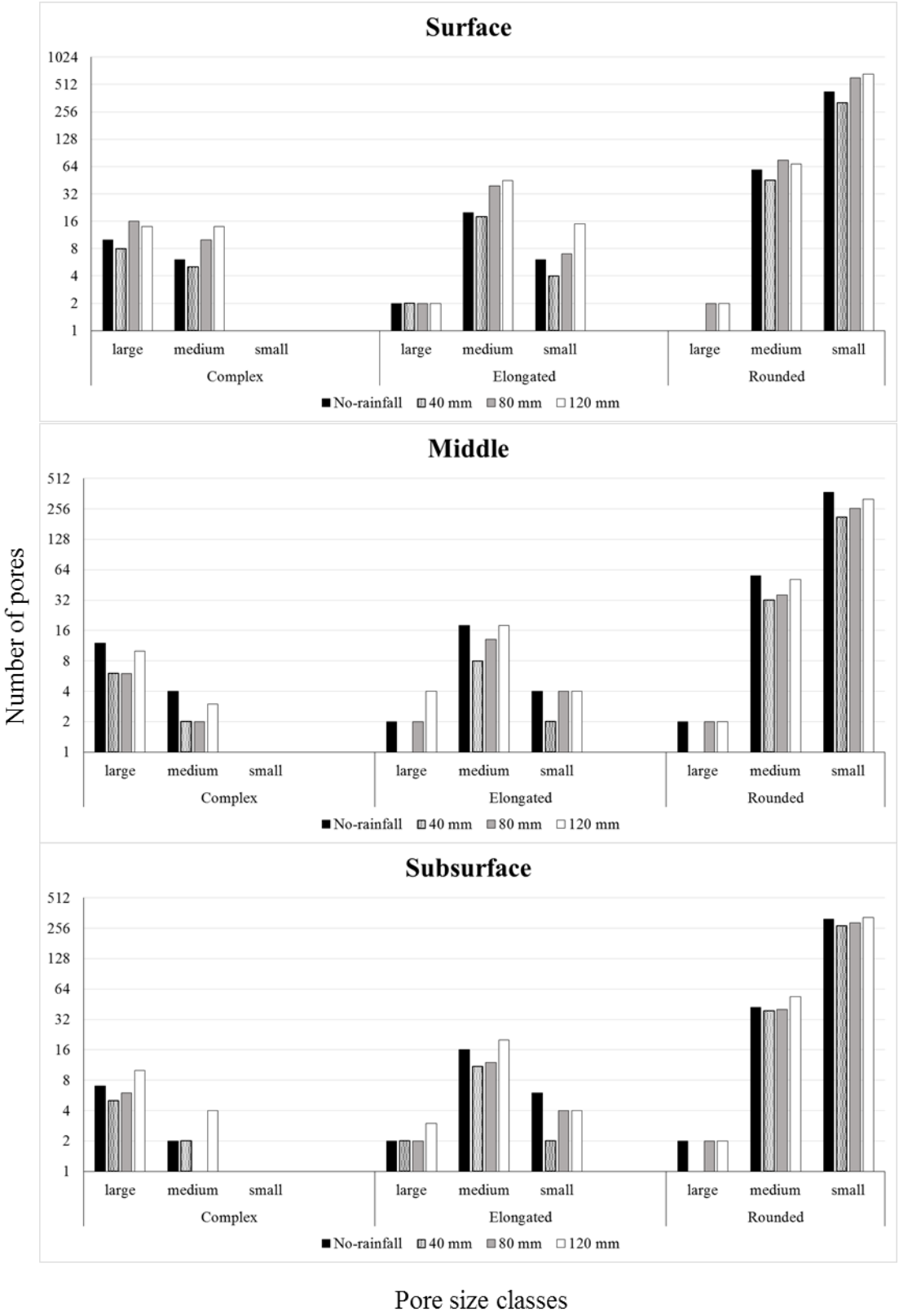

Figure 18 - Distribution of number of pores by shape and size classes in a Rhodic Kandiudalf before (No-rainfall) and after rainfall simulations (40, 80 and 120 mm). Results are means from quadruplicate soil blocks having triplicate images within rainfall amount and depth of measurement. Images were taken, parallel to the real surface of the soil, for three depths,: surface (0-10 mm), middle (20- 30 mm) and subsurface (40 – 50 mm)

2.3.4.2 Multifractal analyses of pores

When we first look at the average multifractal spectra by rainfall amount and depth (Figure 19) is a little difficult to observe a standard behavior according to rainfall. At surface, the spectrum after 120 mm of rainfall presents the minimum *f(α)* at both left and right side, and also the wider *α* range, which could mean that sealing causes an increase on the fragmentation of the pore system, with big pores becoming less frequent along the system (i.e. smaller *f(α)* at left side) at same time small pores become more frequent, since this is the only treatment that presents a right spectrum side. In the subsequent layer, after the first rainfall (40 mm) the pores became less fragmented, reaching higher *f(α)* values for most part of the spectra. At subsurface all treatments were much more similar. All rainfall amounts induced a more fragmented left side, indicating that big pores distribution did not change at this layer with increasing rainfall. At the same time, the spectrum before rainfall had a wider right side, which could mean that, for this treatment, small pores are more equally distributed along scales. Other interpretations are difficult to be made only by a visual approach. Thus, we now take our attention to the parameters contained in Table 12.

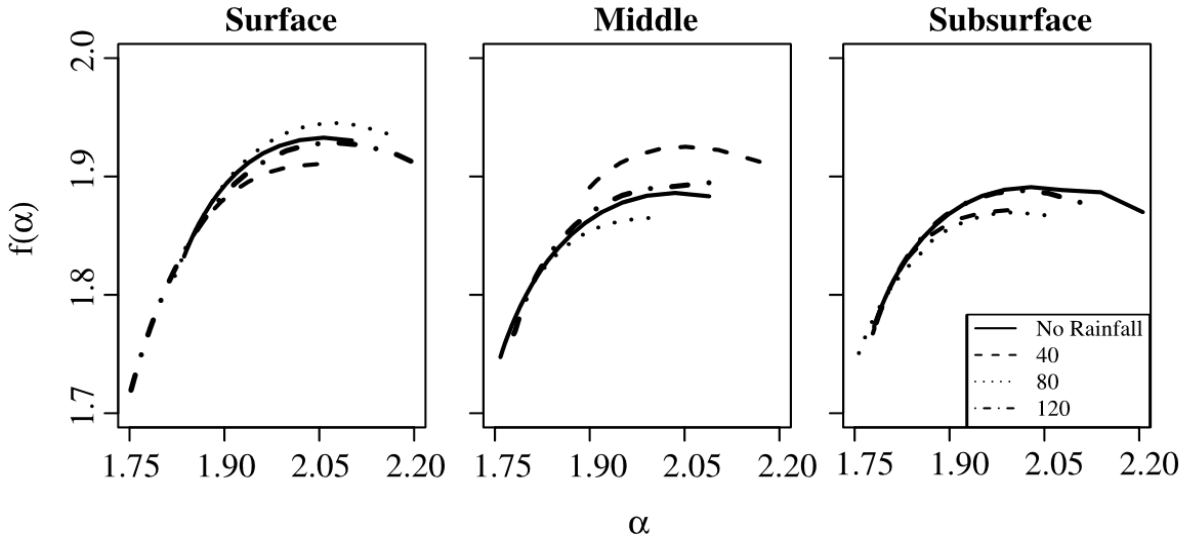

Figure 19 – Multifractal spectra of area of pores from a Fine Rhodic Kandiudalf before (No rainfall) and after rainfall simulations (40, 80 and 120 mm), obtained from the average of triplicate images of quadruplicates blocks of soil. Soil blocks were impregnated and images taken in three depths, parallel to the real surface of the soil: surface (0-10 mm), middle (20- 30 mm) and subsurface (40 – 50 mm)

At surface, differences ($p < 0.10$) with rainfall increase occurred positively for *D0-D1*, *D0-D2*, *D1-D2*, *LΔf(α)* and *ΔLα*, and negatively for $Lf(\alpha)_{min}$ and α_{min}. *D1* is the entropy dimension, following the information entropy definition (SHANNON; WEAVER, 1949). Thus, *D1* represents the heterogeneity of the system (MARTÍNEZ et al., 2009), since it measures the decrease in information as the box size increase during the box-counting

analysis (POSADAS et al., 2003). A decrease in *D1* when compared to *D0*, i.e., an increase in *D0-D1*, implicates an increase in heterogeneity. As mentioned in the soil roughness discussion section, *D2* represents the correlation of the measure contained in a L size box (POSADAS et al., 2003). Therefore, a decrease in *D2* with regard to *D0*, i.e., *D0-D2*, implicates diminishing correlation, and in comparison to *D1*, i.e., *D1-D2*, means that correlation drops faster than the rate in which information is lost. Rainfall caused an increase in heterogeneity, noted by *D0-D1* (0.07, 0.07, 0.09 and 0.10), and a decrease in correlation marked by *D0-D2* (0.15, 0.14, 0.21 and 0.21). The fact that *D0* did not change significantly shows that the system's average is not altered, which would mean that all changes are related to the displacement between small and big pores distributions, without big changes in the total area of pores. This agrees with the summarized micromorphometrical results, where, while no differences ($p > 0.10$) were found for area of pores on most of the sizes (large, medium and small) and classes (complex, elongated and rounded), there were several differences ($p < 0.10$) in the number of pores, indicating an increase in the fragmentation of the porosity with rainfall increase.

Rainfall also increased *D1-D2* intervals (0.07, 0.06, 0.12 and 0.11). While large complex pores decreased most in area, the increase in the number of pores was more pronounced for the class of small rounded ones, going from 424 before rainfall, to 662 after 120 mm (Table 11). Considering the creation of new rounded pores from the collapse of big complex pores as spatial dependent, and that spots where the structure is weaker are going to fade more easily and faster than others, we can imagine that the final geometry of the pore system is going to be unequally distributed. Therefore, correlation between different regions would drop fast with increasing rainfall. In contrast, *D1* gives the probability of pore occupation of the *i*th L size box without considering the way they are distributed (VÍDAL VAZQUEZ et al., 2008). Thus, even if information loss along scales is affected by rainfall, any geometrical distribution would promptly affect *D2*, making it to drop faster than *D1*. Vidal Vázquez et al. (2008) also used the multifractal formalism to evaluate changes caused by rainfall, but with regard to the pores size distribution obtained by Hg porosimetry. Their results were very similar for *D1*, *D0-D1* and $Lf(\alpha)_{min}$. However, their differences for *D2* were not significant ($p < 0.5$).

Table 12 – Multifractal parameters calculated from area of pores of a fine Rhodic Kandiudalf before (No-rainfall) and after rainfall simulations (40, 80 and 120 mm), obtained from the average of triplicate images of quadruplicates blocks of soil. Soil blocks were impregnated and images taken in three depths, parallel to the real surface of the soil: surface (0-10 mm), middle (20- 30 mm) and subsurface (40 – 50 mm)

Multifractal parameters	Surface				Middle				Subsurface			
	No-rainfall	40 mm	80 mm	120 mm	No-rainfall	40 mm	80 mm	120 mm	No-rainfall	40 mm	80 mm	120 mm
D0	1.93 A	1.91 A	1.95 A	1.93 A	1.89 bB	1.93 aA	1.86 bB	1.89 abB	1.89 B	1.87 B	1.87 B	1.89 B
D1	1.86 A	1.84 AB	1.86 A	1.83	1.80 bB	1.86 aA	1.81 bB	1.82 ab	1.81 B	1.81 B	1.79 B	1.82
D2	1.80 A	1.79	1.74	1.72	1.72 bB	1.81 a	1.75 B	1.76 b	1.74 B	1.76	1.73	1.71
D0-D1	0.07 b	0.07 B	0.09 ab	0.10 aA	0.09	0.07	0.07	0.08 AB	0.08	0.06	0.08	0.07 B
D0-D2	0.15 b	0.14 B	0.21 aA	0.21 aA	0.16	0.13	0.12 B	0.14 B	0.15	0.11	0.14 B	0.17 AB
D1-D2	0.07 b	0.06 B	0.12 aA	0.11 aA	0.07	0.05	0.05 B	0.06 B	0.07 ab	0.04 b	0.06 abB	0.08 abAB
$Rf(\alpha)_{min}$	1.70 B	1.72	1.65 B	1.67	1.82 aA	1.71 ab	1.77 abAB	1.68 b	1.74 AB	1.82	1.79 A	1.71
$Lf(\alpha)_{min}$	1.74 ab	1.78 A	1.50 bB	1.56 bB	1.69 b	1.80 a	1.73 abA	1.74 abA	1.73	1.78	1.73 A	1.70 AB
$R\Delta f(\alpha)$	0.23 A	0.19 AB	0.29 A	0.26	0.07 bB	0.21 aA	0.09 abB	0.21 ab	0.15 AB	0.05 B	0.08 B	0.18
$L\Delta f(\alpha)$	0.19 b	0.13 B	0.44 aA	0.37 aA	0.20	0.13	0.13 B	0.15 B	0.17 a	0.09 b	0.14 abB	0.19 abB
$f(\alpha)_{ratio}$	1.39 A	1.21	0.75	0.84	0.38 bB	1.71 a	0.79 ab	1.53 ab	1.10 AB	0.60	0.89	1.41
α_{min}	1.80 aA	1.80 A	1.71 b	1.70 b	1.73 bB	1.82 a	1.76 ab	1.77 ab	1.76 AB	1.79	1.75	1.75
α_{max}	2.55	2.50 A	2.62 A	2.62	2.31 b	2.57 aA	2.29 abB	2.51 ab	2.41	2.17 B	2.25 B	2.43
$\Delta\alpha$	0.75	0.70 A	0.91 A	0.92	0.57	0.75 A	0.53 B	0.74	0.65	0.38 B	0.50 B	0.68
$\Delta R\alpha$	0.49 A	0.45 A	0.55 A	0.55	0.27 bB	0.52 aA	0.30 abB	0.47 ab	0.38 AB	0.18 B	0.25 B	0.42
$\Delta L\alpha$	0.26 b	0.25 B	0.36 aA	0.37 aA	0.30	0.23	0.23 B	0.26 B	0.27	0.20	0.25 B	0.26 B
α_{ratio}	1.96 A	1.67 AB	1.55	1.59	0.91 bB	2.24 aA	1.20 ab	1.78 ab	1.47 AB	0.84 B	1.11	1.71
q_{min}	-0.6 abB	-0.5 aB	-0.8 bB	-0.7 ab	-0.3 aA	-0.5 Bb	-0.4 abA	-0.5 ab	-0.5 abAB	-0.2 aA	-0.3 abA	-0.6 b
q_{max}	3.6 ab	2.5 B	5.3 aA	4.4 aA	3.5	2.7	2.7 B	3.1 AB	3.3	2.3	2.8 B	3.0 B

Lower case letters represent significant differences ($p < 0.10$) between rainfall amounts within depths and uppercase letters represent significant differences ($p < 0.10$) between depths within rainfall. Differences were checked by Tukey HSD test in case of homoscedasticity, otherwise, DTK test was applied. RR_i: random roughness index; *D0*: capacity dimension; *D1*: entropy dimension; *D2*: correlation dimension; $Rf(\alpha)_{min}$: minimum Hausdorff dimension at right of *D0*; $Lf(\alpha)_{min}$: minimum Hausdorff dimension at left of *D0*; $\Delta Rf(\alpha)$: range of Hausdorff dimensions at right of *D0*; $\Delta Lf(\alpha)$: range of Hausdorff dimensions at left of *D0*; $f(\alpha)_{ratio}$: ratio between $\Delta Rf(\alpha)$ and $\Delta Lf(\alpha)$; α_{min}: minimum Lipschitz-Holder exponent; α_{max}: maximum Lipschitz-Holder exponent; $\Delta\alpha$: the complete range of Lipschitz-Holder exponents; $\Delta R\alpha$: range of Lipschitz-Holder exponents at right of *D0*; $\Delta L\alpha$: range of Lipschitz-Holder exponents at left of *D0*; α_{ratio}: ratio between $\Delta R\alpha$ and $\Delta L\alpha$; q_{min}: minimum generalized dimension; q_{max}: maximum generalized dimension

Other parameters from the left side of the spectrum that also increased ($p < 0.10$) with rainfall are $L\Delta f(\alpha)$ and $\Delta L\alpha$, while, in contrast, $Lf(\alpha)_{min}$ and α_{min} decreased. The left side shows the Hausdorff dimensions and the Lipschitz-Holder exponents related to the large pores. A decrease in $Lf(\alpha)_{min}$ indicates an increase on the fragmentation of large pores, which was discussed before considering *D1* and *D2*. The decrease of α_{min} was followed by the increase of $\Delta L\alpha$, i.e., there was no displacement of $\alpha(f(\alpha)_{max})$. This shows that the scale relation for the fragmentation of large pores has also changed. Narrower α ranges are related to more homogeneous pore systems (POSADAS et al. 2003; VIDAL VÁZQUEZ et al., 2010), where, sometimes, *D0* is enough to represent the whole system. Increasing $\Delta L\alpha$ followed by a decrease in $Lf(\alpha)_{min}$ indicate that larger pores were fragmented into smaller pores, which are distinguished from the previous class by featuring a distinct degree of fractality, i.e., a different Hausdorff dimension.

When we examine the middle layer, more differences ($p < 0.10$) are noted: *D0*, *D1*, *D2*, $Rf(\alpha)_{min}$, $Lf(\alpha)_{min}$, $R\Delta f(\alpha)$, $f(\alpha)_{ratio}$, α_{min}, α_{max}, $\Delta R\alpha$ and α_{ratio}. However, these differences look random at first, i.e., they do not follow a trend across rainfall amount. Nevertheless, this is further evidence that, during the sealing process, changes do occur at deeper layers, even if it is difficult to find a pattern. What we note is that, instead of a linear trend, most differences occur after the first rainfall (40 mm). *D0*, *D1* and *D2* reach their maximum after this rainfall amount. As explained before, *D1* and *D2* increase implicates in a decrease in information loss over scales and an increase in correlation between different regions of the measure, respectively. Posadas et al. (2003) found high correlations between *D0* and total area of pores. Since *D0* is the average Hausdorff dimension of the system, which represents the underlying fragmentation process, this is expected to happen. The middle layer had a much higher percentage of pores area after 40 mm of rainfall (46.45 %) when compared to other treatments (32.25, 39.96 and 34.40 %).

Many other parameters follow the same behavior, by peaking ($Lf(\alpha)_{min}$, $f(\alpha)_{ratio}$, α_{min} and α_{ratio}) after 40 mm of rainfall. In contrast, $Rf(\alpha)_{min}$ decreases with rainfall input, reaching its minimum after 120 mm of rainfall. $Rf(\alpha)_{min}$ is the Hausdorff dimension, i.e. the fragmentation index, of very small pores. Thus, a decreasing $Rf(\alpha)_{min}$ indicate a reduction of the contribution of small pores, i.e., the area of small pores is reduced. This corroborates in parts the micromorphometrical data, since smaller $Rf(\alpha)_{min}$ after 40 mm of rainfall (1.82, 1.71, 1.77 and 1.68) is paired with smaller area covered by small elongated (0.04, 0.02, 0.03 and 0.04) and rounded (1.52, 0.94, 1.09 and 1.37) pores. In the case of 120 mm, even if the area of these

classes of pores increase when compared to 80 mm, we note that the number of pores in such classes also increase, which also interferes in the fragmentation of the system.

At the deepest layer (subsurface) two parameters of the left side of the spectra presented differences ($p < 0.10$) with rainfall increase (*D1-D2*, $L\Delta f(\alpha)$). However attentions must be paid to the significance of the differences for q_{min} values. While differences were significant ($p < 0.10$) for q_{min} in all layers, two facts contributed to the lack of discussion of this parameter in other depths. First, differences were less pronounced at surface and middle, with ranges of 0.3 and 0.2, respectively, than at subsurface, ranging 0.4. Secondly, the magnitude and order of parameters from the left side did not always accompanied the differences between q_{min} values at upper layers. For example, at surface, the minimum $Lf(\alpha)_{min}$ was 1.78, even with when $L\Delta f(\alpha)$ was the shortest.

Considering this last statement, is important to remember that fragmentation is a measure of two things: the filling capacity of a process, i.e., larger the area covered by the object, larger its Hausdroff dimension is; and the degree of brokenness, i.e. more divided the object is in the system, smaller its Hausdroff dimension is. The results above for the porosity of a Rhodic Kandiudalf, measured by two-dimensional image analysis, seems to demonstrate that most multifractal parameters are associated not only to the area of pores, but also to the number of pores at each level of size and shape.

The differences ($p < 0.10$) between depths within each rainfall amount show that the surface had higher values when compared to the underlying layers of soil, for all the left side parameters, while the contrary holds for some parameters of the right side. Most of the time, the middle layer was the opposite of the surface. For example, while D0, D1 and D2 had the highest values at surface before rainfall (1.93,1.86 and 1.80), the middle had the lowest (1.89, 1.80 and 1.72), while the subsurface got intermediate values (1.89,01.81,1.74). This just indicates that, at surface, the area of big pores was higher during all rainfalls, which corroborates some of the micromorphometrical results. The middle layer works as a transition between a very opened surface, i.e. a layer with high percentage of pores, to a mild fragmented subsurface. When rainfall starts to act on the soil, transformations seems to be more pronounced in this transition, especially on the right side of the spectrum. This means that, although this layer has smaller pores, those are less stable than the ones at the surface, since particles tend to close more the pores at this layer than at surface.

3 CONCLUSIONS

The multifractal spectra is sensitive to structure changes caused by rainfall. Considering the soil surface roughness, the multifractal parameterization is useful to evaluate modifications, caused by rainfall, on very fine scales. However, for the soil of this study, it is not possible to use the multifractal approach in datasets with resolutions coarser than 10 mm, since a pattern could not be found in such scale, i.e., MRM. There seems to be a relation between decreasing grid resolution and increase in randomness of heights, since other classical index, i.e., RR_i, also could not distinguish changes provoked by rainfall. The multifractal behavior of this soil is not distinguishable ($p < 0.10$) between measurements made at minimum resolutions of 0.074 mm and 0.5 mm. Therefore, is more convenient to use the device that work closer to the upper part of this range, i.e., MLT, for two reasons: its lower cost and greater area coverage. Considering the area and number of pores, obtained by micromorphometrical techniques, the multifractal behavior changed according to sealing development and depth of measurement, being sensitive to the changes in the pores size distribution and their fragmentation degree within each size class. Whereas this soil presents dominant complex pores across rainfall amounts and layers, it is not possible to correlate any spectra parameter to pores shape modification.

Some multifractal parameters are suitable for modeling steps of soil surface degradation by rainfall. The Hausdorff dimensions at the left side of the spectrum are the parameters most sensitive to physical changes related to rainfall erosion. $Lf(\alpha)_{min}$, $L\Delta f(\alpha)$ and *D2* were the parameters that often showed a linear behavior with increasing rainfall amount, considering both surface roughness and area of pores measurements. However, *D2* from porosity was not different ($p > 0.10$) along rainfall amounts at surface. In this case, *D0-D1*, *D0-D2* and *D1-D2* presented as parameters that could be used to describe the changes in the pore system.

REFERENCES

ANDERSLAND, O.B.; WIGGERT, D.C.; DAVIES, S.H. Frozen soil subsurface barriers: formation and ice erosion. **Journal of Contaminant Hydrology,** Amsterdam, **v.** 23, n. 1/2, p. 133–47, 1996.

ALLMARAS, R.R.; BURWELL, R.E.; LARSON, W.E.; HOLT, R.F.; NELSON, W.W. **Total porosity and random roughness on the interrow zone as influenced by tillage.** Washington: USDA, Agriculture Research Service, 1966. 22 p. (Conservation Research Report, 7).

ANDERSON, J.M.; INGRAM, J.S.I. **Tropical soil biology and fertility:** a handbook of methods. Wallingford: CAB International, 1992. 171 p.

ANDERSON, S.H.; PEYTON, R.L.; GANTZER, C.J. Evaluation of constructed and natural soil macropores using X-ray computed-tomography. **Geoderma,** Amsterdam, v. 46, n. 1/3, p.13-29, 1990.

ANDERSON, S.H.; PEYTON, R.L.; WIGGER, J.W.; GANTZER, C.J. Influence of Aggregate Size on Solute Transport as Measured Using Computed Tomography. **Geoderma,** Amsterdam, v. 53, n. 3, p. 387–98, 1992.

ASSOULINE, S.; BEN-HUR, M. Effects of rainfall intensity and slope gradient on the dynamics of interrill erosion during soil surface sealing. **Catena,** Amsterdam, v. 66, n. 3, p. 211–20, 2006.

BALL, B.C.; CAMPBELL, D.J.; DOUGLAS, J.T.; HENSHALL, J.K.; O'SULLIVAN, M.F. Soil structural quality, compaction and land management. **European Journal of Soil Science**, Malden, v. 48, n. 4, p. 593–601, 1997.

BAYAT, H., DAVATGAR, N.; JALALI, M. Prediction of CEC using fractal parameters by artificial neural networks. **International Agrophysics,** Lublin, v. 28, n. 2, p.143–52, 2014.

BERGSMA, E.; CHARMAN, P.; GIBBONS, F.; HURNI, H.; MOLDENHAUER, W.C.; PANICHAPONG, S. **Terminology for soil erosion and conservation:** concepts, definitions and multilingual list of terms for soil erosion and conservation in English, Spanish, French and German. Wageningen: Grafisch Service Centrum, 2000. 313 p. (Reprinted)

BERTONI, J.; LOMBARDI NETO, F. **Conservação do solo.** São Paulo: Ícone, 2005. 355 p.

BERTUZZI, P., RAUWS, G.; COURAULT, D. Testing roughness indices to estimate soil surface roughness changes due to simulated rainfall. **Soil and Tillage Research,** Amsterdam, v. 17, n. 1, p. 87–99, 1990.

BESICOVITCH, A.S. On linear sets of points of fractal dimension. **Mathematische Annalen, New York**, v. 101, n. 1, p. 161–193, 1929.

BESICOVITCH, A.S.; URSELL, H.D. Sets of fractional dimensions (V): on dimensional numbers of some continuous curves. **Journal of the London Mathematical Society,** London, v. 12, n. 1, p. 18–25, 1937.

BIEGANOWSKI, A.; CHOJECKI, T.; RYZAK, M; SOCHAN, A.; LAMORSKI, K. Methodological aspects of fractal dimension estimation on the basis of particle size distribution. **Vadose Zone Journal,** Madison, v. 12, n. 1, 2013.

BODDY, L., WELLS, J.M.; CULSHAW, C.; DONNELLY, D.P. Fractal analysis in studies of mycelium in soil. **Geoderma,** Amsterdam, v. 88, n. 3–4, p. 301–28, 1999.

BORSELLI, L., TORRI, D.; POESEN, J.; SANCHIS, P.S. Effects of water quality on infiltration, runoff and interrill erosion processes during simulated rainfall. **Earth Surface Processes and Landforms**, Chichester, v. 26, n. 3, p. 329–42, 2001.

BORSELLI, L.; TORRI, D. Soil roughness, slope and surface storage relationship for impervious areas. **Journal of Hydrology,** Amsterdam, v. 393, p. 389–400, 2010.

BOUMA, J.; JONGERIUS, A.; BOERSMA, O.; JAGER, A.; SCHOONDERBEEK, D. Function of different types of macropores during saturated flow through 4 swelling soil horizons**. Soil Science Society of America Journal,** Madison, v. 41, n. 5, p. 945-950, 1977.

BURWELL, R.E.; LARSON, W.E. Infiltration as influenced by tillage-induced random roughness and pore space. **Soil Science Society of America Proceedings,** Madison, v. 33, p. 449-452, 1969.

BURWELL, R.E.; ALLMARAS, R.R.; AMEMIYA, M. A Field measurement of total porosity and surface micro relief of soils. **Soil Science Society of America Proceedings,** Madison, v. 27, n. 6, p.697-700, 1963.

CARVALHO, A. C. P; História da Tomografia Computadorizada, **Revista da Imagem**, São Paulo, v. 29, n. 2, p. 61-66, 2007.

CASTILHO, S.C.P.; COOPER, M.; JUHÁSZ, C.E.P. Influence of crust formation under natural rain on physical attributes of soils with different textures. **Revista Brasileira de Ciência do Solo,** Viçosa, v. 35, p. 1893-1905, 2011.

CASTRO, L.G.; COGO, N.P.; VOLK, L.B.D. Alterations in soil surface roughness by tillage and rainfall in relation to water erosion. **Revista Brasileira de Ciência do Solo,** Viçosa, v. 30, p. 339-352, 2006.

CASTRO, S.S.; COOPER, M.; SANTOS, M.C.; VIDAL TORRADO, P. Soil micromorphology: concepts and applications. **Topics in Soil Science,** Viçosa, v. 3, p. 107–164, 2003.

CHESWORTH, W. (Ed.) **Encyclopedia of soil science**. Dordrecht: Springer, 2008. 902 p.

CHHABRA, A.; JENSEN, R.V. Direct determination of the f(alpha) singularity spectrum. **Physical Review Letters,** College Park, v. 62, n. 12, p. 1327-1330, 1989.

CHHABRA, A.B.; MENEVEU, C.; JENSEN, R.V.; SCREENIVASAN, K.R. Direct determination of the f (alpha) singularity spectrum and its application to fully-developed turbulence. **Physical Review A**, College Park, v. 40, n. 9, p. 5284-5294, 1989.

CHU, D. Complexity: against systems. **Theory in Biosciences,** New York, v. 130, n. 3, p. 1431-7613, 2011.

COOPER, M.; BOSCHI, R. S.; SILVA, V. B.; SILVA, L. F. S. Software for micromorphometric characterization of pores obtained from 2d image analysis. **Scientia Agricola,** Piracicaba, 2016 (in press)

CORÁ, J.E.; FERNANDES, C., BERALDO, J.M.G.; MARCELO, A.V. Use of sand for soil dispersion in granulometric analysis. **Revista Brasileira de Ciência do Solo,** Viçosa, v. 33, n. 2, p. 255–62, 2009.

CRAWFORD, J.W.; SLEEMAN, B.D.; YOUNG, I.M. On the relation between number size distributions and the fractal dimension of aggregates. **Journal of Soil Science**, Philadelphia, v. 44, n. 4, p. 555–65, 1993.

CRESTANA, S.; MASCARENHAS, S.; POZZIMUCELLI, R.S. Static and dynamic 3-dimensional studies of water in soil using computed tomographic scanning. **Soil Science,** Baltimore, v. 140, n. 5, p. 326-332, 1985.

CURRENCE, H.D.; LOVELY, W.G. The analysis of soil surface roughness. **Transactions of the American Society of Agricultural Engineering,** St. Joseph, v. 13, p. 710-714, 1970.

DALLA ROSA, J.; COOPER, M.; DARBOUX, F.; MEDEIROS, J.C. Soil roughness evolution in different tillage systems under simulated rainfall using a semivariogram-based index. **Soil and Tillage Research,** Amsterdam, v. 124, p. 226–232, 2012.

DARBOUX, F.; DAVY, P.; GASCUEL-ODOUX, C.; HUANG, C. Evolution of soil surface roughness and flowpath connectivity in overland flow experiments. **Catena**, Amsterdam, v. 46, p. 125-139, 2001.

DARBOUX, F.; HUANG, C. Does soil surface roughness increase or decrease water and particle transfers? **Soil Science Society of America Journal,** Madison, v. 69, p. 748-756, 2005.

DE GRYZE, S.; JASSOGNE, L.; SIX, J.; BOSSUYT, H.; WEVERS, M.; MERCKX, R. Pore structure changes during decomposition of fresh residue: X-ray tomography analyses. **Geoderma,** Amsterdam, v. 134, n. 1/2, p. 82-96, 2006.

DESCROIX, L.; BRRIOS, J.L.G.; VIRAMONTES, D.; POULENARD, J.; ANAYA, E.; ESTEVES, M.; ESTRADA, J. Gully and sheet erosion on subtropical mountains slopes: Their respective roles and the scale effect. **Catena**, Amsterdam, v. 72, p. 325-339, 2008.

DEXTER, A.R. Soil physical quality part I: theory, effects of soil texture, density, and organic matter, and effects on root growth. **Geoderma,** Amsterdam, v.120, p.201-214, 2004a.

DEXTER, A. R. Soil physical quality part II: friability, tillage, filth and hard-setting. **Geoderma,** Amsterdam, v.120, p.215-225, 2004b.

DEXTER, A.R.; KROESBERGEN, D.B. Methodology for determination of tensile-strength of soil aggregates. **Journal of Agricultural Engineering Research,** San Diego, v. 31, n. 2, p. 139–47, 1985.

DORAN, J.W.; COLEMAN, D.C.; BEZDICEK, D.F.; STEWART, B.A. **Defining soil quality for a sustainable environment.** Madison: Soil Science Society of America; American Society of Agronomy, 1994. 244 p. (SSSA Special Publication, 35).

DROOGERS, P.; STEIN, A.; BOUMA, J.; DE BOER, G. Parameters for describing soil macroporosity derived from staining patterns. **Geoderma,** Amsterdam, v. 83, n. 3/4, p. 293-308, 1998.

ELLIOT, T.R.; REYNOLDS, W.D.; HECK, R.J. Use of existing pore models and x-ray computed tomography to predict saturated soil hydraulic conductivity. **Geoderma,** Amsterdam, v. 156, n. 3–4, p. 133–42, 2010.

ELTZ, F.L.F.; NORTON, L.D. Surface roughness changes as affected by rainfall erosivity, tillage, and canopy cover. **Soil Science Society of America Journal,** Madison, v. 61, n. 6, p. 1746–55, 1997.

EMBRAPA. **Sistema brasileiro de classificação de solos**. Brasília: Embrapa Serviço de Produção de Informação; Rio de Janeiro: Centro Nacional de Pesquisa de Solos, Embrapa Solos, 2013. 412 p.

ERSAHIN, S.; GUNAL, H.; KUTLU, T.; YETGIN, B.; COBAN, S. Estimating specific surface area and cation exchange capacity in soils using fractal dimension of particle-size distribution. **Geoderma,** Amsterdam, v. 136, n. 3–4, p. 588–97, 2006.

FEDOTOV, G.N.; SHOBA, S.A. Current ideas on the possible pathways for the formation of humic substances in soils. **Eurasian Soil Science,** New York, v. 46, n. 12, p. 1263–69, 2013.

FERREIRA, B.A.; FABRIS, J.D.; SANTANA, D.P.; CURI, N. Iron oxides of sand and silt fractions in a nitossolo developed from basalt. **Revista Brasileira de Ciência do Solo,** Viçosa, v. 27, n. 3, p. 405–13, 2003.

FOX, J.; WEISBERG, S. **An {R} companion to applied regression**, Second Edition. Thousand Oaks CA: Sage. 2011. URL: http://socserv.socsci.mcmaster.ca/jfox/Books/Companion

FULLEN, M.A.; YI, Z.; BRANDSMA, R.T. Comparison of soil and sediment properties of a loamy sand soil. **Soil Technology**, Amsterdam, v. 10, p. 35-45, 1996.

GABET, E. J. “Fire Increases Dust Production from Chaparral Soils.” **Geomorphology,** Amsterdam, v. 217, p. 182–92, 2014.

GARCÍA MORENO, R.; DÍAZ ÁLVAREZ, M.; SAA REQUEJO, C.A.; TARQUIS, A.M. Multifractal analysis of soil surface roughness. **Vadose Zone Journal,** Madison, v. 7/2, p. 512-520, 2008.

GEE, G. W.; OR, D. The solid phase. In: DANE, J. H. e TOPP, G. C. (Ed.). **Methods of soil analyses:** part 4 - physical methods. Madison, Wisconsin, USA: Soil Science Society of America, 2002. cap. 2, p.201-414. (Soil Science Society of America Book Series).

GERANIAN, H.; MOKHTARI, A.R.; COHEN, D.R. A comparison of fractal methods and probability plots in identifying and mapping soil metal contamination near an active mining area, Iran. **Science of the Total Environment,** Amsterdam, v. 463, p. 845–54, 2013.

GHANBARIAN-ALAVIJEH, B., MILLAN, H.; HUANG, G. A review of fractal, prefractal and pore-solid-fractal models for parameterizing the soil water retention curve. **Canadian Journal of Soil Science**, Ottawa, v. 91, n. 1, 2011.

GIMENEZ, D.; ALLMARAS, R.R.; NATER, E.A.; HUGGINS, D.R. Fractal dimensions for volume and surface of interaggregate pores: scale effects. **Geoderma,** Amsterdam, v. 77, n. 1, p. 19-38, 1997.

GRASSBERGER, P.; PROCACCIA, I. Estimation of the kolmogorov-entropy from a chaotic signal. **Physical Review A**, College Park, v. 28, n. 4, p. 2591-2593, 1983.

GREVERS, M.C.J.; DEJONG, E.; STARNAUD, R.J. The characterization of soil macroporosity with ct scanning. **Canadian Journal of Soil Science,** Ottawa, v. 69, n. 3, p. 629-637, 1989.

GROSSMAN, R. B.; REINSCH, T. G. The solid phase. In: DANE, J. H. e TOPP, G. C. (Ed.). **Methods of soil analyses:** part 4 - physical methods. Madison, Wisconsin, USA: Soil Science Society of America, 2002. cap. 2, p.201-414. (Soil Science Society of America Book Series).

GUARRACINO, L.; ROETTING, T.; CARRERA, J. A fractal model to describe the evolution of multiphase flow properties during mineral dissolution. **Advances in Water Resources,** Oxford, v. 67, p. 78–86, 2014.

GUO, M.; JIAN, J; ZHAO, Z.; JIAO, J. Measurement on physical parameters of raindrop energy. **SpringerPlus**, New York, v. 2, n. Suppl 1, 2013.

GUZHA, A.C. Effects of tillage on soil microrelief, surface depression storage and soil water storage. **Soil & Tillage Research,** Amsterdam, v. 76, p. 105–114, 2004.

HAINSWORTH, J.M.; AYLMORE, L.A.G. The use of computer-assisted tomography to determine spatial-distribution of soil-water content. **Australian Journal of Soil Research,** Melbourne, v. 21, n. 4, p. 435-443, 1983.

HANSEN, B.; SCHJØNNING, P.; SIBBESEN, E. Roughness indices for estimation of depression storage capacity of tilled soil surfaces. **Soil & Tillage Research,** Amsterdam, v. 52, p. 103-111, 1999.

HÅKANSSON, I. A method for characterizing the state of compactness of the plough layer. **Soil and Tillage Research,** Amsterdam, v.16, p.105-120, 1990.

HAUSDORFF, F. Dimension und äußeres Maß. **Mathematische Annalen,** New York, v. 79, n. 1/2, p. 157–179, 1919.

HECK, R.J. X-ray computed tomography of soil. **Topics in Soil Science,** Viçosa, v. 5, p. 1–30, 2009

HENTSCHEL, H.; PROCACCIA, I. The infinite number of generalized dimensions of fractals of strange attractors. **Physical Review D**, College Park, v. 8, p. 435-444, 1983.

HIRMAS, D.R.; GIMÉNEZ, D.; MOME FILHO, E.A.; PATTERSON, M.; DRAGER, K.; PLATT, B.F.; ECK, D.V. Quantifying soil structure and porosity using three-dimensional laser scanning. In: Hartemink, Alfred E., and Budiman Minasny, eds. **Digital soil morphometrics**. Progress in Soil Science. Cham: Springer International Publishing, 2016.

HUANG, C.; WHITE, I.; THWAITE, E.G.; BENDELI, A. A noncontact laser system for measuring soil surface-topography. **Soil Science Society of America Journal,** Madison, v. 52, n. 2, p. 350–55, 1988.

HOLDEN, N.M. Description and classification of soil structure using distance transform data. **European Journal of Soil Science,** Malden, v. 52, n. 4, p. 529-545, 2001.

HORGAN, G.W. Mathematical morphology for analysing soil structure from images. **European Journal of Soil Science,** Malden, v. 49, n. 2, p. 161-173, 1998.

HUANG, C.H.; BRADFORD, J.M. Applications of a laser scanner to quantify soil microtopography. **Soil Science Society of America Journal,** Madison, v. 56, p. 14-21, 1992.

HUANG, C.H.; BRADFORD, J.M; LAFLEN, J.M. Evaluation of the detachment-transport coupling concept in the weep rill erosion equation. **Soil Science Society of America Journal,** Madison, **v.** 60, n. 3, p. 734–39, 1996.

HUDSON, N.W. **The influence of rainfall on the mechanics of soil erosion with particular reference to Southern Rhodesia.** 1965. 316 p. Thesis (Master in Science) - University of Cape Town, Cape Town, 1965.

JOSCHKO, M.; GRAFF, O.; MULLER, P.C.; KOTZKE, K.; LINDNER, P.; PRETSCHNER, D.P.; LARINK, O. A non-destructive method for the morphological assessment of earthworm burrow systems in three-dimensions by X-ray computed tomography. **Biology and Fertility of Soils,** New York, v. 11, p. 88-92, 1992.

JOSCHKO, M.; MULLER, P.C.; KOTZKE, K.; DRHRING, W.; LARINK, O. Earthworm burrow system development assessed by means of X-ray computed tomography. **Geoderma,** Amsterdam, v. 56, p. 209-221, 1993.

JUHÁSZ, C.E.P.; COOPER, M.; CURSI, P.R.; KETZER, A.O.; TOMA, R.S. Savanna woodland soil micromorphology related to water retention. **Scientia Agricola,** Piracicaba, v. 64, n. 4, p. 344-354, 2007.

KAMPHORST, E.C.; JETTEN, V.; GUERIF, J.; PITKANEN, J.; IVERSEN, B.V.; DOUGLAS, J.T.; PAZ, A. Predicting depressional storage from soil surface roughness. **Soil Science Society of America Journal,** Madison, v. 64, p. 1749-1758, 2000.

KOOISTRA, M.J.; SIDERIUS, W. Micromorphometrical aspects of crust formation in a savanna climate under rainfed subsistence agriculture. In: CALLEBAUT, C.; GABRIELS, D.; DE BOODT, M. **Assessment of soil surface sealing and crusting:** proceedings of the symposium held in Ghent, Belgium, 1985. Ithaca: Flanders Research Centre for Soil Erosion and Soil Conservation, 1986. 374p.

LAL, R. Soil Degradation by Erosion. **Land Degradation & Development**, Chichester, v. 12, n. 6, p. 519–39, 2001.

LAU, M.K. DTK: Dunnett-Tukey-Kramer pairwise multiple comparison test adjusted for unequal variances and unequal sample sizes. (2013) R package version 3.5. https://CRAN.R-project.org/package=DTK.

LE BISSONNAIS, Y. Aggregate stability and assessment of soil crustability and erodibility .1. Theory and methodology. **European Journal of Soil Science,** Oxford, v. 47, p. 425-437, 1996.

LEVY, G.J.; EISENBERG, H.; SHAINBERG, I. Clay dispersion as related to soil properties and water permeability. **Soil Science**, Philadelphia, v. 155, n. 1, p. 15–22, 1993.

MAGUNDA, M.K.; LARSON, W.E.; LINDEN, D.R.; NATER, E.A. Changes in microrelief and their effects on infiltration and erosion during simulated rainfall. **Soil Technology,** Amsterdam, v. 10, p. 57-67, 1997.

MANDELBROT, B. How long is the Coast of Britain? Statistical self-similarity and fractional dimension. **Science,** New Series, Washington, v. 156, n. 3775, p. 636-638, 1967.

MENDIBURU, F. agricolae: statistical procedures for agricultural research. (2015) R package version 1.2-3. https://CRAN.R-project.org/package=agricolae.

MOLDRUP, P.; OLESEN, T.; KOMATSU, T.; SCHJONNING, P.; ROLSTON, D.E. Tortuosity, diffusivity, and permeability in the soil liquid and gaseous phases. **Soil Science Society of America Journal,** Madison, v. 65, n. 3, p. 613–23, 2001.

MORAN, C.J.; MCBRATNEY, A.B.; KOPPI, A.J. A micromorphometric method for estimating change in the volume of soil induced by weathering. **Journal of Soil Science**, Philadelphia, v. 39, n. 3, p. 357–73, 1988.

MORGAN, R.P.C. **Soil erosion & conservation**. 2nd ed. Oxford: Blackwell, 2005. 316 p.

MOMOLI, R.S.; COOPER, M.; CASTILHO, S.C.P. Sediment morphology and distribution in a restored riparian forest. **Scientia Agricola,** Piracicaba, v. 64, n. 5, p. 486-494, 2007.

MULLINS, C.E.; BLACKWELL, P.S.; TISDALL, J.M. Strength development during drying of a cultivated, flood-irrigated hardsetting soil .1. comparison with a structurally stable soil. **Soil and Tillage Research,** Amsterdam, v. 25, n. 2–3, p. 113–28, 1992.

MURPHY, C.P. **Thin section preparation of soils and sediments.** Berkhamsted: A.B. Academic, 1986. 149 p.

MURPHY, C.P.; BULLOCK, P.; TURNER, R.H. The measurement and characterization of voids in soil thin sections by image analysis. Part I. Principles and techniques. **Journal of Soil Science**, Oxford, v. 98, p.498-508, 1977.

NEARING, M.A.; BRADFORD, J.M.; HOLTZ, R.D. Measurement of waterdrop impact pressures on soil surfaces. **Soil Science Society of America Journal,** Madison, v. 51, n. 5,p. 1302–6, 1987.

NEARING, M.A.; PARKER, S.C. Detachment of soil by flowing water under turbulent and laminar conditions. **Soil Science Society of America Journal**, Madison, v. 58, p. 1612–1614, 1994.

OLSEN, P.A.; BORRESEN, T. Measuring differences in soil properties in soils with different cultivation practices using computer tomography. **Soil & Tillage Research,** Amsterdam, v. 44, n. 1/2, p. 1-12, 1997.

ORFORD, J.D.; WHALLEY, W.B. The Use of the Fractal Dimension to Quantify the Morphology of Irregular-Shaped Particles. **Sedimentology**, Malden, v. 30, n. 5, p. 655–68, 1983.

OXFORD ENGLISH DICTIONARY. Oxford: Oxford University Press. Disponível em: <http://www.oed.com/viewdictionaryentry/Entry/11125>. Acesso em: 28 ago. 2015.

PACHEPSKY, Y.; YAKOVCHENKOB, V.; RABENHORSTC, M.C.; POOLEYD, C.; SIKORAB, L.J.. Fractal parameters of pore surfaces as derived from micromorphological data: effect of long-term management practices. **Geoderma,** Amsterdam, v. 74, n. 3/4, p. 305-319, 1996.

PAGLIAI, M.; DENOBILI, M. Relationships between soil porosity, root development and soil enzyme-activity in cultivated soils. **Geoderma,** Amsterdam, v. 56, n. 1/4, p. 243-256, 1993.

PAGLIAI, M.; VIGNOZZI, N.; PELLEGRINI, S. Soil structure and the effect of management practices. **Soil & Tillage Research**, Amsterdam, v. 79, p. 131-143, 2004

PARISI, G.; FRISCH, U. On the singularity structure of fully developed turbulence in Turbulence and predictability in geophysical fluid dynamics and climate dynamics. In: GHIL, M.; BENZI, R.; PARISI, G. (Ed.). **Turbulence and predictability in geophysical fluid dynamics.** Amsterdam: Elsevier Science, 1985. p. 84–87. (Proceedings of the International School of Physics. Book, 88).

PAZ FERREIRO, J.; WILSON, M.; VIDAL VAZQUEZ, E. Multifractal description of nitrogen adsorption isotherms. **Vadose Zone Journal,** Madison, v. 8, n. 1, p. 209–19, 2009.

PENG, G.; XIANG, N.; SHENG-QIAO, L.V.; ZHANG, G.C. Fractal characterization of soil particle-size distribution under different land-use patterns in the Yellow river delta wetland in China. **Journal of Soils and Sediments**, v. 14, n. 6, p. 1116–22, 2014.

PERFECT, E.; KAY, B.D. Applications of fractals in soil and tillage research: a review. **Soil & Tillage Research,** Amsterdam, v. 36, p. 1-20, 1995.

PETROVIC, A. M.; SIEBERT, J. E.; RIEKE, P. E. Soil bulk-density analysis in 3 dimensions by computed tomographic scanning. **Soil Science Society of America Journal,** Madison, v. 46, n. 3, p. 445-450, 1982.

PHOGAT, V.K.; AYLMORE, L.A.G. Evaluation of soil structure by using computer-assisted tomography. **Australian Journal of Soil Research,** Melbourne, v. 27, n. 2, p. 313-323, 1989.

PIRES, L.F.; BACCHI, O.O.S.; REICHARDT, K. Assessment of soil structure repair due to wetting and drying cycles through 2D tomographic image analysis. **Soil & Tillage Research,** Amsterdam, v. 94, n. 2, p. 537-545, 2007.

POSADAS, A.; GIMÉNEZ, D.; QUIROZ, R.; PROTZ, R. Multifractal characterization of soil pore systems. **Soil Science Society of America Journal,** Madison, v. 67, p. 1361-1369, 2003.

R DEVELOPMENT CORE TEAM. **R**: a language and environment for statistical computing. Vienna: R Foundation for Satatistical Computing. 2015. url: {http://www.R-project.org}.

RAATS, P.A.C. Developments in soil-water physics since the mid 1960s. **Geoderma,** Amsterdam, v. 100, n. 3–4, p. 355–87, 2001.

RAIJ, B. van; QUAGGIO, J.A. Determinação de fósforo, cálcio, magnésio e potássio extraídos com resina trocadora de íons. In: RAIJ, B. van; ANDRADE, J.C.; CANTARELLA, H.; QUAGGIO, J.A. (Ed.). **Análise química para avaliação da fertilidade de solos tropicais**. Campinas: Instituto Agronômico de Campinas, 2001. p. 189-199.

RICE, J.A.; LIN, J.S. Fractal nature of humic materials (vol 27, pg 413, 1993). **Environmental Science & Technology**, Washington, v. 27, n. 8, p. 1696–1696, 1993.

RICE, J.A.; TOMBACZ, E.; MALEKANI., K. Applications of light and x-ray scattering to characterize the fractal properties of soil organic matter. **Geoderma,** Amsterdam, v. 88, n. 3–4, p. 251–64, 1999.

RICHARDSON, L.F. The problem of contiguity: an addendum to statistics of deadly quarrels. **General Systems Yearbook,** Washington, v. 6, p. 139-187, 1961.

RINGROSE-VOASE, A.J. A scheme for the quantitative description of soil macrostructure by image analysis. **Journal of Soil Science,** Philadelphia, v. 38, p. 343-356, 1987.

RINGROSE-VOASE, A.J.; BULLOCK, P. The automatic recognition and measurement of soil pore types by image analysis and computer programs. **Journal of Soil Science,** Philadelphia, v. 35, p. 673-684, 1984.

RINGROSE-VOASE, A.J. Micromorphology of soil structure: description, quantification, application. **Australian Journal of Soil Research**, Melbourne, v. 29, p. 777-813, 1991.

RIEU, M.; SPOSITO, G. Fractal fragmentation, soil porosity, and soil-water properties .1. theory. **Soil Science Society of America Journal,** Madison, v. 55, n. 5, p. 1231–38, 1991.

RIZZI, F.R.; STOLL, S.; SENESI, N.; BUFFLE, J. A transmission electron microscopy study of the fractal properties and aggregation processes of humic acids. **Soil Science**, Philadelphia, v. 169, n. 11, p. 765–75, 2004.

RODRÍGUEZ-CABALLERO, E.; CANTÓN, E.; CHAMIZO, S.; AFANA, A.; SOLÉ-BENET, A. Effects of biological soil crusts on surface roughness and implications for runoff and erosion. **Geomorphology,** Amsterdam, v. 145/146, p. 81–89, 2012.

RÖMKENS, M.J.M.; HELMING, K.; ;PRASAD, S.N. Soil erosion under different rainfall intensities, surface roughness, and soil water regimes. **Catena,** Amsterdam, v. 46, p. 103–123, 2001.

SALLES, C.; POESEN, J.; GOVERS, G. Statistical and physical analysis of soil detachment by raindrop impact: rain erosivity indices and threshold energy. **Water Resources Research,** Washington, v. 36, n. 9, p. 2721–29, 2000.

SAN JOSÉ MARTÍNEZ, F.; CANIEGO, J.; GUBER, A.; PACHEPSKY, Y.; REYES, M. Multifractal modeling of soil microtopography with multiple transects data. **Ecological Complexity,** Amsterdam, v. 6, p. 240–245, 2009.

SEGINER, I. Random walk and random roughness models of drainage networks. **Water Resources Research,** Washington, v. 5, n. 3, p. 591-607, 1969.

SENESI, N. Aggregation patterns and macromolecular morphology of humic substances: a fractal approach. **Soil Science**, Philadelphia, v. 164, n. 11, p. 841–56, 1999.

SHAKESBY, R. A. Post-Wildfire Soil Erosion in the Mediterranean: Review and Future Research Directions. **Earth-Science Reviews**, Amsterdam, v. 105, n. 3–4, p. 71–100, 2011.

SHARMA, P.P. Interrill erosion. In: AGASSI, M. (Ed.). **Soil erosion conservation and rehabilitation**. New York: Marcel Dekker, 1996. p. 125-152.

SHANNON, C.E.; WEAVER, W. **The mathematical theory of communication.** Urbana: University of Illinois Press, 1949. 125 p.

SMITH, M.W. Roughness in the Earth sciences. **Earth-Science Reviews**, Amsterdam, v. 136, p. 202–25, 2014.

SOIL SURVEY STAFF. **Keys to soil taxonomy.** 12th ed. Washington: USDA, Natural Resources Conservation Service, 2014. 360 p.

SOKOLOWSKA, Z.; WARCHULSKA,P.; SOKOLOWSKI, S. Trends in soil fractal parameters caused by accumulation of soil organic matter as resulting from the analysis of water vapor adsorption isotherms. **Ecological Complexity**, Amsterdam, v. 6, n. 3, p. 254–62, 2009.

STANCHI, S.; BONIFACIO, E.; ZANINI, E.; PACKEPSKY, Y. Presence and prediction of fractal behavior in particle-size distributions as affected by the sample pretreatment and soil properties. **Soil Science**, Philadelphia, v. 171, n. 4, p. 283–92, 2006.

STANLEY, H.E.; MEAKIN, P. Multifractal phenomena in physics and chemistry: review. **Nature,** London, v. 335, n. 6189, p. 405–409, 1988.

TURCOTTE, D.L. Fractals and Fragmentation. **Journal of Geophysical Research**, Washington, v. 91, n. B2, p. 1921–26, 1986.

TYLER, S.W.; WHEATCRAFT, S.W. Fractal scaling of soil particle-size distributions - analysis and limitations. **Soil Science Society of America Journal,** Madison, v. 56, n. 2, p. 362–69, 1992.

UIJLENHOET, R.; STRICKER, J.N.M. A consistent rainfall parameterization based on the exponential raindrop size distribution. **Journal of Hydrology,** Amsterdam, v. 218, n. 3–4, p. 101–27, 1999.

Van GENUCHTEN, M.T. A closed form equation for predicting the hydraulic conductivity of unsaturated soils. **Soil Science Society of America Journal**, Madison, v.44, p.892–898, 1980.

Van OOST, K.; GOVERS, G.; DESMET, P. Evaluating the effects of changes in landscape structure on soil erosion by water and tillage. **Landscape Ecology**, Dordrecht, v. 15, n. 6, p. 577–89, 2000.

VIDAL VÁZQUEZ, E.; VIVAS MIRANDA, J.G.; PAZ GÓNZALEZ, A. Characterizing anisotropy and heterogeneity of soil surface microtopography using fractal models. **Ecological Modelling,** Amsterdam, v. 182, p. 337–353, 2005.

VIDAL VÁZQUEZ, E., VIVAS MIRANDA, J.G. AND PAZ GÓNZALEZ., A. A multifractal approach to characterize cumulative rainfall and tillage effects on soil surface microtopography and to predict depression storage. **Biogeosciences**, Gottingen, v. 7, p. 2989-3004, 2010.

VOSS, R.F. Fractals in nature: from characterization to simulation. In: PEITGEN, H.-O.; SAUPE, D. (Ed.). **The science of fractal image.** New York: Springer, 1988. p. 21-69.

WISCHMEI,W.H.; MANNERIN, J.V. Relation of soil properties to its erodibility. **Soil Science Society of America Proceedings**, Madison, v. 33, n. 1, p. 131 – &, 1969.

WISCHMEIER, W.H.; SMITH, D.D. Soil-loss estimation as a tool in soil and water management planning. **International Association Of Hydrological Sciences**, Wallingford, v. 59, p. 148-159, 1962.

YOUNG, I.M.; CRAWFORD, J.W. The fractal structure of soil aggregates - its measurement and interpretation. **Journal of Soil Science**, Philadelphia, v. 42, n. 2, p. 187–92, 1991.

ZHOU, H.U.; PENG, X.; PERFECT, E.; XIAO, T.; PENG, G. Effects of organic and inorganic fertilization on soil aggregation in an ultisol as characterized by synchrotron based x-ray micro-computed tomography. **Geoderma,** Amsterdam, v. 195, p. 23–30, 2013.

ZHOU, X.; LIN, H.S.; WHITE, E.A. Surface soil hydraulic properties in four soil series under different land uses and their temporal changes. **Catena,** Amsterdam, v. 73, n. 2, p. 180–88, 2008.